universität wien

MASTERARBEIT / MASTER'S THESIS

Titel der Masterarbeit / Title of the Master's Thesis

Worms' migration through the redox discontinuity layer: Evidences from the Thiosymbion physiology?

verfasst von / submitted by

Tobias Viehböck, BSc

angestrebter akademischer Grad / in partial fulfilment of the requirements for the degree of

Master of Science (MSc)

Wien, 2018 / Vienna 2018

Studienkennzahl lt. Studienblatt / degree programme code as it appears on the student record sheet:	A 066 830
Studienrichtung lt. Studienblatt / degree programme as it appears on the student record sheet:	Masterstudium Molekulare Mikrobiologie, Mikrobielle Ökologie und Immunbiologie
Betreut von / Supervisor:	Priv.-Doz. Dr. Silvia Bulgheresi

Ich habe mich bemüht, sämtliche Inhaber der Bildrechte ausfindig zu machen und ihre Zustimmung zur Verwendung der Bilder in dieser Arbeit eingeholt. Sollte dennoch eine Urheberrechtsverletzung bekannt werden, ersuche ich um Meldung bei mir.

Table of Contents

Abstract

Free-living marine nematodes belonging to the subfamily Stilbonematinae carry symbiotic, autotrophic sulfur-oxidizing Gammaproteobacteria of the genus *Candidatus* Thiosymbion on their cuticle. As a prominent member of the thiobios, they may occur at extremely high abundances (>10^5 per m^2) in shallow water sediments characterized by an oxygen-sulfide gradient with oxygenated upper layers and anoxic deeper sulfide-rich sands. Therefore, these chemoautotrophic symbioses might substantially contribute to S, C and N cycling in shallow water marine sediments and affect their biogeochemistry. It has long been hypothesized that the symbionts associate to the nematodes to exploit their vertical migrations through this redox zone as these can alternatively expose them to sulfide (electron donor) and oxygen (electron acceptor). In this work, we studied the metabolic adaptions of stilbonematid symbionts by (1) reconstructing symbiont metabolic pathways and adaptions that might be beneficial to a symbiotic existence by using a combining short (Illumina) and ultra-long-read (Oxford Nanopore Technologies) sequencing technologies for genome assembly; (2) measuring their vertical distribution and physicochemical parameters they encounter in the sediment of Carrie Bow Cay, Belize, and Piran, Slovenia; (3) determining the effect of high and low oxygen environments on symbiont S, C, N metabolisms by quantifying the transcription of key metabolic genes (*aprA*, *dsrA*, *norB*, *cbbL*, *nifH*) over 72 h by qPCR.

The complementation of Illumina reads with long reads (max. 121 kbp) greatly improved the overall assembly statistics. As determined by COG and Pfam annotation, *Cand.* Thiosymbion oneisti possesses a high number of transposases and toxin-antitoxin systems in addition to a high number of repeats, and fully encodes for a type II secretion pathway of proteins (with Sec and Tat pathways), type IV pili and a type VI secretion system, all of which points to a mobile genome and an extracellular, versatile ecological lifestyle. Moreover, the diversity in toxin-antitoxin systems poises them as cellular adaptions to nutrient limitation and environmental stress. In contrast, metabolic reconstruction revealed that all pathways necessary for a host-independent lifestyle are complete and its genome (4.3 Mbp) is not reduced. These include auto- and heterotrophy (Calvin cycle, TCA cycle), sulfur oxidation (Sox/reverse Dsr pathway), denitrification, nitrogen fixation, biosynthesis of all amino acids, genes encoding for cofactor and vitamin biosynthesis (biotin, folate, polyhydroxybutyrate, riboflavin, cobalamin, heme) and ABC transporters (i.e. for acetate, ammonium, molybdate, urea, phosphate, zinc, lipoproteins, heme).

The vertical distribution of Stilbonematinae, in particular *Laxus oneistus*, shows a distinct maximum at low sulfidic (< 20 µM) and low oxygen (< 20 µM) concentrations. Ammonia, nitrate, nitrite and DOC concentrations varied between sites, with ammonium potentially being the main nitrogen source for the ectosymbionts.

The genome-derived hypotheses tested in oxic and hypoxic incubations elucidated simultaneous respiration of oxygen and nitrate for carbon fixation, both enhanced in the hypoxic incubation. Both genes for sulfur oxidation (*aprA*, dsrA) decreased over time supposedly due to exhaustion of the internal sulfur storage. Moreover, nitrogen fixation (*nifH* transcription) might increase upon 72 h-long hypoxia.

All in all, the data suggest a versatile stilbonematid symbionts' metabolism optimized to exploit environment with low redox potential.

Introduction

The thiobios, life in an extreme environment

Fenchel & Riedl introduced the 'sulfide system' in 1970 [1] to describe (meiobenthic) life (termed 'thiobiome' or 'thiobios' [2]) and trophic significance of anaerobic decomposition beneath oxidized marine sediments in the 'black zone'. As this is characterized by strongly reducing, micro- to anaerobic conditions with high concentrations of sulfide, it was previously considered to be azoic. Microbial reduction of virtually unlimited sulfate is the driving force through with sulfide develops and accumulates in deeper, organically rich and oxygen-depleted layers [3,4]. In this complex habitat, marine benthic meiofauna – that is animals 44 to 500 µm in size - represents a relevant biological and ecological unit on its own [5–8]. Nematodes of the subfamily of Stilbonematinae – the subjects of this thesis and further discussed below - are members of the thiobios and occur world-wide from temperate to tropical waters [9]. The extreme environments they inhabit include shallow water seeps [10–13], deep sea [14], gas-hydrothermal vents [15], shallow water vents [15–17], mangroves and hypoxic/anoxic environments and are adapted to the upper and lower limits of life [9] (as reviewed in [18]).

Life in anoxia has particular advantages such as sufficient food supply under low competitive stress and avoidance of competition because of low meiofaunal density [16,19–22], prevention of detrimental epigrowth [19], stability of physical parameters (O_2, redox potential, pore water content, temperature, salinity) due to lack of influence of heavy rainfall, strong currents and waves in shallow water ecosystems [20,21].

The existence of life in anoxia was thought to be a Precambrian relict because the anaerobic biosystem preceded aerobic life on Earth [1,2,23–26]. Opposing this idea, there are specific physical and structural adaptions that have developed that allow survival and flourishing of this complex and specific biome [10,27–32]. Although Powell (1989) [28] concluded that life in high sulfidic environments, which are normally lethal[1] [33–40], is only possible if the organisms are sulfide insensitive, no report of sulfide intolerance or a sulfur insensitive respiration chain is known [41–43], and thus, a detoxification system such as an effective export mechanism [16,44] or protective proteins (hematins) [45,46] must be present to prevent H_2S toxification. Only in oxygen-dependent macrobenthic freshwater fauna

[1] by binding to cytochrome c at the heme site or by reducing disulfide bridges [31]

inhabiting the thiobios high abundance of sulfide-insensitive enzymes was found [47]. Some meiobenthic metazoans deposit sulfur granules in their epidermis that reduce the toxic effect and serve as an energy deposit [41,48,49] or excrete sulfur droplets [16]. Others precipitate ferrous sulfide on their body surface to inhibit the flow of sulfide into the body [41,48–52]. Sulfur oxidation in mitochondria coupled to succinate formation was proposed [53–55], but the underlying molecular mechanisms and their efficiencies remain unclear. Only for *Parahaploposthia* (Turbellaria) sulfide (and cyanide) insensitivity was found [56]. In other cases, high sulfidic habitats are simply avoided [11,31,34,57–59].

Metazoan life under oxygen limitation

Sulfide can deplete the interstitial pore water from oxygen. Anaerobic metazoans are defined as "organisms that can complete their life cycle in absolute absence of oxygen" [60]. Extensive literature on microaerophilic invertebrates that tolerate anoxia (or oxygen concentrations below the detection limit) not only for irregular time intervals during low tides [61], but also, in extreme environments, for extended periods of time is available (reviewed in [18]).

Only anecdotal reports of nematodes reproducing in anoxia in a subterranean cave are available and the complete anoxic life cycle suggested for Loricifera from deep hypersaline anoxic basins in the Mediterranean Sea is highly debated [62–65]. Therefore, irrefutable proofs of the existence of anaerobic metazoans are lacking. An increase of body surface area to volume (pronounced in slender bodies) facilitates epidermal absorption of low oxygen concentrations or dissolved organic matter, and allow the thiobios to be mobile even in stiffer clays [16,22,66–70]. Hemoglobins with high oxygen affinity [71–76] or oxygen storage capability [77] may counteract the absence of oxygen. Among the thiobios, marine and limnic nematodes seem tolerant, if not most resistant among the thiobios [2,19,69,77–87] to anaerobic and reducing conditions in deeper layers [20], especially at the redox potential discontinuity (RPD) layer[2] or below [20,67,68,88–92]. Survival of non-symbiotic metazoans at low oxygen levels and high

[2] Upper boundary of the sulfide system, where oxidized change into reduced conditions [1,384], and redox potential (Eh) has a value of 0. The RPD layer is chemically characterized by high oxygen and nitrate concentrations in the upper layer and high concentrations of ferric iron, manganese, and sulfate in the lower layers.

sulfide concentrations has been reported [58,93–100], theoretically possible through oxygen diffusion alone [28,60,101]. Nematodes, including Stilbonematinae, are capable of oxygen uptake [19,102] at low rates [29]. However, long-term anoxic incubations are biased due to death by starvation [20] and only little information about anaerobic energy gain (e.g. eukaryotic denitrification and sulfate reduction) is known [103]. There is no evidence of non-oxidative phosphorylation. High mitochondrial density is an adaptation to low oxygen [104–106], some oxygen-sensitive invertebrates use glycolytic pathway for ATP generation, metabolize stored glycogen or use supplementary fermentative pathways in mitochondria when exposed to short-term anoxia [30,52].

There are various responses of meiofauna to anoxia:

- Reproduction of the annelid *Tubifex* sp. in anoxia was reported [107], although traces of oxygen in the set-up cannot be excluded.
- Anoxia triggered hatching of juveniles of the nematode *Metachromadora vivipararus* possibly due to the stressful conditions anoxia represents to it [80].
- The free-living nematode *Sabatieria* was present permanently in hypoxic or anoxic sediments [69] but on the mechanisms of adaptations can only be speculated [25].
- *Cletocamptus confluens* (Copepoda) enters quiescence when exposed to high sulfide [30].
- Marine annelids have developed mechanisms of production and storage of opines by fermentation of pyruvate that can be used when oxygen becomes available again [108,109].

Other meiofaunal invertebrates inhabit micro-aerobic niches [1,110] or oxygen islands generated by macrofaunal bioturbation [111,112] (Figure 1).

Nematodes live in the interstitial environment of sediment in pore water [113] and thus their distribution is shaped by chemical gradients. Stilbonematinae have a strong chemosensory system, but to what extent chemotaxis can occur is not known [11]. Although the RPD layer defines the sulfide biome and the population density of nematodes is high in its vicinity [1,25], oxygen solely shapes the distribution of benthic organisms [25,68]. Nematodes are a prominent component of deeper meiobenthic fauna [22,29,67,114] and the existence of life exclusive under reducing conditions was hypothesized [19].

Macrobenthos change physicochemical gradients of the sediment, as well as plant growth [115–117], the former representing also a strong biotic influence (e.g. food source, grazing, predation) on animal distribution [20,113].

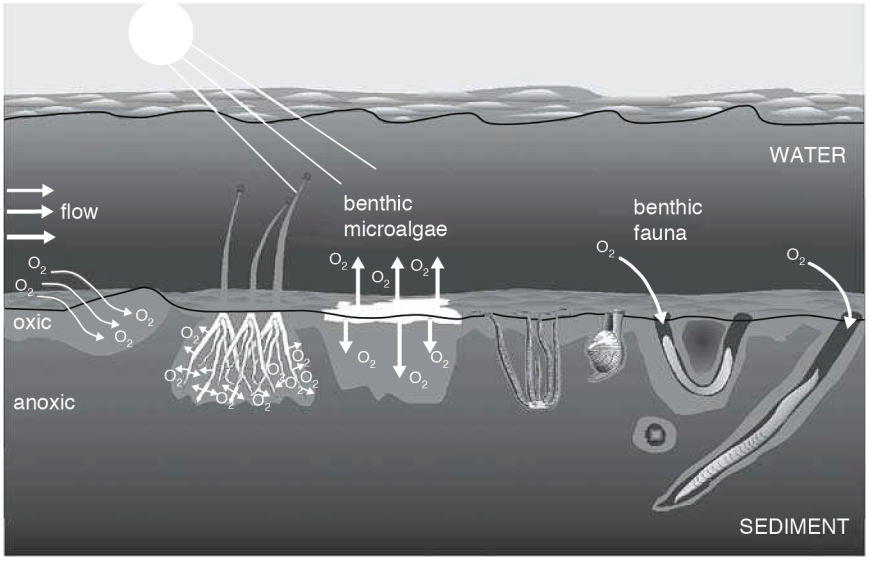

Figure 1. Sources and distribution of oxygen in shallow, subtidal sediment. Sulfide is shaped antagonistically. Taken from Giere (2008) [8].

Microbial association as survival strategy

Another adaptation to life in marine sediment enriched with H_2S and depleted in oxygen is the bacterial coverage [15,29,33,68], as all nematodes of the subfamily Stilbonematinae have [19]. The nematode host might benefit from symbiont-mediated sulfide detoxification and a nutritional symbiosis has been postulated [29,68,118]. Because anaerobic metabolism is less efficient [20], non-symbiotic worms showed reduced survival in anoxic incubations [80]. Evidence that symbionts provide nutrients, and consequently energy, was first given in Pogonophora (Vestimentifera), which lack a mouth, digestive tract, and anus. Chemotrophy, in contrast to phototrophy, does not include light as an energy source but the oxidation of inorganic hydrogen sulfide, elemental sulfur, dihydrogen, ammonia or ferrous iron. Carbon is supplied by fixing inorganic carbon (as in autotrophs, e.g. CO_2) or organic carbon (as in heterotrophs).

The discovery of the association of the vestimentiferan tube worm, *Riftia pachyptila*, with chemoautotrophic bacteria at hydrothermal vents [119,120] revolutionized the view on the impact of bacteria on host nutrition. Lacking a mouth or gut and being unable to obtain organic compounds by diffusion, *R. pachyptila* gains the latter via bacterial, sulfur oxidation-driven

CO_2 fixation. *Riftia* symbionts also play an important role in resource recycling in nutrient-poor habitats [57,70,121–129]. Soon after the *Riftia* symbiosis discovery, additional thiotrophic symbioses were described in more accessible shallow water coastal ecosystems too [114,120,130,131]. So far, seven eukaryotic phyla and one archaeon [132] are known to possess chemoautotrophic, sulfur-oxidizing bacteria. Below, I briefly discuss three among the most intensively studied shallow water symbioses.

Thio- & diazotrophy in Bivalvia symbioses

Five families of bivalves (Lucinidae, Mytilidae, Solemyidae, Thyasiridae, Vesicomyidae, Teredinidae) are known to harbor chemosynthetic symbionts [133,134] in gill filaments and occur from sewage effluent sites [135] to the deep sea [136]. All symbionts are sulfur oxidizers [133] with oxygen or nitrate used as the terminal electron acceptor [137–140], the deep sea bathymodiolin mussels additionally harbor a methanoautotrophic symbiont [141,142]. In addition to symbiont digestion, CO_2 fixation by RuBisCO [135,143–146] as well as nitrogen fixation [147,148] may contribute to the host's nutrition [149–151] and sustain entire ecosystems [152]. Their successful distribution over the globe is partly due to forming a tripartite symbiosis with seagrass. This provides dissolved organic molecules and debris to sulfate reducers and oxygen to the clams and these, in turn, detoxify the sediment for the seagrass [153]. Except for bathymodiolin mussels that rely on diffusion gradients for providing electron acceptors and donors to their symbionts [154], sulfide and oxygen are separately acquired by digging vertically with the foot [11] and are transported via binding to haemoglobin [155,156]. Additionally, cellulolytic activity for wood degradation and nitrogen fixation was also observed in Gammaproteobacteria of shipworms [157–159].

Bacterial syntrophy in gutless oligochaetes

Sulfide concentrations between 2 and 32 µM were detected in the habitat of *Inandrilus leukodermatus* (Phallodrilinae, Annelida) [160], one member of the so-called marine gutless oligochaetes due to the reduction of gut and mouth [161–163]. These organisms with world-wide distribution live buried in the sediment [164] and possess endosymbiotic bacteria below the cuticle [165,166] that oxidize reduced sulfur compounds to fix CO_2 or respire sulfate [105]. Each host species harbors three to six specific symbiont phylotypes that belong to Gamma-, Delta- and Alphaproteobacteria and Spirochaetes and live in syntrophy [167]. Thiotrophic

gammaproteobacterial symbionts of oligochaetes and nematodes are phylogenetically related and grouped in the *Candidatus* genus Thiosymbion formerly known as MONTS cluster [168,169].

In the oligochaete *Olavius algarvensis*, the γ1 symbiont is mainly responsible for the oxidation of reduced sulfur compounds with oxygen for energy generation, whereas the γ3 symbiont is mainly a denitrifying sulfur oxidizer. Both symbionts are able to fix CO_2 via the Calvin-Benson-Bassham cycle, although γ3 additionally generates energy by CO oxidation into CO_2 through the aerobic-type CO dehydrogenase [170]. On the other hand, both δ1 and δ4 symbionts are sulfate reducers, gain energy through H_2 oxidation via hydrogenases and have two anaerobic-type CO dehydrogenases, one of which is possibly connected to the Wood–Ljungdahl pathway (reductive Acetyl-CoA cycle). The capability of heterotrophy is complemented with the reductive TCA cycle. All four symbionts have high-affinity transporters allowing them to inhabit locations with low concentrations of electron donors. Host excretion products can be taken up, more specifically γ1 can recycle fermentative waste and γ3 osmolytes (i.e. glycine betaine) [167,171–173]. Only in some individuals of *O. algarvensis* (Mediterranean Sea) and *O. crassitunicatus* (Peru/Southwest Pacific; has γ1, γ2, δ1, δ2 & δ3 symbionts), a Spirochaete with unknown function has been identified [174]. Symbiotic Alphaproteobacteria were described in *O. loisae* (from Australia; 1 γ symbiont & Spirochaete) [175] and *I. leukodermatus* (γ1, α1a, α1b, α1c & α3) & *I. makropetalos* (γ1 α1b & α2) [50,130,176]. Both *Inandrilus* species bear symbionts encoding for *cbbL* and *aprA* [176].

Stilbonematid symbioses

Nematodes are the most abundant, still existing, metazoan and Nathan Cobb, father of US nematology, draw attention to that fact 100 years ago [177]: "In short, if all the matter in the universe except the nematodes were swept away, our world would still be dimly recognizable, and if, as disembodied spirits, we could then investigate it, we should find its mountains, hills, vales, rivers, lakes, and oceans represented by a film of nematodes. The location of towns would be decipherable, since for every massing of human beings there would be a corresponding massing of certain nematodes." Although the first scientific report of the parasitic lifestyle of a wheat seed infesting nematode started to stress out the agricultural impact of nematodes [178], even in marine sediments nematodes are the most abundant taxon [62,179,180].

An association of marine, free-living nematodes with external, presumably symbiotic (*sensu lato* after de Bary 1879 [181]) microorganisms was described in 1936 [182] and thereafter [15,114,183–188] in all species within the subfamily of Stilbonematinae (Desmodorida) [189]. This association is a specific, binary (one single bacterial phylotype per host species) ectosymbiosis with chemoautotrophic, sulfide-oxidizing Gammaproteobacteria of the genus *Candidatus* Thiosymbion related to free-living members of the Chromatiaceae [168,169,190]. It is neither known whether the symbiosis is obligate for both partners, nor how it is established (reviewed in [191]). However, host-symbiont recognition in *Laxus oneistus*[3] is mediated by the Mermaids, a family of mannose-binding, Ca^{2+}-dependent (C-type) lectins [192] secreted with mucus through glandular sensory organs [193,194]. The mucus-embedded symbionts are arranged in a species-specific pattern on the cuticle of the nematode [12]. Concerning stilbonematid symbiont metabolism, physiological studies reported chemoautotrophy by sulfur-oxidation [195], denitrification [118], and carbon fixation [11,29,195]. Only genomic evidence of nitrogen fixation is available so far [147].

Considering the high host-symbiont specificity, and likely co-evolution [68,169], Stilbonematinae are one evolutionary success story thank to the permanent relationship with a bacterial coat. This must represent a selective advantage as it was suggested in the 'microbial gardening hypothesis' by Riemann & Schrage (1978) [11,196]. Since Stilbonematinae have a reduced alimentary gut [114], ingestion of mucus-embedded ectosymbiotic bacteria has been suggested [66,183] and was observed microscopically for some species [10,197].

Vertical migrations: a thiobios' ace in the hole?

Another way metazoans deal with the disadvantages of living in low oxygen zones (such as lack of oxygen for the respiratory chain) is by migrating vertically towards oxygenated upper layers (Figure 2). This vertical migration behavior can also provide the advantage of avoiding predation and competition and of living under more stable conditions [198]. Stilbonematinae and oligochaetes (see the last two sections above) were shown to migrate through sulfide gradients in agar-filled glass pipettes. Based on these experiments, it was hypothesized that both invertebrates migrate between oxic and anoxic sediment layers [11,167] in order to expose their

[3] from Latin *laxus*, meaning 'loose/relaxed' due to their body, and Greek *oneistus*, meaning 'most useful' due to its relevance as an experimental animal [385]

symbionts alternatively to electron donors (e.g. sulfide) and acceptors (e.g. oxygen, nitrate) [11]. It is not known how long these organisms reside in the respective layers. An experimental ecology study by Giere *et al.* (1991) [199] showed that *Inandrilus leukodermatus* prefers the vicinity of the RPD layer at the oxygen/sulfide interface and is only rarely present in the uppermost layers.

Downward migrations can also be a result of low water content during low tide, changes in salinity because of heavy rainfall or strong currents and waves. According to the 'intermediate disturbance hypothesis', nematodes from disturbed sediments are more adapted to physicochemical changes than those in stable sediments [8,200]. *Leptonomella* was detected exclusively below 6 cm and vertical migrations were hypothesized because of temperature, high light intensity and correlated diatom migrations [198]. Light intensity is also shaping oligochaete distribution [21]. Vertical migration of the nematode *Theristus anoxybioticus* through an oxygen gradient is linked to its reproduction: downwards migration occurs for juveniles to hatch and upwards during adulthood to feed on diatoms, although survival of juveniles was limited to 15 days in anoxia [201].

In turn, meiofaunal migration has a positive ecological impact on nutrient cycling that stimulates bacterial growth. Cycling of oxygen, fractionation of larger organic larger particles, excretion of phosphorus, and nitrogen from animals thrive bacterial communities in the sediment [202].

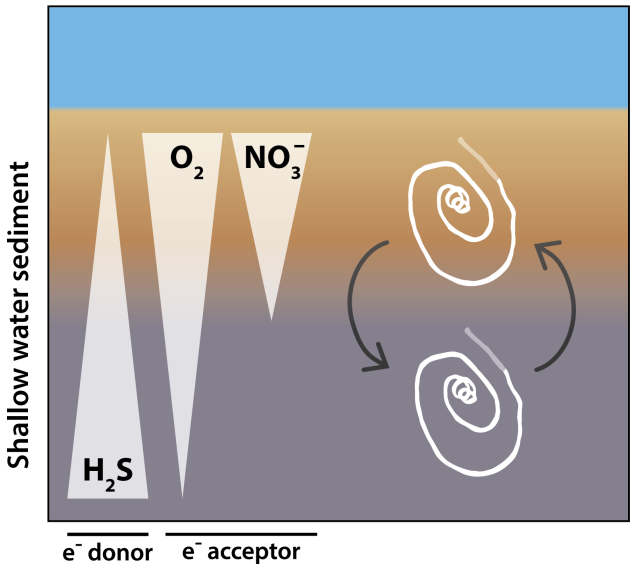

Figure 2. Sketch illustrating a stilbonematid nematode migrating between oxic and anoxic sediment layers. The migrations alternatively expose the symbionts to electron donors (e.g., sulfide) and acceptors (oxygen, nitrate). Adapted from Ott *et al.* 1991 [11].

Aims of this thesis

To study the metabolic adaptations of the stilbonematid symbiont *Cand.* Thiosymbion to the challenging ´black layer´, three synergistic approaches were used:

(1) ***Genome-based prediction of symbiont metabolic pathways (in silico* study).** We predicted the metabolic pathways of *Cand.* Thiosymbion oneisti by combining the available short- (Illumina; [147]) with long (Oxford Nanopore Technologies, ONT)-read sequencing technology. Frequently, short-read sequencing cannot resolve complex genomes containing long repeats. To reduce the high fragmentation of short-read sequencing, long reads obtained with ONT or PacBio can help scaffolding Illumina-based contigs by bridging the gaps [203]. Long read, single-strand sequencing on a handheld device was made possible by sensing the change in ionic current when a DNA-strand passes through a pore as envisioned by David Deamer in 1989 and developed by ONT [204]. Different assembly programs in terms of accuracy, time, and number of annotated features were compared. Finally, a comprehensive annotation pipeline was applied to provide i*n silico* information into the symbiont's metabolic potential since cultivation has not been successful yet. So far, direct genomic analyses of symbiotic entities have provided useful insights about uncultured marine symbionts [167,205–207] such as metabolic independencies, molecular regulation, and mechanisms for host recognition and physiological requirements/adaptations for living in oxygen-depleted, sulfidic habitats.

(2) Characterization of abiotic environmental conditions encountered by the symbionts (field study). We measured the physicochemical parameters to which Stilbonematinae are exposed in their natural habitat. Namely, the vertical distribution of two co-occurring stilbonematid nematodes - *Laxus oneistus* and *Stilbonema* sp. - was related to the concentration of oxygen, sulfide, ammonia, nitrate, nitrite, and dissolved organic carbon (DOC) in the pore water of sediment cores collected at Carrie Bow Cay, Belize, and Piran, Slovenia.

(3) Symbiont metabolic response to oxygen limitation (laboratory study). We exposed *Cand.* Thiosymbion to two types of conditions (oxic and hypoxic) likely encountered in their natural habitat. In this controlled, laboratory setup,

transcriptional levels of key metabolic genes of *Cand.* T. quadrati[4], the symbiont of the stilbonematid nematode *Catanema* sp., for sulfide oxidation, denitrification, CO_2 fixation, and nitrogen fixation were measured over a 72 h time period.

[4] The name will be proposed elsewhere (Weber, Pende *et al.*, in prep.)

Material & Methods

Nematode collection

Individuals of *Laxus oneistus* were collected on multiple field trips (2013-2016) at approx. 1 m depth from a shallow back-reef sand bar off Carrie Bow Cay (16.803058, -88.081783), Belize, by stirring the sediment in seawater and pouring the supernatant through a 212 µm pore-size sieve. The retained meiofauna was transferred into a Petri dish, and single nematodes were identified based on morphological features, picked by hand under a dissecting microscope, fixed in methanol and transported and stored at -20 °C.

For qPCR, *Catanema* sp. was collected by Jean-Marie Volland in 2016-2017 in Guadeloupe, France, off 'Îlet à Cochons' at approx. 0.5 m depth by stirring the sediment in seawater and pouring the supernatant through a 212 µm pore-size sieve. The retained meiofauna was transferred into a Petri dish, and single nematodes were identified based on morphological features, picked by hand under a dissecting microscope, fixed in methanol and transported and stored at -20 °C. In total, four sediment extractions was performed (Table 2).

Oxford Nanopore sequencing of symbiont *Cand.* Thiosymbion oneisti

DNA extraction

Approx. 800 *Laxus oneistus* individuals were incubated three times for 5 min each in TE-Buffer (10 mM Tris-HCl, 1 mM disodium EDTA, pH 8.0) to dissociate the ectosymbionts. Dissociated symbionts were collected by 10 min centrifugation at 7,000 x g and subsequent removal of the supernatant. DNA was extracted from this pellet using the Blood and Tissue Kit (Qiagen) according to the manufacturers' instructions. Namely, the pellet was resuspended in 180 µl Buffer ATL by carefully pipetting up and down, 20 µl proteinase K (600 mAU/ml) added and incubated at 56 °C overnight on a thermoblock at 300 rpm. To degrade RNA, 4 µl of Riboshredder RNase blend (1 U/µl, Epicentre) and incubated 5 min at 37 °C. After adding 200 µl buffer AL and 200 µl 100 % ethanol, the mixture was pipetted into a DNeasy Mini spin column and centrifuged for 1 min at 6,000 x g. The column was washed once with 500 µl buffer AW1, centrifuged for 1 min at 6,000 x g, then washed with 500 µl buffer AW2 and the column dried for 3 min at 20,000 x g and left open for 10 min for complete drying. For elution, 200 µl preheated (60 °C) buffer AE was added into the column, incubated for 5 min at room temperature and centrifuged for 1 min at 6,000 x g. For up concentrating, the eluant was mixed

with 100 µl DNA binding buffer of DNA Clean & Concentrator-5 (Zymo Research) and centrifuged through the provided column for 30 s at 12,000 x g, then washed once with 200 µl DNA wash buffer and centrifugation for 30 s at 12,000 x g and dried at room temperature for 10 min. DNA was eluted twice with 10 µl nuclease free water, incubated for 5 min and centrifuged for 30 s at 12,000 x g.

DNA concentration was measured on Qubit 2.0 Fluorometer (Life technologies) and purity measured using NanoDrop (ND-1000, PeqLab). DNA size was estimated on a 0.3 % agarose gel in-gel stained with ethidium bromide using 0.6 µg GeneRuler High Range DNA Ladder (0.1 µg/µl, Thermo Fisher Scientific).

ONT MinION library preparation

Oxford Nanopore Technologies' (ONT) 1D sequencing library was prepared according to the SQK-RAD002 Rapid Sequencing kit protocol. In short, 200 ng DNA was mixed with 2.5 µl Fragmentation Mix (ONT) in a final volume of 10 µl with nuclease-free water and incubated at 30 °C for 1 min followed by 75 °C for 1 min. 1 µl Rapid Adapter (ONT) was added to the tagmented DNA, gently mixed and 0.2 µl Blunt/TA Ligase Master Mix (New England Biolabs) added, mixed and incubated for 5 min at room temperature.

The sequencing mix was prepared with 11 µl of DNA library, 3.5 µl nuclease-free water, 35 µl Running Buffer with Fuel Mix (ONT) and 25.5 µl Library Loading Beads (ONT).

ONT MinION sequencing and base calling

To assess the number of active pores on a R9.4 flow cell (FLO-MIN106; ONT), platform QC was carried out according to the manufacturer's protocol by running the MinKNOWN platform QC (ONT). The sequencing mix was added to the flow cell R9.4 for a 24 h run.

Base calling of raw MinION reads was performed automatically with the Metrichor Agent v1.4.2 (ONT), the resulting data were retrieved in fast5 format and reads sorted into 'passed' and 'failed' automatically.

Read statistics

Read statistics and read quality plots were calculated using PRINSEQ-lite v0.20.4 [208]. Coverage was estimated with a genome size of 4.3 Mbp. Poretools v0.6.0 [209] and NanoOK

v1.31 [210] was used to calculate and visualize statistics based on the fast5 reads, GC content in % was calculated with a custom script and visualized with SPSS v24 (IBM).

De novo assemblies

Raw reads for one stilbonematid individual including its symbiont, obtained by Illumina HiSeq 2 x 100 bp paired-end sequencing as well as a genome draft assembled of these reads [147] were provided by Harald Gruber-Vodicka (referred to SPAdes Illumina).

For the raw reads, adapters were removed and filtered using bbduk (BBMap v37.22 [211]), with a minimum length of 36 and a minimum phred score of 2. Trimmed reads were mapped onto the genome draft using the bwa-mem algorithm (bwa v0.7.16a-r1181 [212]). Reads that did not map back were discarded.

Illumina-nanopore hybrid assembly (referred to as SPAdes hybrid) was done with SPAdes v3.11 [213] and MaSuRCA v3.2.2 [214] including only 'passed' reads obtained from nanopore. Spades-hybrid assembly was run according to [147] including the `--nanopore` option. Contigs lower than 200 bp and a coverage lower than 5X were filtered out with a custom python script. MaSuRCA-hybrid assembly was run with default parameters (referred to as MaSuRCA hybrid). Canu v1.5 [215] was run with `-genome=4.7m` and `correctedErrorRate=0.105`.

All contigs of the Illumina assembly were mapped to the hybrid assemblies using the bwa-mem algorithm (bwa v0.7.16a-r1181 [212]) and statistics calculated using samtools stats v 1.6 (using htslib 1.6).

Comparative analysis

Metrics

For SPAdes assembly, SPAdes-hybrid assembly filtered and unfiltered and MaSuRCA-hybrid assembly, statistics were calculated with GenomeTools v1.5.10 (N50, L50, longest contig, number of contigs, total contig length) [216]. CPU time for each assembler was measured using the `time` command as integrated into Linux. User time and system time was reported. Illustration of the contig sizes, cumulative length, and distribution of GC (%) was achieved with Quast v4.6.0 [217].

Ribosomal RNAs were predicted with RNAmmer v1.2 (specifying `bacteria` as a super kingdom) [218], tRNAs and tmRNAs with ARAGORN v1.2.37 [219], and completeness,

contamination, and strain heterogeneity checked with CheckM v1.0.7 [220] using a lineage-specific marker gene set. Average GC content was calculated with a custom python script. Non-coding RNAs (ncRNAs) were predicted using Infernal v1.1.2 [221] with Rfam database v12.2 [222], clustered regularly interspaced short palindromic repeats (CRISPR) found with MinCED v2.0 [223] and number of signal peptide cleavage sites with SignalP v4.1 [224] (after [207]).

Homopolymers (5-mers) were counted with a custom script and visualized with SPSS v24 (IBM).

Whole genome alignment

For aligning the SPAdes assembly against the SPAdes-hybrid filtered assembly and the SPAdes-hybrid filtered assembly against the MaSuRCA-hybrid assembly, MUMmer v3.23 [225] with the nucmer alignment script, suitable for aligning two draft genomes, was used. The alignment file was converted to contain coordinates and filtered in 'contigs with high similarity' with a nucleotide identity ≥ 99 % and a coverage of ≥ 90 %, and in 'contigs with medium similarity' with a nucleotide identity < 99 % and a coverage of < 90 %. Alignments were illustrated with Circos v0.69-6 [226].

Whole-genome based average nucleotide identity was calculated with ANIcalculator v1.0 [227]. Hierarchical clustering using euclidean distance and the UPGMA method and plotting of the heatmap was performed in R v3.3.2 [228] using `heatmap.2` of the gplots library [229].

Genome annotation

Contigs of the SPAdes-hybrid assembly were annotated using Prokka v1.12 (presets genetic code `11`, `gram neg`., kingdom `Bacteria`) [230]. Venn diagrams were generated with jvenn [231]. Assignment of the predicted proteins to Clusters of Orthologous Groups (COGs) was done using rpsblast of the NCBI package blast v2.6.0 [232,233] against NCBI's COG database (ftp://ftp.ncbi.nih.gov/pub/mmdb/cdd/little_endian/Cog_LE.tar.gz, as of March 28, 2017) with a 10^{-5} e-value cutoff and only the top hit retained, followed by manually assigning functional categories (ftp://ftp.ncbi.nih.gov/pub/COG/COG2014/data/fun2003-2014.tab) to COG numbers (after [234]). Protein family (Pfam) domains were assigned using hmmscan of the HMMER v3.1b2 [235] package against Pfam HMM v31.0 database [236] with a 10^{-5} e-value cutoff. Clans were assigned to Pfam domains with a custom script. CRISPR loci

were predicted with the CRISPR finder tool [237] only reporting confirmed CRISPRs with more than 3 spacers. Proteins with signal peptides were predicted using SignalP 4.1 Server [224], PECAS (genomics.cicbiogune.es/PECAS/index.php) and Phobius v1.01 [238], and reported if it was predicted with at least two of the methods. Proteins containing transmembrane helices were identified with TMHMM Server v2.0 [239]. For screening of carbohydrate-active domains, proteins were compared using hmmscan against the dbCAN database v6 [240] containing profile hidden Markov models (HMM). Overlapping hits were discarded using the micropan package [241] in R v3.3.2, and the hit with the lowest e-value retained. After filtering, an e-value cutoff of 10^{-5} was applied for alignments longer than 80 amino acids and an e-value cutoff of 10^{-3} for alignments shorter than 80 amino acids. Localization of predicted proteins was done by PSORTb v3.0 [242]. RepSeek [243] has been used to detect approximate repeats. Repeats, non-coding genes, and protein-coding genes (found by Prokka) were mapped back onto the draft genome using blastn and tblastn of the NCBI package blast v2.6.0 [232,233] and visualized with Circos v0.69-6 [226]. The same pipeline was applied to *Escherichia coli* K12 substr. MG1655 (RefSeq acc. no. NC_000913.3) and *Shigella dysenteriae* Sd197 (RefSeq acc. no. NC_007606.1). Pathways were reconstructed by assigning Kyoto Encyclopedia of Genes and Genomes (KEGG) K-numbers [244] to the protein sequences using BlastKOALA Server v2.1 [245]. *Nif* gene cluster was plotted using DNAfeaturesViewer (Edinburgh Genome Foundry, unpubl.).

Habitat characterization of *Laxus oneistus* and *Stilbonema* sp.

Sampling of sediment cores

Sediment cores were collected in July 2017 in a Caribbean Sea shallow (~0.5 m depth) sand bar off Carrie Bow Cay, Belize (16.803058, -88.081783) and in September 2017 in a Mediterranean Sea sand bar off the coast of Piran, Slovenia (45.514848, 13.571020). Plexiglas cores (60 mm inner diameter) were forced into the sediment down to a depth of 30 cm (for Carrie Bow Cay) and 10 cm (for Piran), in total 15 cores for Carrie Bow Cay and seven cores for Piran were retrieved. For the Carrie Bow Cay cores, sediment cores are grouped into cores away from seagrass beds (approx. 1 m from *Thalassia* sp. beds [246]) and cores in proximity to seagrass (at the sand - *Thaliassia* sp. bed interface). Corers were closed with rubber lids and brought immediately to the laboratory without further disturbance. Pore water was extracted in 6 cm (for Carrie Bow Cay cores) and 3 cm (for Piran cores) intervals using 0.15 µm pore-

size Rhizon MOM samplers (Rhizosphere) within 1 h (Figure 3). For each measurement point, 6 ml (Carrie Bow Cay cores) and 9 ml (Piran cores) pore water was taken, starting from the top hole. Oxygen (O_2) was measured using Fibox 4 trace (PreSens Precision Sensing) with a flow-through cell FTC-PSt3 (PreSens Precision Sensing). The sample for sulfide measurement was immediately analyzed, the sample for nitrate measurement stored was at -80 °C. For assessing the nematode distribution, animals were extracted after the sampling of pore water by subdividing the core in 6 cm fractions (for Carrie bow Cay) and 3 cm (for Piran), stirring the sediment in seawater and pouring the supernatant through a 212 µm pore-size sieve for three times. Nematodes were identified and counted under a dissecting microscope. The volume of extracted sediment was 169.64 cm^3 (6 cm core diameter, 6 cm length).

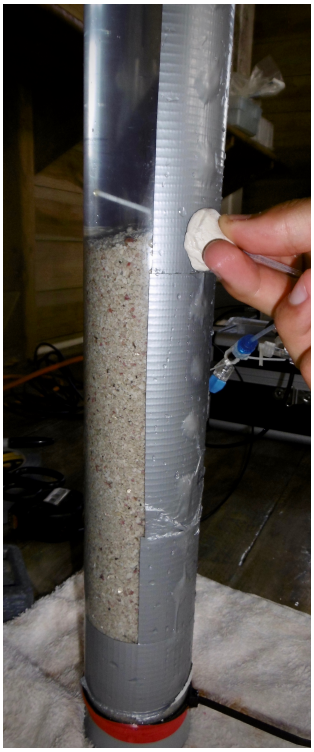

Figure 3. Image showing the sampling of pore water from sediment cores. The Plexiglas tube was sealed with waterproof tape before forcing it into the sediment. Pore water was taken with Rhizon MOM samplers (Rhizosphere) connected to a syringe. For oxygen measurements, a flow-through optical oxygen sensor (PreSense Precision Sensing) was connected in between.

Pore water chemistry measurements

Sulfide (S_2^-, HS^-, H_2S) was measured in triplicates using a quantitative colorimetric assay after Cline (1969) [247] that is based on the conversion of total sulfide into methylene blue. In

short, 670 µl of a 2 % zinc acetate solution was mixed with 335 µl sample and subsequently 335 µl 0.5 % N,N-Dimethyl-p-phenylenediamine and 17 µl 10 % ferrous ammonium sulfate added and incubated for 30 min in the dark. Blank was superficial seawater instead of the sample. After measuring the absorbance at 670 nm, the concentration was calculated from a standard curve. Nitrate (NO_3^-) and nitrite (NO_2^-) concentrations were determined according to the Griess method [248] with Vanadium(III) chloride [249]. For NO_2^- measurements, 900 µl sample was mixed with 90 µl Griess reagent (50:50 2 % sulphanilamide : 0.2 % N-(1-naphtyl)-ethylenediamine dihydrochloride) in triplicates and left 15 min at 30 °C in the dark before measuring the absorbance at 540 nm in a Tecan Sunrise microplate reader. NO_3^- was measured in triplicates by adding 350 µl Griess reagent and 350 µl 8.3 % Vanadium(III) chloride to 350 µl sample, incubated for 15 min at 30 °C and measuring absorbance at 540 nm in a Tecan Sunrise microplate reader. Ammonium (NH_4^+) was measured according to [250] by mixing 1 ml of sample with 40 µl phenol-nitroprusside (3.5 % phenol & 0.04 % sodium nitroprusside) and alkaline hypochlorite (28 % $Na_3C_6H_5O_7$, 2.2 % NaOH, 4 % NaClO), incubating for 6 h in the dark at room temperature and measuring the absorbance at 630 nm in a Tecan Sunrise microplate reader. For all three measurements, a standard curve using $NaNO_2$, KNO_3, and NH_4Cl, respectively, was prepared fresh for each measurement with artificial seawater [251] and measured in triplicates. As blank artificial seawater was used instead of the sample. For the Piran cores, sample and reactant volume were increased proportionally for measuring on a spectrophotometer DR1900 (Hach). Concentration of dissolved organic carbon (DOC) was determined by Andreas Maier (Department of Geography and Regional Research, University Vienna).

The total number of recorded measurements (O_2, total sulfide, NH_4^+, NO_2^-, NO_3^-, DOC, the abundance of *Stilbonema* sp. and *Laxus oneistus*) is given in Table 1. For the Piran cores, measurements (oxygen, total sulfide, ammonium, nitrite, nitrate) were taken for all 7 cores.

Approx. water holding capacity was determined by first slicing the cores at 5 cm intervals and drying the sediment at 80 °C for 24 h, then adding seawater until saturation was reached.

Table 1. Number of measurements taken away from and in proximity to seagrass beds in Carrie Bow Cay, Belize.

Location	Depth	O_2	Sulfide	NH_4^+	NO_2^-	NO_3^-	DOC	Abundance	
								Stilbonema sp.	*Laxus oneistus*
away from seagrass	0	9	9	4	4	4	5	10	10
	-6	9	9	4	4	4	5	10	10
	-12	9	9	4	4	4	5	10	10
	-18	9	9	4	4	4	5	10	10
	-24	9	9	4	4	4	5	10	10
	-31	5	5	4	4	4	4	3	3
in proximity to seagrass	0	5	5	1	1	1	5	5	5
	-6	5	5	1	1	1	5	5	5
	-12	3	3	1	1	1	3	5	5
	-18	5	5	1	1	1	5	5	5
	-24	5	5	1	1	1	5	5	5

Statistical analysis

For the Carrie Bow Cay cores, an unpaired two-tailed Welch's test (for unequal variances) was performed in Microsoft Excel 2016 v15 to test a significant difference of measurement points with 1 cm distance. If the result was insignificant ($p > 0.05$), the measurement points were shifted to 0, 6, 12, 18, 25, 31 cm final depth. Plots for concentrations of the chemical compounds were generated with Microsoft Excel 2016 v15.

The abundance and distribution of *Laxus* oneistus and *Stilbonema* sp. across the sediment layers were expressed in percentage and calculated relative to the total abundance of nematodes found in one sediment core.

SPSS v24 (IBM) was used for statistical testing and for generating the bar plots. A Kolmogorov-Smirnov test was used to inspect the sample distribution and equality of variances checked with Levene's test ($\alpha = 0.05$). An independent two-sample Student's t-test was used if the variable distribution was normally distributed and variances were equal. If the variable was not normally distributed, a Kruskal-Wallis H-test was used, if variances were unequal, a Welch's t-test was used. If applicable, Dunn-Bonferroni *post hoc* multiple comparison test was used. A correlation of the distribution of *Laxus oneistus* and *Stilbonema* sp. was calculated using Spearman's rho (no normal distribution could be assumed according to one-sample Kolmogorov-Smirnoff test). 3D scatter plots were generated in R v3.3.2 [228] using the scatterplot3D library [252].

Quantitative PCR

RNA extraction, gDNA digestion, cDNA synthesis (by reverse transcription PCR), quality control and qPCR were carried out by the author and by Gabriela Paredes following the same protocol (see below).

Preparation of standard plasmids

Table 2. Overview of sample list, duration of incubation, and from which sediment the nematodes originated.

Sample	Incubation		Sediment extraction
1	oxic	24 h	A
2	oxic	24 h	A
3	oxic	24 h	A
4	oxic	24 h	A
5	hypoxic	24 h	B
6	hypoxic	24 h	B
7	hypoxic	24 h	B
8	hypoxic	24 h	B
9	oxic	48 h	C
10	oxic	48 h	C
11	oxic	48 h	C
12	oxic	48 h	C
13	hypoxic	48 h	C
14	hypoxic	48 h	C
15	hypoxic	48 h	C
16	hypoxic	48 h	C
17	oxic	72 h	D
18	oxic	72 h	D
19	oxic	72 h	D
21	hypoxic	72 h	D
22	hypoxic	72 h	D
23	hypoxic	72 h	D

Primer design

Sequences for *aprA*, *dsrA*, *norB*, *cbbL*, *nifH*, *rpoB,* and 16*S* rDNA were retrieved from the genome draft '*Cand.* Thiosymbion Catanema 'bump' GU16 SB19' annotated by the RAST server [253]. To ensure a correct annotation, sequences were compared with the NCBI non-redundant protein sequences database (nr-protein) using blastx of the NCBI package blast v2.6.0 [232,233]. Primers were designed by using the web-based tool Primer3Plus (www.bioinformatics.nl/primer3plus) [254], modifying the settings as follows: product size ranges: 150-250 bp, primer size 18-27 bp (opt. 20 bp), primer melting temperature (T_m) 58-

60 °C (opt. 59 °C), 40-60 % primer GC, max. T_m difference 2 °C, 1 GC clam. Suggested primers were evaluated based on the formation of hairpin structures, homo-dimers, and hetero-dimers as calculated by OligoAnalyzer 3.1 (https://eu.idtdna.com/calc/analyzer). Specificity of primers was assessed by blasting the primer sequences against the genome draft using blastn of the NCBI package blast v2.6.0 [232,233]. Synthesis of primers (desalted, genomics synthesis scale; Table 3) was done by Microsynth AG.

Table 3. Primer sets used for the preparation of standard plasmids and quantitative PCR.

Target gene	Primer name	Primer sequence (5'-3')	GC (%)	T_m (°C)	Amplicon length
aprA	aprA_qCat_F	AGAACTACCACCGCATCCTC	55	59.2	177
	aprA_qCat_R	TGAAGCAGGTCCACTTTTTG	45	58.9	
dsrA	dsrA_qLo_F	TCCTACTCAGGCATTGACCC	55	58.9	214
	dsrA_qLo_R	GGACTCGTAGTCTTCCTCGG	55	59.2	
norB	norB_qCat_F	TGCTGGAGATGTGGAGTTTC	50	58.8	166
	norB_qCat_R	TCACGCAGCCAGTAGAAGAG	55	59.3	
cbbL	cbbL_qCat_F	GACTTACTGGATGCCCGATT	50	59.0	239
	cbbL_qCat_R	CGACGAAGGCGTAGTAACAC	55	58.5	
nifH	nifH_qCat_F	CCTACGACGAGGACCTGAAC	60	59.7	165
	nifH_qCat_R	CGATCCCCTTGGAGATATTG	50	59.3	
rpoB	rpoB_qCat_F	GCCTACGGTTCCTCCTACAC	60	58.7	177
	rpoB_qCat_R	CTCCACATTGATACCCAACG	50	58.8	
16*S*	16S_qCat_F	TAGCGGTGAAATGCGTAGAG	50	54.7	76
	16S_qCat_R	CCTCAGCGTCAGTATTGGTCC	57.1	57.5	

PCR amplification

Methanol-fixed nematodes were washed 3 times for 5 min each in 1X PBS (136.9 mM NaCl, 2.7 mM KCl, 10.0 mM Na_2HPO_4, 2.0 mM KH_2PO_4, pH 7.6) for hydration and removal of methanol. Single nematodes were sonicated 45 s in 6 µl 1X PBS for dissociation of bacterial ectosymbionts. PCR reactions were set up with nuclease-free water, containing 1X Green GoTaq Reaction Buffer (contains 1.5 mM $MgCl_2$; Promega), 0.2 µM forward Primer, 0.2 µM reverse primer, 0.2 mM dNTP-Mix (Thermo Fisher Scientific), 0.025 U GoTaq G2 DNA polymerase (Promega) and 2 µl of the bacterial solution was used as a template in 25 µl final volume. The negative control contained 2 µl nuclease-free water instead of the bacterial solution. Hot start PCR conditions were as follows: 95 °C 5 min, followed by 30 cycles at 95 °C 1 min, 55 °C for 1 min, 72 °C for 30 s, and a final elongation step for 6 min at 72 °C. For evaluating the PCR products, amplicons were visualized by gel electrophoresis on a 1 – 1.5 %

agarose in 1X TAE Buffer (40 mM TRIS, 20 mM acetic acid, 1 mM EDTA, pH 7.6) with in-gel stain ethidium bromide. The electrophoresis was run for 40 min at 100 V and an image of the gel taken with Gel Dock XR+ (Bio-Rad). If the amplicon size and the primer specificity were adequate (i.e. no primer dimers), DNA was purified using Monarch PCR & DNA Cleanup Kit (New England Biolabs) according to manufacturer's protocol. Purity and approx. quantity was assessed on NanoDrop (ND-1000, PeqLab).

Cloning, colony PCR and sequencing

Purified amplicons were ligated using either pGEM-T Easy Vector System (Promega) or CloneJET PCR cloning kit (Thermo Fisher Scientific) according to the manufacturers' protocols. For transformation, TOP10 *E. coli* competent cells (Thermo Fisher Scientific) were thawed for 30 min on ice. 1 µl ligation mix was incubated with 10 µl Top10 cells for 15 min on ice. Heat shock was performed for 45 s at 42 °C and cooling down for 5 min on ice. The entire mix was incubated at 37 °C for 1h at 150 rpm with 200 µl SOC (2 % tryptone, 0.5 % yeast extract, 10 mM NaCl, 2.5 mM KCl, 10 mM $MgCl_2$, 10 mM $MgSO_4$, 20 mM glucose), plated on LB-agar plates containing 100 mg/L ampicillin, 0.1 mM IPTG and 60 mg/L X-Gal, and incubated at 37 °C overnight. White clones were picked and used as a template in PCR. Hot start PCR conditions were as follows: 94 °C 5 min, followed by 31 cycles at 94 °C 15 s, 55 °C for 20 s, 72 °C for 1.5 min, and a final elongation step for 10 min at 72 °C. Amplicons were visualized by gel electrophoresis as stated above, purified using Monarch PCR & DNA Cleanup Kit (New England Biolabs) and the purity and approx. quantity were checked on NanoDrop (ND-1000, PeqLab). Amplicons were sent to Eurofins Genomics for sequencing with primer pairs M13F/R (for pGEM-T Easy Vector System) or PJET12_blunt_FWD/REV (for CloneJET PCR cloning kit) (Table 4).

Table 4. Sequencing primers used for sequencing.

Primer name	Primer sequence (5'-3')
M13F	GTTTTCCCAGTCACGAC
M13R	CAGGAAACAGCTATGAC
pJET12_blunt_FWD	CGACTCACTATAGGGAGAGCGGC
pJET12_blunt_REV	AAGAACATCGATTTTCCATGGCAG

Sequences were checked with CodonCode Aligner 3.7.1 software (CodonCode Corporation) and blasted against the genome draft using blastn of the NCBI package blast v2.6.0 [232,233]. Only cloned sequences which were full length and had > 99 % nucleotide identity were further processed.

Clone inoculation and restriction digest

Clones that passed the sequence control were inoculated in 10 ml liquid LB medium containing 100 mg/L ampicillin at 37 °C overnight. Plasmid DNA was isolated using PureYield Plasmid Miniprep System (Promega). Plasmids were linearized with the restriction enzymes Pst1-HF (for *aprA*, *dsrA*, *cbbL*, *nifH*, *rpoB,* 16*S*; New England Biolabs) or HindIII-HF (for *norB*; New England Biolabs) in 1X CutSmart Buffer (New England Biolabs). DNA was separated on a 0.8 % agarose gel in 1X TAE buffer. Linearized plasmids with the correct length were cut out from the gel and purified using Monarch DNA Gel Extraction Kit (New England Biolabs), and sent again for sequencing with the respective primers, applying the same sequence quality cutoffs as above. The concentration of plasmid DNA was assessed on Qubit 2.0 Fluorometer (Life technologies).

Gradient PCR

In order to determine the optimal annealing temperature of the targeted genes for quantitative realtime PCR (qPCR), a PCR reaction was set up using linearized plasmid DNA as a template (protocol described above). PCR conditions were as follows: 95 °C 5 min, followed by 30 cycles at 95 °C 1 min, 55 °C + 0.5 °C per lane for 1 min, 72 °C for 30 s, and a final elongation step for 6 min at 72 °C. Amplicons were visualized on a 1 % agarose gel.

Oxic and hypoxic incubations

Incubations were set up by Jean-Marie Volland. Individuals of *Catanema* sp. were collected in May and August 2017 as described above. Batches of 50 *Catanema* sp. were incubated for 24 h, 48 h and 72 h in oxic, 0.2 µm filtered natural seawater in the dark without agitation. Vials were kept open during the incubations. For the hypoxic incubations, an inflatable, oxygen tight polyethylene glove box was used to create an artificial N_2 atmosphere. To deoxygenate, 0.2 µm filtered, natural seawater, was bubbled for 30 min with N_2 gas before adding 50 *Catanema* sp. for 24 h, 48 h, and 72 h. Vials were closed and kept in the dark inside

the glove box. Four biological replicates were carried out for the 24 h and 48 h incubation and three biological replicates for the 72 h incubation. Oxygen was measured at the beginning and at the end of each incubation using Fibox 3 (PreSens Precision Sensing GmbH) and NH_4^+, NO_2^-, NO_3^-, pH and salinity at the beginning. At the end of each incubation, worms were sucked out with plastic single-use pipettes and directly transferred into fresh RNAlater (13.3 mM EDTA, 16.3 mM sodium citrate, 2 M ammonium sulfate, pH 5.2) and RNAlater renewed once. Nematodes were stored in fresh RNAlater at -80 °C prior to shipping on dry ice.

Isolation of host & symbiont RNA

Nematodes in RNAlater were centrifuged for 10 min at 16,000 x g to collect the symbionts. RNAlater was removed and nematodes washed in 400 µl 1X PBS to dilute residual RNAlater. The sample was again centrifuged for 10 min at maximum speed before removing all liquid and adding 1 ml 4 °C cool TRIzol (Invitrogen). The mixture was vortexed and transferred to a bead beating tube Lysing Matrix E (MP Biomedicals). Bead beating was done in a FastPrep-24 (MP Biomedical) for 2 times 30 s with a 30 s break in between (5.5 m/s speed), and the lysate incubated for 5 min at room temperature. 200 µl chloroform was added and vortexed 2 min to better remove protein, and again 3 min incubated at room temperature. The mixture was centrifuged at 12,000 x g for 15 min at 4 °C. The upper aqueous phase was carefully transferred into a new tube and 1 volume of 100 % ethanol added and mixed. The sample was then transferred to RNA Clean & Concentrator-25 column (Zymo Research) and the manufacturer's protocol followed. All centrifugation steps were carried out at 10,000 x g and the final elution done in 30 µl nuclease-free water.

Purity was assessed on NanoDrop (ND-1000, PeqLab), quantity on Qubit 2.0 Fluorometer (Life technologies) and the degree of degradation checked on the 2100 Bioanalyzer using the RNA 6000 Pico Kit (Agilent) and the Eukaryote Total RNA Pico assay.

Genomic DNA digestion and cDNA synthesis

Total RNA was mixed with 1X RQ1 DNase Reaction Buffer (Promega) and 1 U of RQ1 DNase (Promega) and incubated for 60 min at 37 °C. To verify the absence of DNA contamination, a PCR targeting *rpoB* with specific primer pairs rpoB_qCat_F/R was carried out and the amplicon visualized on a 2 % agarose gel (as above) aiming at highly intense bands.

If no band was visible, DNase was inactivated for 10 min at 65 °C in presence of 3 µl RQ1 DNase Stop Solution (Promega; containing 20 mM EGTA, pH 8.0).

For first strand cDNA synthesis, the reaction mix was incubated with 1 mM dNTP-Mix (Thermo Fisher Scientific), 60 µM random hexamer primers (Thermo Fisher Scientific) and nuclease-free water in a final volume of 30 µl at 65 °C for 5 min. Nuclease-free water, 1X ProtoScript II Buffer (Promega), 10 mM DTT (Promega) and 10 U ProtoScript II RT (Promega) was mixed in a final volume of 50 µl and incubated for 5 min at 25 °C, 1 h at 42 °C and 20 min at 65 °C. Single-stranded DNA yield was assessed on a Quibit 2.0 Fluorometer (Thermo Fisher Scientific).

Quantitative PCR cycling conditions

Standard plasmid DNA dilution series ranging from 10^8 to 10^1 ng/µl DNA was prepared with nuclease-free water. The reaction mix for quantitative PCR (qPCR) was prepared as follows: 1X GoTaq qPCR Master Mix (Promega), 0.4 µM of the respective forward and reverse qPCR primers (see Table 3), 2.5 ng cDNA as PCR template in a final volume of 20 µl with nuclease-free water. The negative control contained nuclease-free water instead of cDNA. Standards were carried out in technical duplicates, samples in technical triplicates. The run protocol included 2 min at 95 °C, followed by 40 cycles of 15 s at 95 °C and 1 min at 60 °C with measurement of fluorescence at the end. The subsequent melting curve analysis at the end of the 40 cycles consisted of 15 s at 95 °C, 15 s at 55 °C, continuous fluorescence measurement from 55 °C to 95 °C (temperature increased in regular increments over 20 min), and 15 s at 95 °C. All reactions were carried out on a Mastercycler ep gradient S realplex^2 (Eppendorf).

qPCR amplicons were purified using Monarch PCR & DNA Cleanup Kit (New England Biolabs) according to manufacturer's protocol and sent for sequencing at Eurofins Genomics. Sequences were checked with CodonCode Aligner 3.7.1 software (CodonCode Corporation) and blasted against the genome draft using blastn of the NCBI package blast v2.6.0 [232,233].

Data analysis of quantitative PCR

Relative gene expression was calculated according to [255]. In brief, for each biological replicate an average C_q of all technical replicates was calculated, followed by calculating pairwise $\Delta\Delta C_q$ ratios taking into consideration the efficiency of the qPCR. The number of biological replicates is given in Table 5. All the data were substracted from the respective oxic

incubation ('control') and normalized to *rpoB* 24 h oxic incubation as a reference gene. The reference gene was identified by the lowest standard deviation (SD) over all experimental treatments for each transcript compared.

Table 5. Number of biological replicates used for qPCR data analysis.

	24 h		**48 h**		**72 h**	
	oxic	**hypoxic**	**oxic**	**hypoxic**	**oxic**	**hypoxic**
aprA	4	3	2	4	3	3
dsrA	3	4	4	4	3	3
norB	4	4	4	4	3	3
cbbL	4	4	4	4	3	3
nifH	4	4	3	4	3	3
rpoB	4	3	4	4	3	3
16*S*	4	4	4	4	-	-

One technical replicate of the biological replicate #2/*dsrA* 24 h was removed from further analysis because of a pipetting error, as well as pairwise $\Delta\Delta C_q$ values beyond pairwise $\Delta\Delta C_q$ mean ± 2 standard deviations (Table 6) in order to reduce the high biological variation. The average of pairwise $\Delta\Delta C_q$ ratios (relative mRNA expression values) and the standard error (SE) was plotted in SPSS v24 (IBM), a Kolmogorov-Smirnov test used for testing the variable $\Delta\Delta C_q$ against normal distribution. A Kruskal-Wallis test was calculated with Dunn's test as *post hoc* correction.

Table 6. Number of outliers excluded from data analysis. Outliers were detected by using a threshold of 2 standard deviations around the mean of pairwise $\Delta\Delta C_q$.

Gene	Incubation	Outliers excluded
aprA	24 h	1
	48 h	1
	72 h	1
dsrA	24 h	1
	48 h	1
	72 h	1
norB	24 h	2
	48 h	1
	72 h	1
cbbL	24 h	1
	48 h	0
	72 h	1
nifH	24 h	1
	48 h	1
	72 h	0

Results

Oxford Nanopore sequencing of symbiont *Cand.* Thiosymbion oneisti

Illumina HiSeq 2 x 100 bp paired-end raw reads of a *Laxus oneistus*/*Cand.* Thiosymbion oneisti single worm metagenome and an assembly of the symbiont were provided by Harald Gruber-Vodicka. For long-read sequencing with ONT, genomic DNA extraction and subsequent purification yielded in 52.4 µg/µl DNA (1,048 ng) with a purity of 1.38 $A_{260/280}$ ratio. As determined by agarose gel electrophoresis, the majority of fragments were about 30 kbp.

Read statistics

With ONT, a total of 1,602 reads with a total size of 5,250,548 bp was generated with a mean phred score of 5, being equivalent to 1 in 30 wrong base calls. The basecaller automatically classifies reads into 'passed' and 'failed' reads, depending whether base calling was successful and are high-quality reads. Taking only the 'passed' reads, the longest read was 121,466 bp (mean = 3277.50 bp, standard deviation = 6603.54 bp; Table 7, Figure 5A). Based on the SPAdes-assembled draft genome, the coverage produced by ONT sequencing was 1.22X. The mean GC content was 52.62 % (Figure 5B).

By mapping the trimmed Illumina reads back against the SPAdes draft genome, 7,280,712 reads of symbiont origin were obtained (19.60 %), with an average length of 99.98 bp and an average phred score of 36 (99.975 % base call accuracy; Figure 4). The symbiont genome was 169X covered.

Table 7. Statistics of short-read Illumina data after trimming and long-read ONT data.

	Trimmed & mapped Illumina reads	ONT reads
Number of reads	7,280,712	1,602
Length (mean ± SD)	99.98 ± 1.12 nt	3277.50 ± 6603.54 nt
Maximum length	100 nt	121,466 nt
Minimum length	30 nt	23 nt
Coverage	169X	1.22X

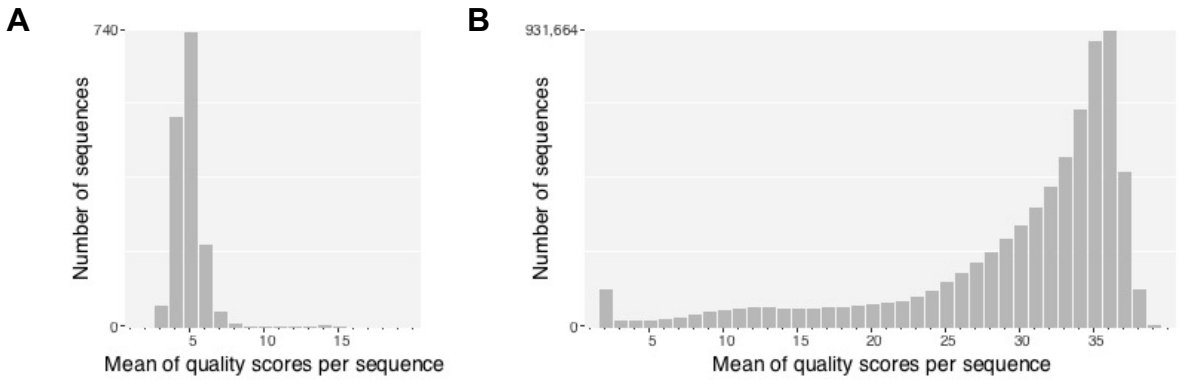

Figure 4. ONT reads and Illumina quality histogram. Mean quality scores (phred score) for (A) ONT reads and (B) Illumina reads after trimming. ONT sequencing resulted in reads with a mean phred score of 5, being equivalent to a 32 % error rate. Illumina HiSeq reads passed ONT read quality by far with a mean phred score of 36 (error rate 0.025 %).

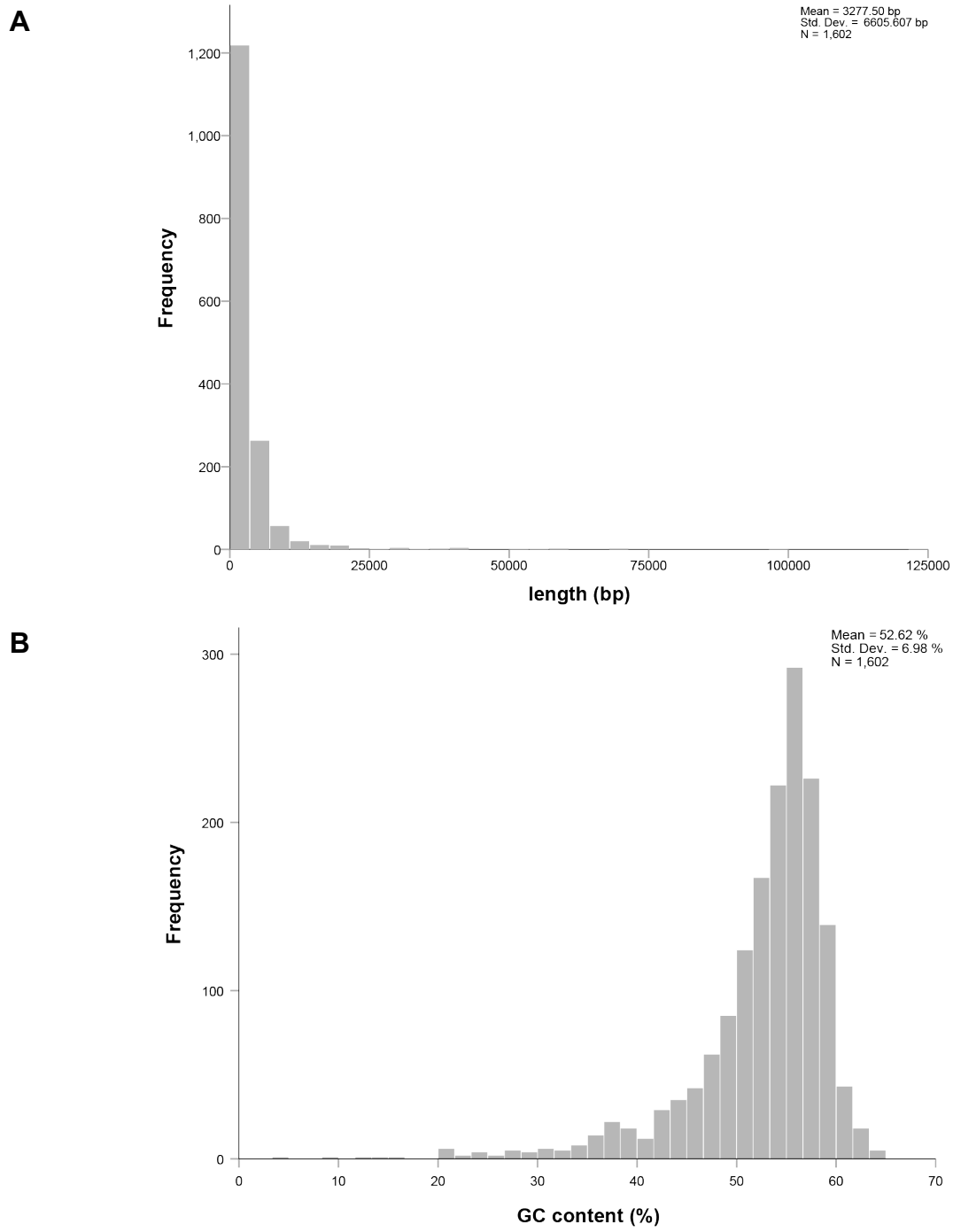

Figure 5. Distribution of read length (A) and GC content (B) of ONT reads. (A) The 1,602 reads ONT reads had a mean length of 3,277.5 bp, ranging from 23 to 121,466 bp. (B) Distribution of the GC content resulted in one clear maximum at 52.62 %, which indicates that only one organism was sequenced.

De novo assemblies

Tree separate assemblies were performed: one non-hybrid assembly (canu) using 'passed' ONT reads, and two hybrid assemblies (MaSuRCA, SPAdes) with the trimmed and mapped Illumina reads. Canu failed at the correction-trimming step and could therefore not be

pursued. The MaSuRCA Illumina-ONT hybrid assembly was made of 2,202 contigs with an N50 of 2,300 and a total contig length of 3.5 Mbp (Table 8). The hybrid assembly with SPAdes yielded the highest N50 value (27,060 bp, longest contig 96,688 bp) and the lowest number of contigs 401 (Figure 6, Figure 7A) after filtering out 446 low coverage, short contigs (coverage < 5X, length > 200 bp). Total contig length is 4.37 Mbp. The Illumina assembly were mapped to the hybrid assemblies. For the Illumina-ONT-hybrid assembly, 100 % of the Illumina contigs mapped, whereas only 86 % mapped to the MaSuRCA hybrid assembly. Three protein-coding genes were removed from the assembly by the filtering step, namely two hypothetical proteins and the Zinc transporter ZitB. MaSuRCA hybrid assembly was substantially faster than SPAdes hybrid assembly (37 min and 145 min user time, respectively). The average GC content was 58.5 % for the SPAdes hybrid assembly. As for the GC content, Figure 5A shows a Gaussian curve indicating the absence of contaminants [256]. In the cumulative length plot (Figure 5B) ordered from largest to smallest, the SPAdes hybrid assembly reached the plateau in a smaller number of contigs than the other two, representing many large contigs and a relatively low number of short contigs. GC content for SP

Ades hybrid and SPAdes Illumina assembly was similar, but was generally lower for the MaSuRCA hybrid assembly (Figure 7B).

5*S*, 16*S* and 23*S* rRNA genes were detected in all assemblies (16*S* and 23*S* only partially), but the highest number of tRNA coding genes was detected in SPAdes hybrid assembly (53 tRNAs; Table 8). Additionally, CheckM reported the highest completeness for SPAdes Illumina assembly and SPAdes hybrid assembly (94.28 %) and low contamination (0.8 %), whereas the MaSuRCA hybrid assembly was highly contaminated (7.06 %) and had a high strain heterogeneity (68.29 %). The two SPAdes assemblies were therefore high-quality drafts [257]. The filtering step did not decrease the number of marker genes present (Table 9). Using a total number of 581 gammaproteobacterial marker genes, 63 were only found in the SPAdes Illumina and SPAdes hybrid assembly (Figure 8).

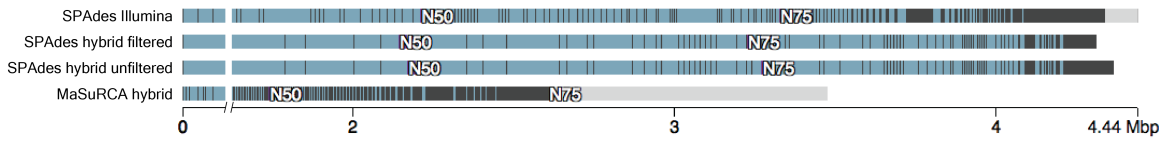

Figure 6. Contig overview of the assemblies SPAdes Illumina, SPAdes hybrid unfiltered and filtered, and MaSuRCA hybrid. The N50 values for the first three were comparable, only the MaSuRCA hybrid assembly yielded a lower N50 value. Grey regions indicate very short contigs (< 170 bp).

Table 8. Comparison of provided SPAdes Illumina assembly with MaSuRCA hybrid, SPAdes hybrid *de novo* assemblies. The filtering step for the SPAdes hybrid assembly removed 446 short (< 200 bp) contigs. Assembly metrics include N50 (sequence length at 50 % of the total genome), L50 (number of contigs that produces the N50 value), largest contig length ('longest contig'), number of contigs, total contig length. Run time was reported as user time (time spent outside the kernel within the process) and system time (amount of CPU time; all assemblies have been run on the same number of CPU). Three CRISPR for the SPAdes Illumina were predicted, consisting of 3, 3 and 4 spaces and only one CRISPR for the SPAdes hybrid assembly, consisting of 10 spacers. Thus, CRISPR was not well resolved in the SPAdes Illumina assembly.

Item		MaSuRCA hybrid	SPAdes Illumina	SPAdes hybrid filtered	SPAdes hybrid unfiltered
assembly metrics	N50 (bp)	2,300	11,049	27,060	27,005
	L50	488	117	48	49
	longest contig (bp)	10,156	47,141	96,688	96,688
	number of contigs	2,202	2,026	401	847
	total contig length (bp)	3,476,084	4,440,236	4,312,079	4,365,553
Run time	user time	37 min	n.d.	145 min	n.d.
	system time	1 min	n.d.	13 min	n.d.
number of rRNAs [a]	5*S*	1	1	1	1
	16*S*	1	1	1	1
	23*S*	1	1	1	1
number of tRNAs		27	47	53	53
number of tmRNAs		1	1	1	1
GC %		59.3	58.7	58.7	58.5
Number coding sequences		3,604	3,918	3,966	3,970
Number of ncRNAs		24	43	35	35
Number of CRISPR		0	3	1	1
Number of signal peptide cleavage sites		85	164	171	171

[a] partial and full sequences
n.d. not determined

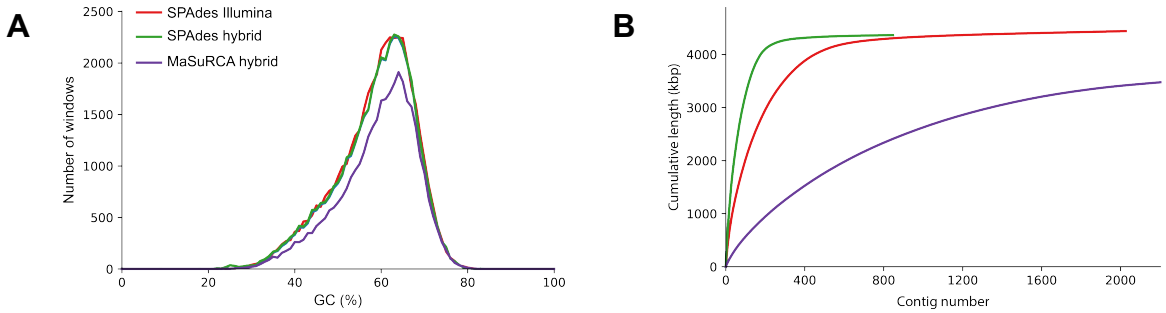

Figure 7. GC content in the contigs calculated in non-overlapping 100 bp windows (A) and cumulative length plots (B) for the assemblies SPAdes Illumina, SPAdes hybrid and MaSuRCA hybrid.

Table 9. Presence or absence of 581 gammaproteobacterial marker genes as determined by CheckM. % completeness indicates presence/absence of marker genes, taking into account a possible co-localization; % contamination indicates whether a marker gene was present more than once in the assembly, and strain heterogeneity whether multiple copies were found with a > 80 % amino acid identity.

	marker gene present						
Assembly	**0x**	**1x**	**2x**	**3x**	**Complete-ness**	**Contami-nation**	**Strain heterogeneity**
MaSuRCA hybrid	85	457	38	1	82.44 %	7.06 %	68.29 %
SPAdes Illumina	22	555	4	0	94.28 %	0.80 %	0.00 %
SPAdes hybrid filtered	22	555	4	0	94.28 %	0.80 %	0.00 %
SPAdes hybrid unfiltered	22	555	4	0	94.28 %	0.80 %	0.00 %

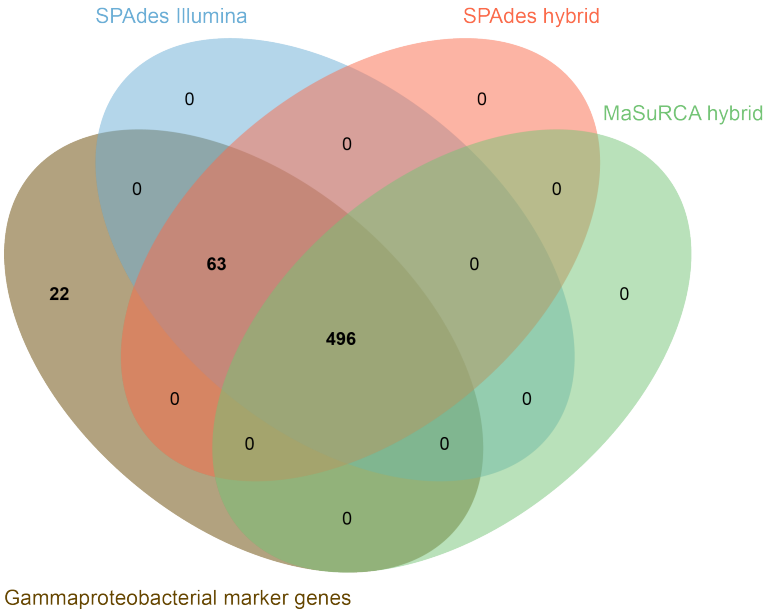

Figure 8. Venn diagram of number of putative single copy genes identified by CheckM.

Of the 581 gammaproteobacterial marker genes, 22 were absent in each assembly (Figure 8). The MaSuRCA assembly was not resolving the genome sequence well, as 39 genes were found more than once, resulting in a strain heterogeneity of 68.29 %.

Whole genome based average nucleotide identity revealed highest sequence identity percentage of the SPAdes hybrid assembly to the SPAdes Illumina (99.98 %; Figure 9). Both SPAdes assemblies aligned to 98.94 % to the MaSuRCA hybrid assembly.

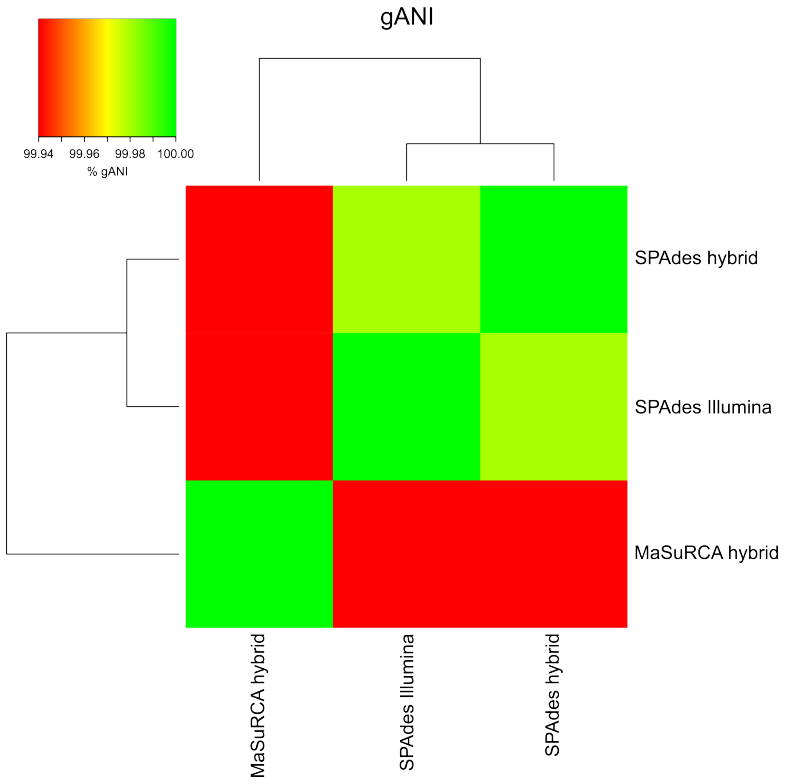

Figure 9. Genomic average nucleotide identity (gANI) for the three assemblies. gANI is a measure of nucleotide similarity between two genomes and used for species delineation based on bi-directional-best-blast hits (i.e. at a cutoff of 95 % [258]). SPAdes hybrid and SPAdes Illumina are identical at 99.98 % gANI, the MaSuRCA hybrid and the SPAdes assemblies only at a 99.94 %.

Only 15 contigs of the MaSuRCA hybrid assembly showed good alignment to the SPAdes hybrid assembly compared to the SPAdes Illumina assembly. The number of alignments was substantially higher (115) when aligning the SPAdes Illumina assembly to the SPAdes hybrid (Figure 10).

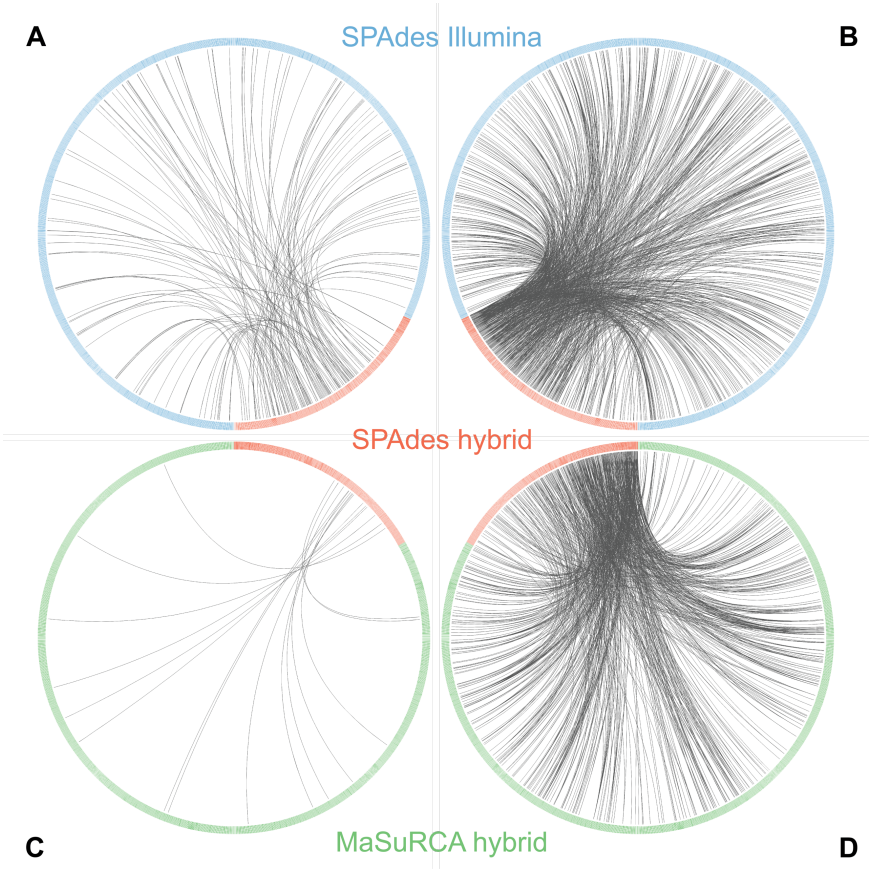

Figure 10. Whole genome alignments of SPAdes hybrid assembly against SPAdes Illumina assembly (A, B) and MaSuRCA assembly (C, D). Links are split into 'high alignment', if nucleotide identity was more than 99 % and more than 90 % of the contig covered (A, C), and 'low alignment', if nucleotide identity was less than 99 % and less than 90 % of the contig was covered (B, D). Contigs produced by the SPAdes Illumina assembly clearly showed a higher number of alignment (120) compared to the MaSuRCA assembly (15). Links with low alignment were similar (887 links for SPAdes Illumina assembly, 726 for MaSuRCA hybrid assembly).

Homopolymeric 5-mers were not well resolved in the MaSuRCA hybrid assembly, particularly AAAAA and TTTTT (Figure 11). SPAdes hybrid assembly yielded a comparable amount of 5-mers, with Illumina short-reads and Illumina short-reads complemented with ONP long-reads.

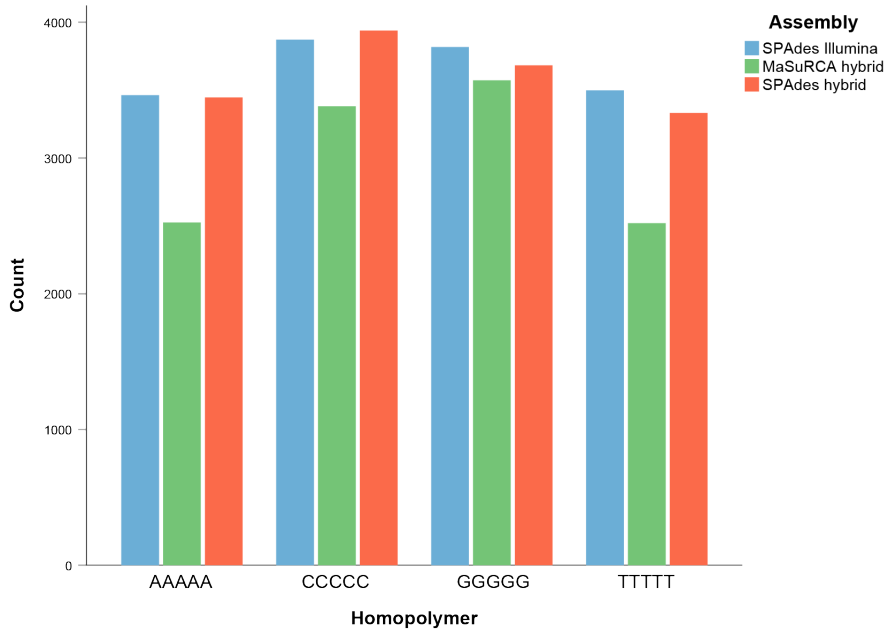

Figure 11. Counts of homopolymeric 5-mers in the SPAdes Illumina, the SPAdes hybrid and MaSuRCA hybrid assembly.

In summary, de Bruijn graph assembler SPAdes was most successful for an Illumina-ONT hybrid approach with highest N50, highest completeness, number of annotated features and information transferred from an Illumina-only assembly.

Genome annotation

As the filtered SPAdes hybrid assembly was superior to the other two in terms of assembly metrics, completion/contamination and number of annotated features, a full genome annotation pipeline was applied to annotate the 4.37 Mbp genome (Table 10). In total, 4,023 genes were predicted, of which 98.58 % protein-coding and 1.41 % RNA genes. Of all protein-coding genes, 69.77 % could be at least annotated other than 'hypothetical protein' or at least one Pfam domain or COG function other than 'unknown' or 'general function prediction only' could be assigned. For 55.87 % of proteins, a subcellular localization could be predicted and for 19.19 % a transmembrane helix predicted. Two CRISPR arrays with 5 and 9 spacers were predicted. Only one copy of 5*S*, 16*S* (partial) and 23*S* (partial) rRNAs were found with 109 bp, 1049 bp and 2001 bp, respectively.

When compared to the SPAdes Illumina assembly, 48 new proteins were identified, of which only 6 could be functionally annotated (Figure 12). The elongation factor Tu (thermo unstable) was lost in the SPAdes hybrid annotation.

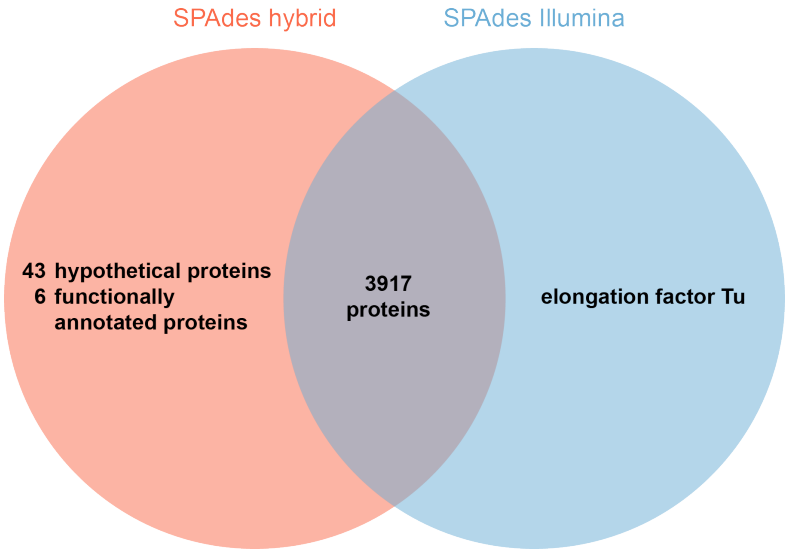

Figure 12. Venn diagram comparing protein annotations of SPAdes Illumina and SPAdes hybrid assembly. In total 49 new proteins were identified with the SPAdes hybrid assembly, including 6 with functional annotation (D-glycero-alpha-D-manno-heptose-1,7-bisphosphate 7-phosphatase, outer membrane porin protein 32, major outer membrane protein P.IB, pyruvate-flavodoxin oxidoreductase, tRNA 2-thiocytidine biosynthesis protein TtcA, zinc transporter ZitB). The essential protein elongation factor Tu [259] could not be recovered by the SPAdes assembly.

Table 10. *Cand.* Thiosymbion oneisti genome statistics.

Attribute	Value	%
Total genes	4,023	100.00
Protein-coding genes	3,966	98.58
RNA genes	57	1.41
Proteins with function prediction [a]	2,767	69.77
Proteins with COG assignment	2,916	73.52
Proteins with Pfam domains [b]	2,774	69.42
Proteins with signal peptides [c]	211	0.53
Proteins with predicted localization	2,216	55.87
Proteins with transmembrane helices	761	19.19
Proteins with KEGG assignment	1,556	39.20
Proteins with CAZy domain	152	0.04
CRISPR repeats	2	

[a] All protein-coding genes plus proteins with annotation 'hypothetical protein' that either fall into COG category other than R (general function prediction only) or S (unknown function) or proteins where at least one Pfam domain could be assigned to, or both
[b] All proteins where at least 1 Pfam domain could be assigned to
[c] Hit only reported if signal peptide was predicted with 2 out of the 3 tools

COG numbers were assigned to 73.53 % of protein-coding genes (Table 11). Considering only COGs with more than 5 hits, most abundant COG numbers were affiliated with transposases/retrotransposons (129) or toxin-antitoxin systems (TA) (53). Sulphatase-

modifying factor protein (COG1262) and tir protein (COG4916) were another two highly abundant hits with 10 and 12 assignments, respectively. 8 proteins were assigned to TRAP transporters (COG2358, COG4644). When grouping COGs into functional categories, the top three abundant categories were 'Replication, recombination and repair', 'Cell wall/membrane/envelope biogenesis' and 'Energy production and conversion' (Figure 13B). If the e-value for assigning COG numbers through rpsblast was set less restrictive (i.e. 10^{-3}), only the functional classes 'unknown' and 'general function prediction only' did increase (data not shown).

Table 11. COG functional category and number of genes associated with each of it.

Code, Functional category		Value	%
A	RNA processing and modification	2	0.05
B	Chromatin structure and dynamics	1	0.03
C	Energy production and conversion	207	5.22
D	Cell cycle control, cell division, chromosome partitioning	64	1.61
E	Amino acid transport and metabolism	170	4.29
F	Nucleotide transport and metabolism	55	1.39
G	Carbohydrate transport and metabolism	100	2.52
H	Coenzyme transport and metabolism	127	3.20
I	Lipid transport and metabolism	65	1.64
J	Translation, ribosomal structure and biogenesis	149	3.76
K	Transcription	111	2.80
L	Replication, recombination and repair	279	7.03
M	Cell wall/membrane/envelope biogenesis	214	5.40
N	Cell motility	18	0.45
O	Posttranslational modification, protein turnover, chaperones	150	3.78
P	Inorganic ion transport and metabolism	115	2.90
Q	Secondary metabolites biosynthesis, transport and catabolism	34	0.86
R	General function prediction only	318	8.02
S	Function unknown	551	13.89
T	Signal transduction mechanisms	79	1.99
U	Intracellular trafficking, secretion, and vesicular transport	64	1.61
V	Defense mechanisms	43	1.08
W	Extracellular structures	0	0.00
X	Mobilome: prophages, transposons	0	0.00
Y	Nuclear structure	0	0.00
Z	Cytoskeleton	0	0.00
Proteins without COG assignment		1,050	26.47
Total proteins		3,966	100.00

Of the protein-coding genes, 69.42 % were affiliated with at least one Pfam domain. The most abundant domain is WD40, a ~40 aa long domain that often terminates with Trp (W) and Asp (D), and second largest a putative endoribonuclease domain uma2 (PF05685), of which all were annotated as COG4636. Other highly prominent domains were the integrase core domain rve_3, the cro/C1-type helix-turn-helix domain (HTH_3), and the PIN domain, the latter is mostly associated with toxin-antitoxin components [260]. Two proteins had sulfur globule domains (SGP). When grouping related domains into clans, P-loop containing nucleoside triphosphate hydrolase superfamily was the largest group (Figure 13A). Among the top 5 % abundant clans also the PD-(D/E)XK nuclease superfamily were represented. An ABC-transporter domain (ABC_tran) was identified in 35 proteins. 8 proteins were annotated with an ACR_tran domain, a cation or multi drug efflux protein, of which all were presumably located in the cytosolic membrane, have 9 to 13 transmembrane helices, and were heavy metal efflux pumps or acriflavin resistance proteins by COG annotation (COG3696 & COG0841). The toxin clan 'Plasmid toxin-antitoxin system' was another well-represented clan with 56 member families, including the PhdYeFM_antitox domain, that act in a type II TA-system, ParE toxin domains and RelE domains (11 and 17, respectively). The corresponding antitoxin clan 'MetJ/Arc repressor' with the domains ParD, RelB, HicB were detected as well. The HicA domain was not covered by any clan but could be detected in 5 protein-coding genes. The MazE and MazF TA domains were present in 8 and 8 proteins, respectively.

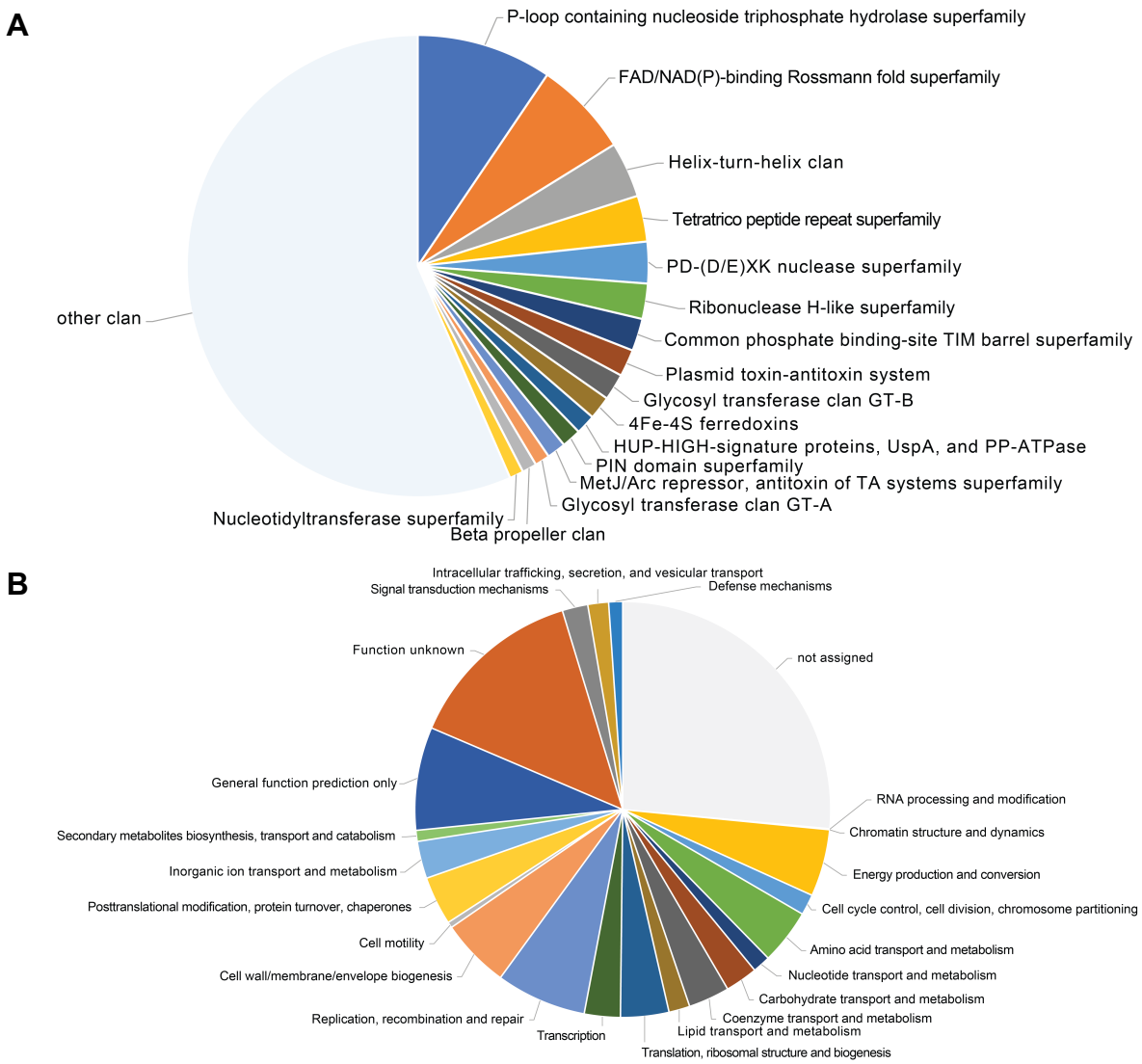

Figure 13. Pie charts showing numerical proportions of protein assigned Pfam clans (A) and COG functional category (B). (A) Only Pfam clans among the top 5 % are shown, others were summarized to 'other clan'.

152 Proteins with Carbohydrate-Active Enzymes (CAZymes) were identified, of which glycosyl transferase GT41 is the most predominant (Figure 14). Generally, over 49 % of all identified CAZymes are glycosyl transferases.

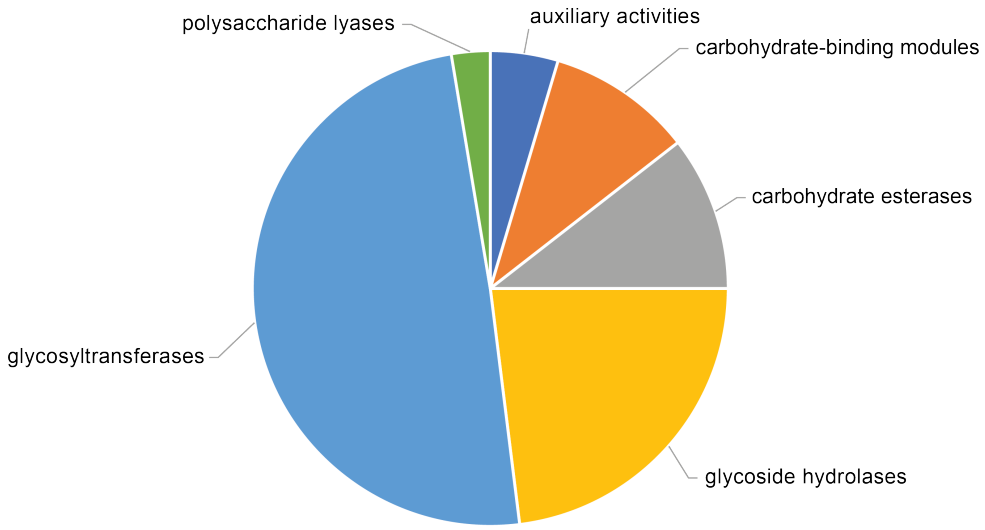

Figure 14. Families of carbohydrate-active enzymes (CAZy) identified in the SPAdes hybrid assembly. In total, *Cand.* T. oneisti contains 152 CAZy domains, of which 5 are predicted to be extracellular enzymes. CAZy degrade, modify, or create glycosidic bonds. The majority of CAZy are glycosyltransferases (68 proteins) that catalyze the formation of glycosidic bonds from phosphorylated sugar donors [261].

Only 0.53 % of all protein-coding genes encode for a signal peptide. SignalP was the most conservative tool and identified only 171 signal peptides in comparison to Phobius (485 predicted signal peptides). Most of the proteins were predicted to be localized in the cytoplasm (1,809 proteins; Figure 15) or in the cytoplasmic membrane (576 proteins). Only 27 extracellular proteins were predicted, including the penicillin-binding protein 1A and three esterase PHB depolymerase, the latter annotated by Pfam domain Esterase_phd and CAZy domain CE1.

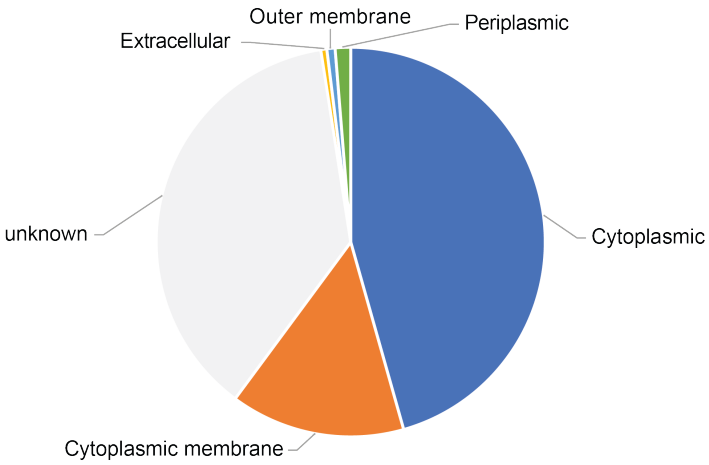

Figure 15. Pie chart visualizing the cellular localization of *Cand.* T. oneisti proteome as predicted by PSORTb. While only 20 proteins were predicted to be extracellular, 654 proteins were predicted to be associated with the membrane, out of which 27 were outer-membrane associated, 51 were periplasmatic and 576 were inner-membrane associated proteins.

Approximate repeats were predicted, resulting in all possible repeats accepting substitutions and indels. Notably, the genome of *Cand.* T. oneisti was richer in repeat sequences (17.33 % of the genome size; (Figure 16B) than the model gram-negative bacterium *E. coli* (4.83 % of the complete genome assembled in 1997 [262] (Figure 16A) and of the human pathogen *S. dysenteriae* (16.26 %). Average repeat length for *E. coli* was 618 bp, for *Cand.* T. oneisti 277 bp (ranging from 39 bp to 2,945 bp) and for *S. dysenteriae* 1,008 bp. The repeats of *Cand.* T. oneisti were more densely distributed with respect to *S. dysenteriae*, and were spread over protein- and non-protein-coding genes.

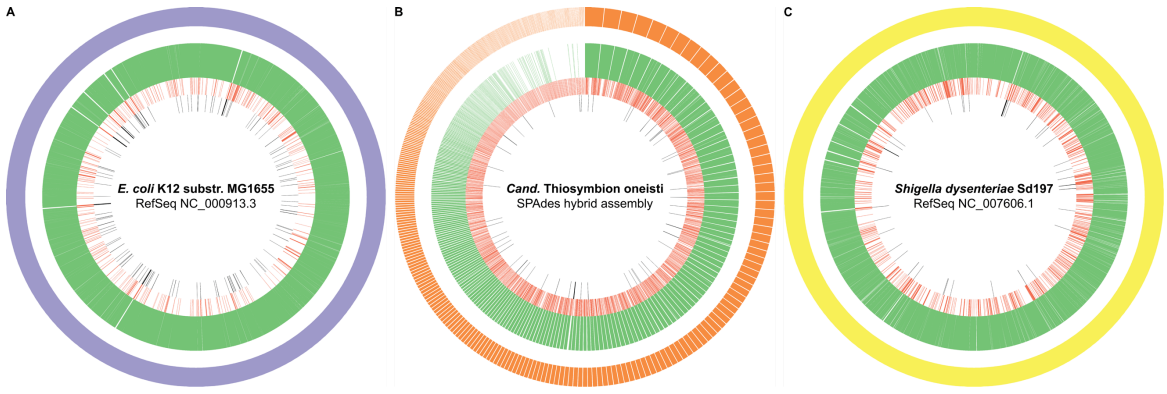

Figure 16. Circular view of *E. coli* K12 substr. MG1655 genome (A), of *Cand.* T. oneisti genome draft (B) and of *S. dysenteriae* Sd197 (C). Circle 1 (outer circle) represents contigs, circle 2 regions on the genome with protein-coding sequences, circle 3 repeat regions identified by RepSeek and circle 4 (inner circle) represents non-protein-coding genes.

Metabolic reconstruction

The Kyoto Encyclopedia of Genes and Genomes (KEGG) was used to further annotate protein-coding genes and for metabolic reconstruction. 1,556 protein-coding genes were annotated, corresponding to 39.2 %.

Cand. Thiosymbion oneisti possesses the complete reductive pentose phosphate cycle (Calvin cycle) for carbon fixation, and although fructose-1,6-bisphosphatase (EC 3.1.3.11) and sedoheptulose-7-phosphatase (EC 3.1.3.32) are absent, they encode for an ATP-dependent 6-phosphofructokinase (EC 2.7.1.90 and EC 2.7.1.11) and can perform nitrogen fixation. One contig compromising *nifA* and *nifL* (transcriptional regulation), *nifB* (formation of a functional Mo-Fe protein), *nifHDK* (dinitrogenase reductase subunit; iron-molybdenum dinitrogenase), two ferredoxins, and the Rnf electron transfer proteins upstream of the nitrogen fixation (*nif*) operon could be retrieved (

Figure **17**). The Rnf transfer proteins might engage in electron transport to the nitrogenase. Remarkably, three components of TA systems were found inside the gene cluster.

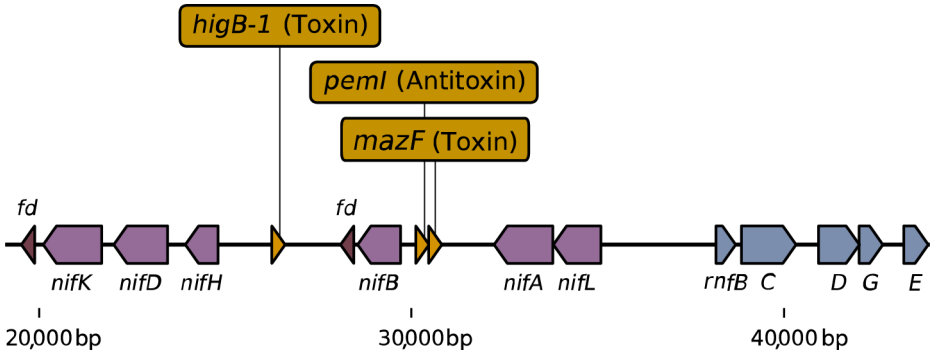

Figure 17. Nitrogen fixation gene cluster in *Cand.* T. oneisti of contig 14. *fd*, ferredoxin, *nifA*, transcriptional regulator, *nifB*, FeMo-cofactor synthesis, *nifH*, nitrogenase reductase and maturation protein, *nifD*, nitrogenase alpha chain, *nifK*, nitrogenase beta chain, *nifL*, nitrogen fixation regulatory protein, *rnf*, electron transport complex.

As energy sources, sulfide and thiosulfate can be oxidized to sulfate via the SOX complex and the reverse dissimilatory sulfite reductase/APS-Sat pathway (dsrAB, AprABM, Sat), whereas nitrate (via denitrification – membrane-bound and periplasmatic nitrate reductase (NarGHI/NapAB and NirS, respectively), membrane-bound nitric oxide reductase (NorBC, with cytochrome bc complex) and periplasmatic nitrous-oxide reductase (NosZ)) and oxygen can be used as electron acceptors. The TCA cycle and the glyoxylate cycle are complete. Sulfide can also be oxidized to elemental sulfur using a membrane-bound flavocytochrome c-sulfide

Dehydrogenase. A cytoplasmic membrane-bound pyrophosphatase can pump inorganic H+ to generate proton motif force and oxidative phosphorylation to generate ATP.

Fatty acids can be synthesized and degraded via beta-oxidation and phospholipids (phosphatidic acid, phosphatidylserine, phosphatidylethanolamine, cardiolipin) produced. *Cand.* T. oneisti can fully synthesize heme, folate, biotin, and riboflavin, polyhydroxybutyrate (PHB) and fully encodes for a heme transport system. The symbiont can transport phosphate, urea, zinc, lipoproteins, LPS using ABC-transporters, acetate via cation/acetate symporter, and ammonium using ammonium channel proteins across the cell membrane, but lack one enzyme each in ABC-transporters of molybdate and L-amino acids.

A type VI secretion system, the general secretion (Sec) and twin-arginine translocation (Tat) pathways and a type IV pilus are completely encoded. The majority of proteins of the type II secretion systems are present. Nitrogen and phosphate can be sensed using the GlnL-GlnG and PhoR-PhoB two-component system.

Habitat characterization of *Laxus oneistus* and *Stilbonema* sp.

Physicochemical conditions of a tropical subtidal shallow water sediment in Carrie Bow Cay, Belize, and of subtidal sediment in 3 m depth in the temperate Northern Adriatic Sea near Piran, Slovenia, were taken in the rainy season (July) and in September, respectively.

In the sediment in Piran, pore water content in the first 16 cm below sea floor was varying between 7 and 14 ml per 28.27 cm^3 sediment (mean water holding capacity 11 ml per 28.27 cm^3 sediment), depending on the layer. In the Carrie Bow Cay, pore water content was between 8 and 16 ml per 28.27 cm^3 sediment (mean value across first 30 cm below sea floor 11.66 ml/28.27 cm^3).

Pore water concentrations varied substantially between cores collected away from- and adjacent to seagrass beds, but also between cores collected close to one another.

For the Carrie Bow Cay sediment cores away from seagrass beds, oxygen was saturated right above the sediment (202.00 µM ± 12.16), but decreased throughout the sediment column to 11.54 µM ± 1.20 at 31 cm below sea floor (Figure 18A). At a salinity of 32 and a temperature of 27.6 °C, as it was measured in Carrie Bow Cay, 195.5 µM oxygen is equal to fully oxygen saturated sea water [263]. Sulfide concentrations varied but generally increased up to a mean concentration of 12.07 µM ± 5.51 at 31 cm below sea floor (bsf). Nitrate and nitrite concentrations were detected up to 0.76 µM and 0.09 µM, respectively (Figure 18B).

Ammonium concentrations ranged between 5.98 µM and 18.78 µM, DOC between 2.37 µM and 16.54 µM. Regarding cores adjacent to seagrass beds, a similar steepness of the gradient of oxygen and sulfide could be observed, although sulfide reached an average maximum concentration of 43.95 µM ± 19.19 (Figure 19A). Nitrate and nitrite concentrations were low with up to 1.41 µM nitrate and ammonium concentrations were considerably higher with a maximum of 126.32 µM (Figure 19B).

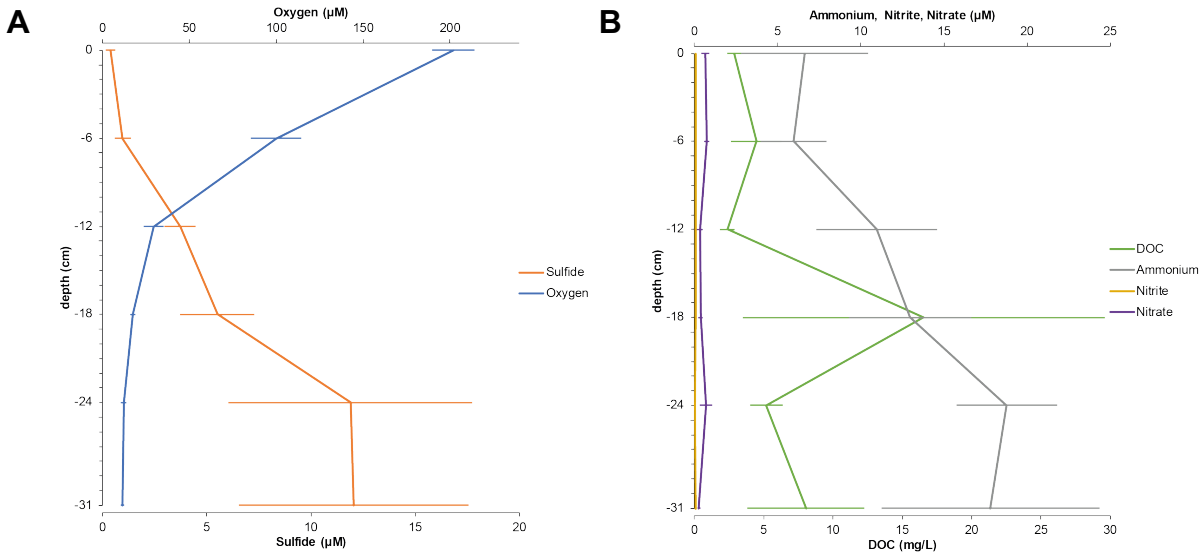

Figure 18. Depth gradients of sulfide and oxygen (A) and ammonium, nitrite, nitrate, and DOC (B) in cores away from seagrass beds in the Carrie Bow Cay sediment. For 0 to 24 cm bsf, each oxygen and sulfide measurement shows the mean and standard error of 9 sediment cores and the standard error; for 31 cm bsf only 5 measurements were taken. The N-species and DOC were measured in four and five replicates, respectively.

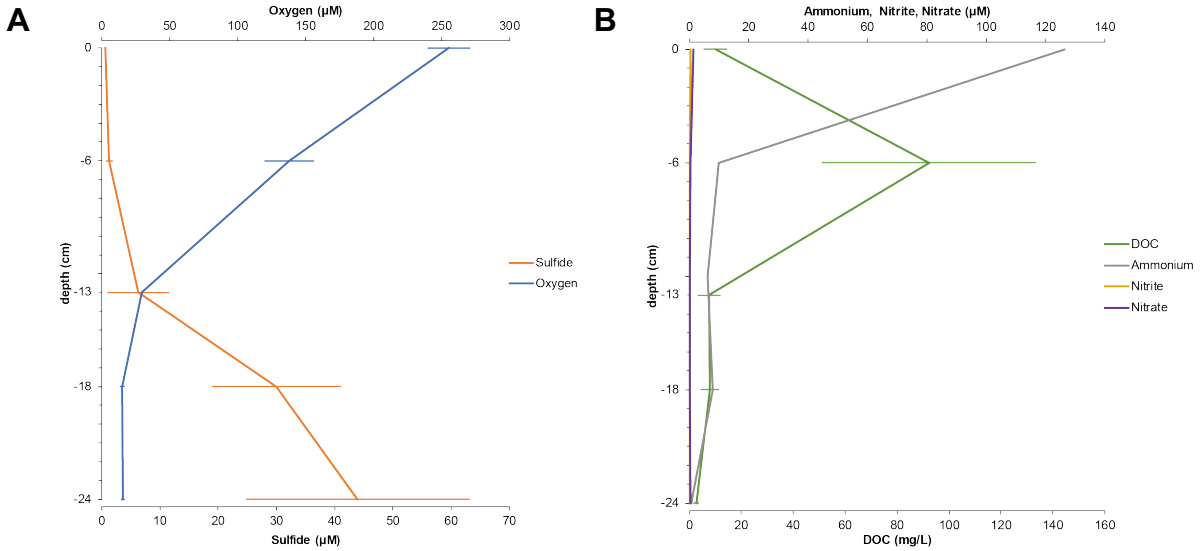

Figure 19. Depth gradients of sulfide and oxygen gradients (A) and ammonium, nitrite, nitrate, and DOC in cores adjacent to seagrass beds in the Carrie Bow Cay sediment. Each oxygen and sulfide measurement shows the mean of 5 sediment cores and the standard error. For only 1 core N-species were measured, DOC was measured in 5 replicates per depth.

Subtidal sediment in the Northern Adriatic Sea near Piran, Slovenia, was considerably enriched in sulfide (131.96 µM ± 68.20) and ammonium (throughout the sediment column 29.67 µM ± 5.65 µM; Figure 20). Oxygen concentrations decreased more rapidly from 185.06 µM ± 5.05 at 2 cm above sea floor down to 5.89 µM ± 1.67 at 10 cm bsf. Nitrite concentrations were low (maximal value 1.31 µM ± 1.06 at 10 cm bsf) as well as nitrate concentrations (throughout the sediment column 0.5 µM ± 0.36).

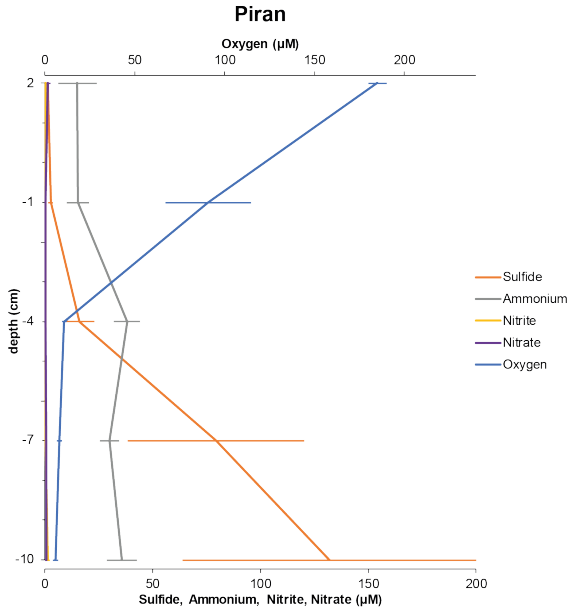

Figure 20. Depth gradient of sulfide, oxygen, ammonium, nitrite and nitrate in costal subtidal sediments of the Northern Adriatic Sea near Piran, Slovenia. Each measurement represents the mean concentration and standard error of 5 measurements.

In the Carrie Bow Cay cores away from seagrass beds, *Laxus oneistus* and *Stilbonema* sp. were found throughout the sand column. However, the maximum abundance of *L. oneistus* was observed at 18 to 24 cm bsf (mean abundance of 34.43 % ± 8.46; **Figure 21**A), where oxygen is low (17.56 µM to 12.29 µM), as well as sulfide (5.51 µM to 11.89 µM). A one-sample Kolmogorov-Smirnov test failed to reject the hypothesis that the nematode abundance was normally distributed ($D(43) = 0.186$ for *L. oneistus*; $D(43) = 0.186$ for *Stilbonema* sp.; $p \leq 0.01$), therefore an independent samples Kruskal-Wallis test was performed. There was a statistically highly significant difference in *L. oneistus* distribution across sediment layers ($H(4) = 17.031$, $p < 0.01$). A Dunn-Bonferroni *post hoc* test revealed that the distribution in the layer 3 (12 to 18 cm bsf) and layer 4 (18 to 24 cm bsf) were statistically higher than in the oxygenated subsurface layer (0 to 6 cm bsf; $p < 0.01$ each) with a mean distribution of 30.80 % ± 3.74 (layer 3), 34.43 % ± 8.46 (layer 4) and 4.09 % ± 1.36 (layer 1). On the other hand, there was no significant difference in the *Stilbonema* sp. distribution between layers ($H(4) = 8.543$, $p > 0.05$).

A similar trend was observed in cores adjacent to seagrass beds, although *L. oneistus* was absent in layer 1 (n = 5; **Figure 21**B), where oxygen concentrations range from 255 to 138 µM. Since the data were not normally distributed ($D(23) = 0.278$, $p < 0.001$ for *L. oneistus*; $D(23) = 0.182$, $p < 0.05$ for *Stilbonema* sp.), a Kruskal-Wallis test with *post hoc* test Dunn-Bonferroni

correction showed a significant difference between layer 1 and layer 3 for *L. oneistus* ($p < 0.05$) with a mean concentration of 60.71 % ± 17.40 in layer 3. Intriguingly, when sulfide levels are increased up to a concentration of 50 µM or 120 µM (supplementary Figures, core N & M), the abundance of *L. oneistus* and *Stilbonema* sp. decreased down to a mean abundance of 10 % for *L. oneistus* while *Stilbonema* sp. is absent at all (n = 2).

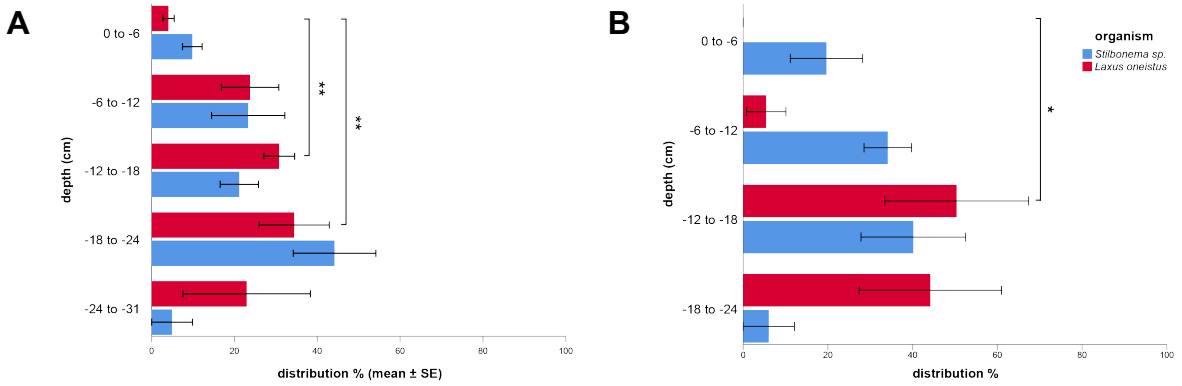

Figure 21. Sand column distribution of *Laxus oneistus* and *Stilbonema* sp. in cores away from seagrass beds (A) and cores adjacent to it (B). Distribution is plotted in percent (calculated based on the total number of individuals for each core) across 5 and 4 layers, respectively. A total of 345 *L. oneistus* and 244 *Stilbonema* sp. was found in cores away from seagrass beds and a total of 176 and 162, respectively, in seagrass adjacent cores. *, $p < 0.05$, **, $p < 0.01$.

A communality that is observed in both away from seagrass and adjacent to it is a low abundance of *L. oneistus* (mean abundance 2.05 % ± 0.68; Figure 22) and of *Stilbonema* sp. (7.21 % ± 2.71) in the most oxygenated layer. The abundance increased with depth and reached a maximum at low sulfidic (< 20 µM) and hypoxic (< 20 µM) conditions. The color of the coarse calcareous sediment changed from yellowish in the upper, oxygenated layer, to a grey zone at gradually at approx. 20 cm below sea floor. The chance to encounter a hot spot with high sulfide concentrations (defined acc. to [10]) is higher close to the seagrass.

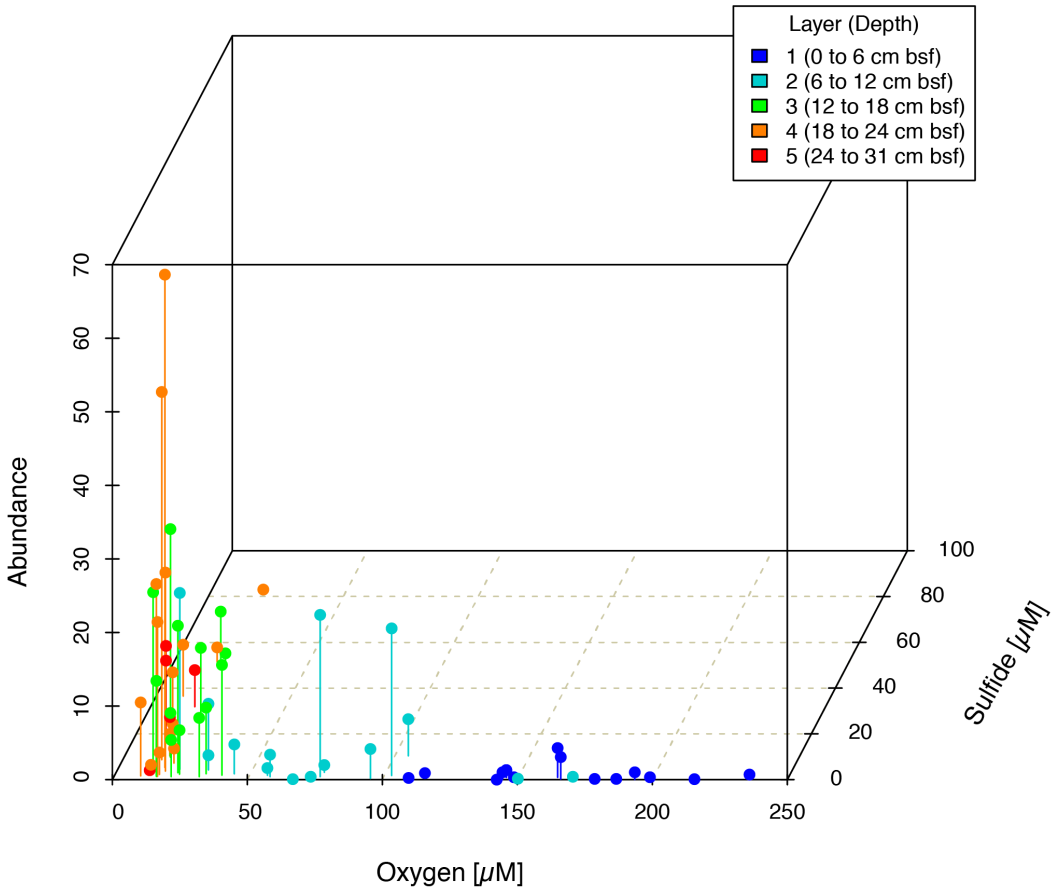

Figure 22. 3D scatter plot of oxygen and sulfide concentrations and abundance of *L. oneistus* colored according to the layer they were retrieved. bsf, below sea floor.

Nematodes of the subfamily Stilbonematinae could not be retrieved by taking sediment cores in Piran, Slovenia. Only some individuals of the genus *Eubostrichus* GREEF [184,264–267] have been collected with a bucket so far (Bulgheresi, pers. communication). The grain size of the sediment reached from small gravel at the upper layers to silt and clay, as well did sediment color change from brown/grey because of the high content of detritus to black in the lower parts of the sediment core.

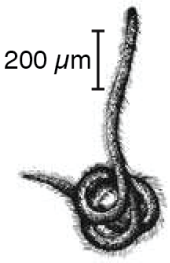

Figure 23. All individual of the genus *Eubostrichus* carry ectosymbiotic bacteria on their cuticule. Taken from Giere (2008) [8].

A Spearman's rank-order correlation was used to determine co-occurrence of *L. oneistus* and *Stilbonema* sp. In the cores away from seagrass beds, we found the correlation of the abundances of the two species to be highly significant (r_S (43) = 0.509, $p < 0.001$; **Figure 24**A). However, this was not the case in proximity to seagrass beds (r_S (20) = -0.089, $p > 0.05$; **Figure 24**B).

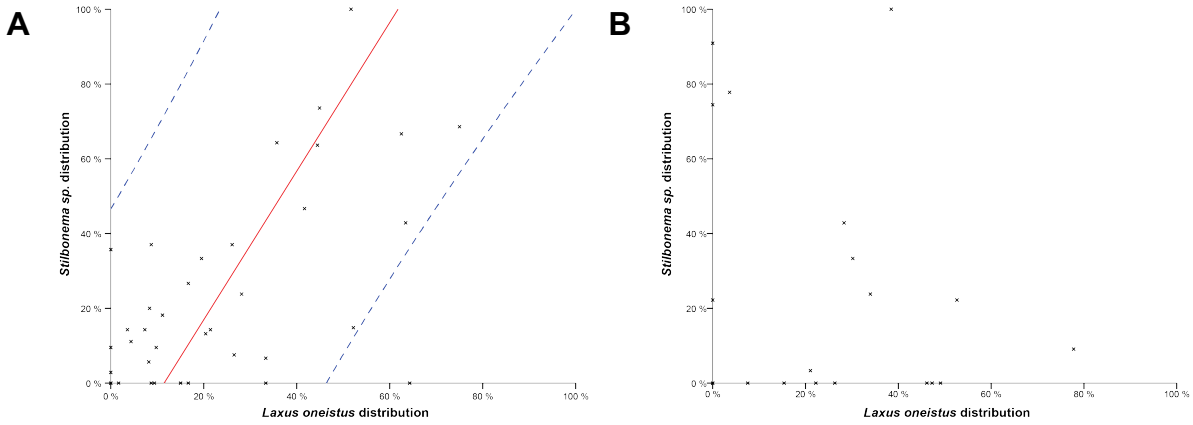

Figure 24. Correlation of *L. oneistus* and *Stilbonema* sp. in cores away from seagrass (A) and in proximity to it (B). (A) There was a moderate, statistically highly significant co-abundance of the two species. A regression line was fitted through the data (R^2 = 37.6 %, red line) and 95 % confidence interval (dashed lines). (B) There was no significant correlation ($p < 0.05$) between the two organisms in seagrass proximity.

In summary, vertical gradients of sediment chemistry were highly dynamic but were characterized by oxygen decreasing with depth and sulfide increasing in Carrie Bow Cay and Piran. Nitrate and nitrite concentrations are in a nanomolar range, although ammonia can be up to 120 µM. Both genera of Stilbonematinae, namely *Laxus oneistus* and *Stilbonema* sp. showed a maximum abundance at low oxic, low sulfidic concentrations.

Quantitative PCR-based assessment of *Cand.* Thiosymbion quadrati metabolic response to different oxygen regimes

Incubations

To detect differential expression of key metabolic genes involved in sulfur oxidation (*aprA, dsrA*), denitrification (*norB*), nitrogen fixation (*nifH*) and carbon fixation (*cbbL*), the symbiotic nematodes were incubated in oxic and hypoxic seawater for 24 h, 48 h and 72 h. For the oxic 24 h and 48 h incubations, the medium had an initial oxygen value close to saturation (184.18 µM and 205.29 µM, respectively; Table 12). For the oxic 72 h incubations, oxygen decreased from 202.69 µM to 79.52 µM ± 11.93 (see discussion). The hypoxic 72 h incubations had on average 4.24 µM oxygen at a salinity of 34.7. The preparation of the hypoxic seawater through gassing with CO_2 decreased the pH from 8.95 to 8.46. Since the water used for incubation originated from the same tank, only the hypoxic medium (48 h incubation) was measured. It contained 3.36 µM ammonium, 0.29 µM nitrate, and 0.24 µM nitrite.

Table 12. Chemical monitoring of the nematodes' incubations medium.

sample	incubation		O_2 (µM) [a]	NH_4^+ (µM)[a]	NO_3^- (µM) [a]	NO_2^- (µM) [a]	pH
1	oxic	24 h	184.18	n.d.	n.d.	n.d.	n.d.
9	oxic	48 h	205.29	n.d.	n.d.	n.d.	n.d.
13	hypoxic	48 h	6.4				n.d.
14	hypoxic	48 h	n.d.	3.36	0.29	0.24	n.d.
15	hypoxic	48 h	n.d.				n.d.
16	hypoxic	48 h	n.d.				n.d.
17	oxic	72 h	68.24	n.d.	n.d.	n.d.	8.95
18	oxic	72 h	78.31	n.d.	n.d.	n.d.	8.95
19	oxic	72 h	92.00	n.d.	n.d.	n.d.	8.95
21	hypoxic	72 h	3.71	n.d.	n.d.	n.d.	8.45
22	hypoxic	72 h	4.53	n.d.	n.d.	n.d.	8.45
23	hypoxic	72 h	4.49	n.d.	n.d.	n.d.	8.45

[a] measured at the end of incubation
n.d. not determined

RNA extraction

Host and symbiont RNA extraction yielded 11.07 ng/µl on average, ranging from 6.25 ng/µl to 14.6 ng/µl with an average purity of 1.61 $A_{260/280}$ (1.52 to 1.82). Electropherograms of all samples obtained by Agilent Bioanalyzer 2100 showed peaks for both host and symbiont

(as a representative electropherogram see Figure 25); the calculation of RNA integrity values (RIN) was therefore obsolete, although RNA was not degraded in any of the samples.

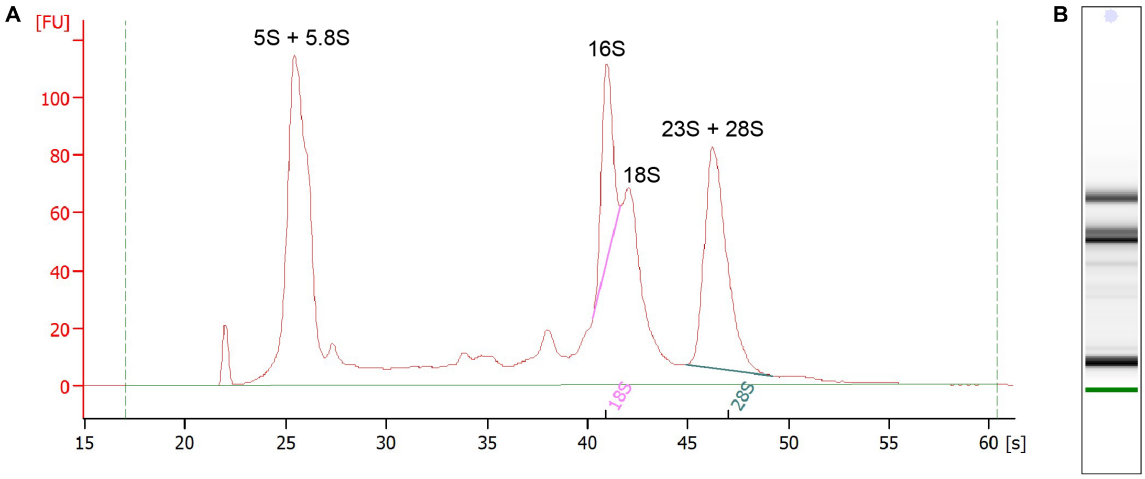

Figure 25. Total RNA was run on a 2100 Bioanalyzer (Agilent) for quality and quantity check. (A) The electropherogram shows an undegraded RNA sample as visible through intact rRNA peaks. The approx. sizes for *Cand.* T. oneisti rRNA are 109 bp (5*S*), 1598 bp (16*S*), 3,335 bp (23*S*); source: SPAdes Illumina and hybrid annotation; approx. sizes for *Caenorhabditis elegans* rRNA are 153 bp (5.8*S*), 1,760 bp (18*S*), 3,509 bp (26*S*); source: RNAcentral since no host genome is available. Dashed green lines (A) and bold line (B) are marker bands. (B) Virtual gel representation of the electropherogram data.

Data analysis of quantitative PCR

The *rpoB* gene showed the most constant expression (lowest standard deviation of 1.23; Table 13, Figure 26) independently of the treatment. *rpoB* was therefore selected as a reference gene.

Table 13. Standard deviation of C_q over all treatments for each transcript.

transcript	C_q standard deviation
aprA	1.69
dsrA	2.99
norB	1.58
cbbL	1.55
nifH	1.30
rpoB	1.23
16*S*	1.60

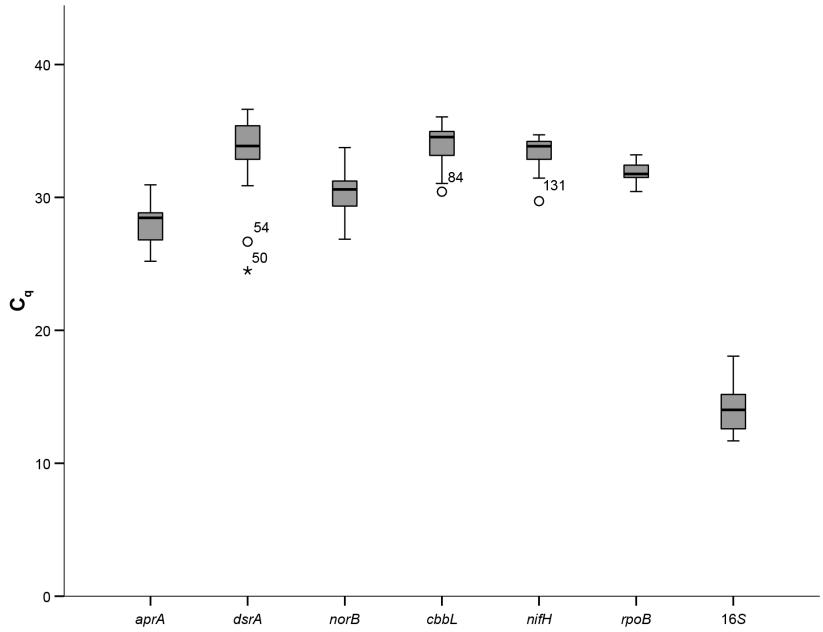

Figure 26. Boxplot displaying the distribution of C_q values across all experimental treatments.

Relative expression values ($\Delta\Delta C_q$) were defined as the expression of the gene-of-interest (*aprA, dsrA, norB, cbbL, nifH*) in the sample-of-interest normalized against the expression of reference transcript *rpoB* in the 24 h incubation (relative quantification). There was generally a high natural variability between biological replicates that was reflected by the standard error of $\Delta\Delta C_q$ (Figure 27). The number of biological replicates varied because some samples did not show any amplification.

Given that the $\Delta\Delta C_q$ values (Table 14) were not normally distributed (Kolmogorov-Smirnov test; $D(171) = 0.363$, $p < 0.001$), a Kruskal-Wallis H test showed a statistically significant difference in $\Delta\Delta C_q$ values between the time points for the transcript *aprA* ($H(26) = 9.960$, $p < 0.01$) and a highly significant difference for *dsrA* ($H(34) = 20.052$, $p < 0.001$). The two transcripts for sulfur oxidation were upregulated in the hypoxic incubation and the level of transcription decreased over time. However, *dsrA* was not differentially expressed after 48 h. A *post hoc* test using Dunn's correction revealed that in the 48 h and 72 h incubations the *dsrA* relative expression elicited a highly significant reduction down to a median $\Delta\Delta C_q$ of 1.56 ± 0.34 ($p < 0.001$ for 48 h time point, $p < 0.01$ for the 72 h compared to 24 h). *aprA* mRNA expression levels significantly decreased in the 72 h compared to the 24 h time point (median $\Delta\Delta C_q$ of 3.00 ± 0.85, median $\Delta\Delta C_q$ of 16.47 ± 3.38, respectively; $p < 0.01$).

Expression levels of nitric oxide reductase subunit B (*norB*) which is involved in denitrification as an electron acceptor showed a significant decrease over time ($H(37) = 6.360$,

$p < 0.05$), with a significant reduction from 48 h to 72 h from a median $\Delta\Delta C_q$ of 9.09 ± 4.28 to 2.38 ± 1.17 ($p < 0.05$), but its expression was upregulated even then.

The overexpression of *cbbL* was not significantly different between the time points ($H(39) = 1.693$, $p > 0.05$) with a median relative mRNA expression of 2.38 throughout the time points.

Expression levels of *nifH* mRNA showed a highly significant increase ($H(35) = 21.785$, $p < 0.001$), especially at 72 h, expression levels increased and turned to a highly significant upregulation from a 24 h median $\Delta\Delta C_q$ of 0.77 ± 0.15 to a 72 h 9.09 ± 4.28. ($p < 0.001$), whereas at 24 h and 48 h *nifH* was not differentially expressed compared to the oxic incubation as relative *nifH* mRNA levels are close to 1.

Sanger sequencing and melting curve analysis of qPCR amplicons confirmed the specificity of the amplification. The investigated transcripts showed qPCR efficiencies from 0.53 (*dsrA* 24 h/48 h) to 1.01 (*norB* 72 h).

Table 14. Mean pairwise $\Delta\Delta C_q$ for each transcript, standard error (SE) and efficiency in amplification (E).

	aprA			***dsrA***			***norB***			***cbbL***			***nifH***		
	ΔΔCq	**SE**	**E**	**ΔΔCq**	**SE**	**E**	**ΔΔ**	**SE**	**E**	**ΔΔCq**	**SE**	**E**	**ΔΔCq**	**SE**	**E**
24 h	14.34	3.39	0.97	44.92	26.17	0.53	9.67	2.55	0.88	2.87	0.62	0.91	0.57	0.11	0.92
48 h	24.42	7.39	0.97	1.91	0.46	0.53	8.87	1.98	0.88	1.71	0.92	0.91	1.39	0.2	0.92
72 h	3.66	0.85	0.94	1.7	0.42	0.67	3.58	1.17	1.01	2.46	0.8	0.71	5.71	1.55	0.85

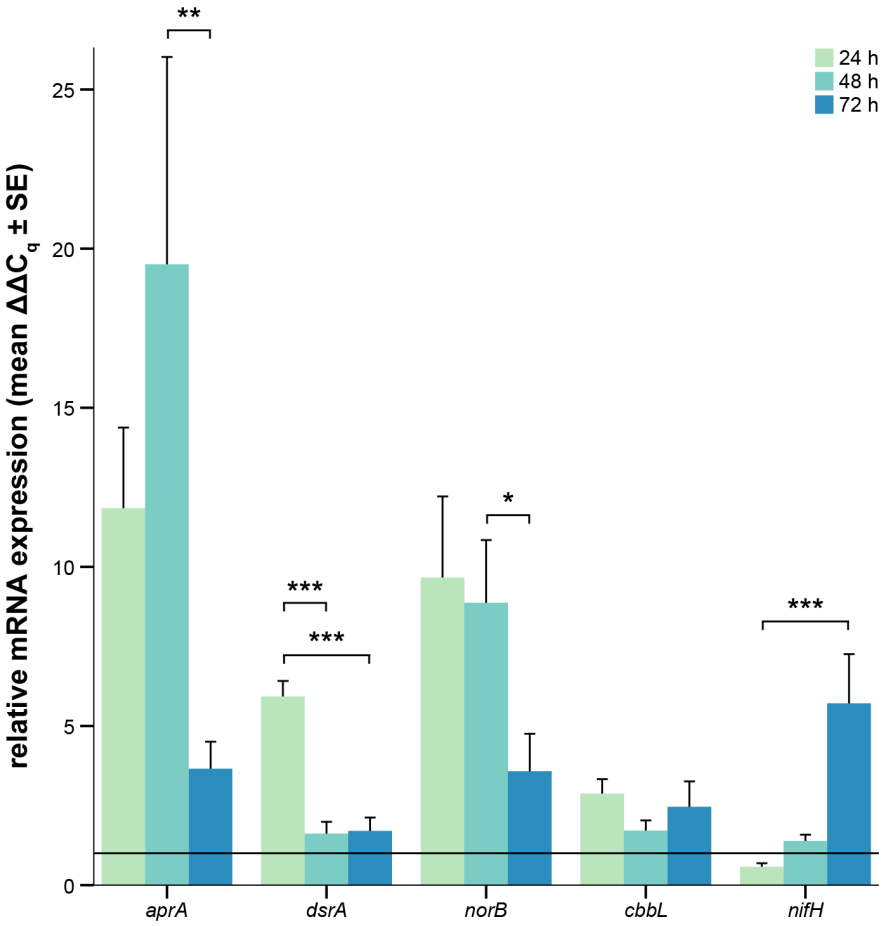

Figure 27. Relative mRNA expression values of key metabolic genes *aprA* (adenosine-5′-phosphosulfate reductase alpha subunit), *dsrA* (dissimilatory sulfite reductase subunit A), *norB* (nitric oxide reductase subunit B), *cbbL* (RuBisCO large subunit), *nifH* (nitrogenase iron protein) in the hypoxic treatment relative to the oxic treatment. C_q values were normalized to the *rpoB* gene expression levels (reference gene). $\Delta\Delta C_q$ values with a value of 1 (black line) are not differentially expressed, values above 1 imply an upregulation in the hypoxic treatment relative to the oxic treatment. Bars represent the mean of pairwise $\Delta\Delta C_q$ values ± standard error ($n \geq 8$). Two to four biological replicates (for details see Table 5) were measured in triplicates each. Significance was determined by a Kruskal-Wallis H test following a *post hoc* test using Dunn-Bonferroni correction. *, $p < 0.05$, **, $p < 0.01$, ***, $p \leq 0.001$.

In summary, mRNA expression of sulfur oxidation genes (*aprA*, *dsrA*) decreased over time and was accompanied by a decrease in mRNA expression of denitrification (*norB*). Expression levels for inorganic carbon is fixation (*cbbL*) were upregulated throughout the 72 h incubation period, while the targeted gene for nitrogen fixation (*nifH*) was only highly significantly upregulated after 72 h.

Discussion

Draft genome assembly of short and long reads reveals adaptions and metabolic versatility in a stilbonematid symbiont

Cand. T. oneisti dissociated from approximately 500 *Laxus oneistus* nematodes from Carrie Bow Cay was sequenced with long-read sequencing technology ONT by which reads with a maximum read length of 121,466 bases and a mean phred score of 5 were obtained. Currently, the longest read obtained with ONT was 1 Mbp (Martin Smith, unpubl.). The third-generation sequencing technology ONT MinION has a similar high error rate compared to PacBio, but its throughput currently is much smaller [203]. However, if coverage is deep enough, error correction is possible by using the generated reads themselves or the Illumina reads [268,269]. Although ONT sequencing is still being actively developed, it is already a powerful tool that yields highly accurate (99 %) *de novo* genome assemblies when compared to Illumina-assembled reference genomes [203,270,271]. Closing of Illumina-based assembly gaps is enabled by a complementing it with long reads [268]. Moreover, due to its low cost ($1000 for the sequencer; $62.5/Gb reads) and high portability [272], real-time genomic data acquisition in resource-limited environments is possible as it was demonstrated in surveillance of Ebola outbreaks [273], for species identification in a remote rainforest [274] or metagenome sequencing on-board of the the TARA Oceans expeditions or at the International Space Station [275]. In particular, DNA methylation can be detected by single molecule sequencing [276] and long reads are critical for resolving structural variation [277,278]. Direct RNA sequencing (without cDNA synthesis) was made available through ONT [279].

Intriguingly, independent of the assembler used, we showed that ONT reads can overcome the high fragmentation of Illumina-based assemblies even at a low sequencing coverage (1.22X coverage). De Bruijn graph-based assemblers originally were written to overcome repetitive sequences in genomes [280]. SPAdes is one of those and includes an initial error correction step, followed by generating and solving an assembling graph and finally scaffolding with long-reads if provided [213]. In contrast, MaSuRCA is a combination of de Bruijn graph and overlap consensus assemblers, and scaffolds are generated by assembling mega-reads out of short (e.g. Illumina) and long reads [214]. Although both assemblers performed best when benchmarked with other assemblers, SPAdes showed over again better performance when larger reads were provided [281,282], because of the above strategy [268].

A promising OLC approach that includes an initial error correction step of long reads through Illumina short reads was implemented in PBcR [268]. In terms of highest N50, completeness, number of annotated features and resolution of homopolymers, this was also shown in this study. Because ONT sequencing relies on measuring the change in voltage when a DNA molecule enters the pore, homopolymers pose a problem because there is no change in signal over time [283]. Canu was written as a *de novo* assembler of high noise sequencing data [215] but failed in our hands, possibly due to the low coverage. With hybrid assembly, it was possible to reach a N50 of 27 kbp with 94.28 % completeness (based on putatively single copy genes) and 99.98 % nucleotide similarity. MaSuRCA hybrid assembly failed in correctly resolving homopolymeric 5-mers, a common problem in ONT. The good accuracy of using Illumina reads together with the continuity that is by using long-reads in a hybrid approach was shown previously [284]. As determined by mapping, there was a substantial loss in information by using MaSuRCA for the assembly. The SPAdes hybrid assembly is smaller because repeats are better resolved. Number of protein-coding sequences and tRNAs was highest in the SPAdes hybrid assemblies. For further improvement of the assembly, a polishing step with racon [285], pilon [286] or nanopolish [270] would be necessary as long as homopolymeric k-mers are not successfully resolved by ONT. New basecallers based on neural networks that are in development are aiming at settling this problem and thus increasing the accuracy.

As the SPAdes hybrid assembly represents a high-quality draft genome [257,258], a comprehensive annotation pipeline was applied to it. The sequence consists of 401 assembled contigs. The genome has a size of 4,312,079 bp and contains 4,023 open reading frames encoding for 3,966 protein-coding genes, 53 tRNA genes for all proteinogenic amino acids (1 to 7 for each type), one incomplete rRNA operon and has an average GC content of 58.7 %. Since this genome is not diminished, it does not point to an obligatory dependence on its host [287].

Functional categorization of the genomic repertoire using clusters of orthologous genes revealed that 16.87 % of all protein-coding genes are devoted to metabolism-related functions (categories CEGHI), whereas conserved functions such as replication, recombination, translation or transcription are represented to a lesser extent [288]. Specifically, transposases and TA proteins were most abundant in the dataset. Expression data suggests that many of these are also actively transcribed (Lena König, pers. comm.). Both protein families might represent key mechanisms for adaption to dynamic environments and host environment [289–

291] by generating genomic diversity [292–294]. High transposon abundances have also been reported in other *Cand.* Thiosymbion symbionts [290,295] such as those of *Olavius algarvensis* [167,296].

Second biggest COG is related to TA systems that point to a putative role in defense [297], stress response [298] or host interaction [299]. In *Bathymodiolus* symbionts or the sponge microbiome, protection of the host against parasites or phages was hypothesized [300,301]. Pfam domain annotation is also covering TA systems as PIN domains, now referred to as VapBC (virulence associated proteins) with VapC as a ribonuclease and inhibited by VapB [302,303]. It was shown that under stressful conditions VapC acts as a 23S rRNA-specific endonuclease and thus inhibiting translational initiation [304,305] so that metabolic levels are adjusted [303,306–308]. Other type II TA systems present in the genome are ParE/ParD, RelE/RelB, and MazE/MazF [309]. ParE inhibits cell division if a DNA fragment (e.g. a phage plasmid) has not been inherited [310], whereas RelE and MazF cleave RNA if cells undergo nutritional stress such as lack of glucose or amino acids [311]. Specifically, unless RelE is inactivated by its antitoxin RelB, it cleaves mRNA codons (preferentially stop codons) at the ribosomal A site [312], thus creating truncated mRNAs that arrest translation and therefore translational rates decrease [313]. In contrast, MazF reversibly cleaves off the Shine-Dalgarno sequence of mRNA and 16*S* rRNA, thus enabling a cell to selectively translate leaderless mRNAs [298,314]. Bacterial adaptation by transposons and defense mechanisms by TA-systems was also shown for sponge microbiota [315–318].

Presence of sulfatases could be involved in sulfur scavenging [319], although in humans sulfatases are involved in sulfolipid turnover [320,321]. Intriguingly, most abundant lipid in phylogenetically closely related *S. majum* symbionts are sulfolipids (Michaela Mauß, pers. comm.). Toll/interleukin-1 receptor/resistance protein (TIR) are widespread in pathogenic and non-pathogenic bacteria where they function in suppression of host immunity and more generally in protein-protein interactions [322]. In rhizobia, evasion of host immunity through TIR-domain containing proteins is important for the establishment of the symbiosis [323]. TRAP transporters (tripartite ATP-independent periplasmatic transporters) as the genome is encoding for six of them are driven by a gradient of electrochemical ions and not by ATP as ABC transporters [324], but elucidation of substrates is mostly lacking. The high abundance of hypothetical proteins with the domain rve_3 (conserved core domain of retroviral integrase) points to a previous encounter with phages [325]. Sulfur globule domains form an envelope

around sulfur globules [326] and are among the most transcribed (Lena König, pers. comm.). The family of Acriflavin resistance proteins are a component in multi-drug efflux systems and serve as a protection against a wide range of hydrophobic inhibitors [327] or antibiotics (e.g. tetracycline, streptomycin, chloramphenicol) [328]. Their expression was confirmed by transcriptomics (Lena König, pers. comm.). Most abundant Pfam clans were identified as conserved clans in fully sequenced bacteria. Due to the low number of CAZymes and extracellular enzymes identified, *Cand.* T. oneisti does not seem to degrade mucus polysaccharides it is embedded into as it is the case for gut microbiota [329,330].

The high number of repeats is supposedly due to the fact that the draft genome was assembled mostly from short-read sequencing reads and scaffolding was only possible with few long reads. Long repeats might therefore be underrepresented. Repeats are a form of genome plasticity and can give rise to differential phenotypes. They are a sign of rearrangements within a genome, through with new functions can evolve, provided that genome integrity is not threatened [331]. Source of repeats are mostly transposable elements [332] and number of repeats ranging from 0 to 21 % is correlated with an organism's lifestyle so that the genomes of intracellular, obligate bacteria contain less mobile elements independent of their phylogenetic placement [295].

Genome size could be underestimated due to the short-read sequencing data as Williamson *et al.* (2016) [333] showed. In contrast, long-read sequencing technology was used for *de novo* assembly of *C. elegans* genome and led to the identification of 2 Mbp of sequences (mostly long repeats) that were missed in the reference genome sequenced in 1998 [334].

All pathways necessary for a host-independent lifestyle are complete. Identified metabolic pathways (i.e. auto- and heterotrophy, sulfur oxidation, denitrification) are consistent with experimental studies of *Cand.* T. oneisti and pathway reconstruction [11,118,147,195]. No fermentative or nitrifying enzymes have been identified. The Calvin cycle possesses the same enzymatic repertoire as in *R. pachyptila* or *O. algarvensis* [296,335]. Oxidation of reduced sulfur compounds occurs via a truncated SOX system with *soxCD* missing and a reverse-acting DsrAB (Lena König, pers. comm.). ABC-transporters have largely been confirmed by the Pfam ABC-transporter domains. Excretion products, in particular ammonium and urea can be used as nitrogen source by the symbiont. *Cand.* T. oneisti might engage in nitrogen fixation as the *nif* operon potentially was horizontally acquired [147], in combination with the nitrogen regulatory system GlnL-GlnG (NtrC) which is present. Analysis

of the *nif* operon revealed presence of components of TA systems (*pemI*, *mazF*, *higB-1*; Harald Gruber-Vodicka, pers. comm.). This mechanism might act as a selective marker and ensures stable maintenance of the *nif* operon [336]. Ammonium can be assimilated through the GS/GOGAT pathway. Storage compounds such as glycogen, PHA, sulfur granules and polyphosphate [147] may function primarily as energy reserve [337] and can be mobilized via amylases, PHB depolymerases, the sulfur oxidation pathway, and phosphatases. The presence of carboxysomes was stated [12]. Besides other cofactors, heme can be synthesized and transported. Intriguingly, the nematode *C. elegans* lacks heme synthesis (Lena König, pers. comm.; [338]), thus an obligate association could have been established with the symbiotic bacteria providing heme to the host since it is scarce in marine habitats [339]. Heme-containing proteins might also engage in sulfide detoxification [45]. The membrane might be primarily composed of phospholipids (phosphatidylserine/ethanolamine, cardiolipin) as it is the case for many diverse marine bacteria in phosphorus-unlimited environments [340]. The genes for sulfolipid biosynthesis that are canonical for photosynthetic bacteria are absent [341].

In addition to host-secreted Mermaids, bacterial Type IV pili might be required for successful colonization, as it is the case for the attachment of the symbiont *Verminephrobacter eiseniae* to earthworm nephridia [342] or *Vibrio fischeri* to its squid host [343]. Twin-arginine translocation pathway and the Sec pathway complementing the type II secretion pathway might export folded and unfolded proteins, respectively, for a symbiosis-specific function or for defense. *Cand.* T. oneisti fully encodes for a type VI secretion system. Although the significance of the T6SS focused on human pathogens, its role extends to a wide range of interbacterial interactions and host environments [344,345]. It acts as a contractile, cell-puncturing system that attaches to bacterial cells via the VgrG subunit [346] and injects effector proteins that have an inter-kingdom role in signaling, host interaction (modification of host cytoskeleton or modulation of inflammatory response) or defense against pathogens [347–349]. The biological effect of the T6SS in light of the symbiosis with ectosymbiotic nematodes might elucidate context-dependent interactions.

Vertical field distribution of symbiotic stilbonematid nematodes and availability of nutrients

The vertical field distribution of two species of Stilbonematinae, *Laxus oneistus* and *Stilbonema* sp., was assessed by taking sediment cores together with physicochemical

properties of the respective layers in which they reside. The volume of interstitial water taken for measurements was lower than the water holding capacity of the sediment, therefore the measurements represented the actual properties of the respective layer.

The vertical distribution of Stilbonematinae, in particular *L. oneistus*, shows a distinct maximum at low sulfidic (< 20 µM) and low oxygen (< 20 µM) concentrations, although their presence cannot be excluded in normoxic pore water in the upper layers. There is a trend that water above the RPD layer (chemocline) has a higher oxygen content and vice versa, but this correlation has to be taken with care since multiple abiotic parameters influence the position of this layer [350]. Generally, the RPD layer constitutes the lower limit of depth for strictly aerobic organisms with small amounts of oxidized and reduced compounds, also because toxic sulfide is produced. In contrast, some species such as *I. leukodermatus* or stilbonematid nematodes thrive under these conditions and reach a maximum in distribution around the RPD layer, where sulfide and oxygen co-occur [1,19,199]. This narrow but dynamic niche is due to oxygen diffusing down from the surface layer and sulfide diffusing up from the deeper layers and is characterized by the presence of photosynthetic and non-photosynthetic sulfur-oxidizing bacteria [351]. In this work, the conducted oxygen measurements were most likely not sensitive enough to distinguish between low hypoxic and completely anoxic (strictly speaking 0 µM oxygen concentration) environments, and contamination of oxygen through the tubes cannot be excluded.

In coarse sediments, the RPD layer is deeper due to the diffusion of oxygen [113]. Therefore, different sediment types influence the physicochemical conditions and, in turn, nematode vertical distribution. In Piran, Slovenia, the low porosity and low permeability due to the increase of clay and silt in the sediment determine the nutrient-rich conditions [21], since oxygen can only penetrate the first few cm [352–354]. As apparent in the Piran sediment cores, sulfur leakage and oxygen consumption because of microbial degradation of organic matter (e.g. DOC) lead to a subsurface layer with less than 100 % oxygen saturation (Figure 20. Depth gradient of sulfide, oxygen, ammonium, nitrite and nitrate in costal subtidal sediments of the Northern Adriatic Sea near Piran, Slovenia. Each measurement represents the mean concentration and standard error of 5 measurements.).

Another feature of deeper sediment layers is the stability of temperature, salinity, pore water content and lack of temporal/seasonal variation that influences meiobenthic distribution [355]. In contrast, upper layers undergo surface cooling and wind action causing a

homogenization of the physical and chemical profiles [351]. A vertical migration of meiobenthic animals might, therefore, be the case if the environment is disturbed [198]. Non-symbiotic nematodes showed directed geotaxis to high CO_2 concentrations or to end products of fermentation [356,357] since these small animals cannot span oxygenated and sulfidic layers as bivalves and pogonophores do.

The upper few centimeters are mostly inhabited by autotrophic bacteria due to light and presence of free oxygen, but their abundance decreases with depth. Since sulfate is highly available throughout the sand column, sulfate reduction is the dominating process [358]. Nitrification processes contribute to nitrate and nitrite concentrations which were low throughout the sand columns. Uptake of nitrate in low concentrations is known from photoautotrophic symbioses [359]. In Piran and CBC, ammonia concentrations generally increased with depth, whereas nitrate and nitrite showed irregular patterns [355]. Ammonia concentrations varied as previously reported [360,361], but is the main nitrogen source for bacteria besides free amino acids in tropical sands [148,362]. Ammonia leaking from hosts and recycling within the symbiosis are other typical sources [363–366].

Throughout the world, sulfide is present in all deeper layers in marine sediments [1,367,368], although stilbonematid nematodes do not encounter high sulfidic habitats [10,11]. In addition, H_2S can precipitate as ferrous sulfide (pyrite) that appears black in deeper layers where no oxygen is present [1]. The yellow color of the sediment in the upper layers is mostly due to ferric iron [1]. Since oxygen is rapidly consumed in the lower layers, organisms rely on alternative electron acceptors such as nitrate, manganese (Mn^{4+}) or iron (Fe^{3+}) for sulfide oxidation. Since the potential for denitrification or usage of other electron acceptors was not known at that time, a temporal and spatial separation in oxygen and sulfide consumption was postulated [199,369,370].

All Stilbonematinae described so far develop in the interstitial waters of coarse sands and harbor chemoautotrophic bacteria [131,185,371]. Therefore, a common vertical migration and thus co-occurrence was assumed [10,11]. This co-occurrence holds true for *Laxus oneistus* and *Stilbonema* sp., although the latter was more evenly distributed across the layers (Figure 21B). No stilbonematid nematodes were retrieved from sediment cores taken in Piran, although a maximum abundance at 4 to 7 cm bsf can be assumed due to the low oxygen and moderate sulfide concentrations. Stilbonematinae belonging to the *Eubostrichus* genus were collected during previous field trips (Silvia Bulgheresi and Harald Gruber-Vodicka, pers. comm.).

Metabolic response of nematode symbionts to different oxygen conditions

The holobiont *Catanema quadratus* with *Cand.* T. quadrati was incubated in oxic and hypoxic seawater and the symbiont's metabolic response measured via qPCR. The incubation medium contained ammonium, nitrate and nitrite concentrations comparable to those measured *in situ* (Figure 18, Table 12). There was a substantial decrease in oxygen for the oxic 72 h incubations which is likely due to the closure of the incubation vials and subsequent oxygen consumption by the nematodes and bacterial contaminants in the medium.

For normalization of gene expression data, various genes are taken depending on the system and context [372,373]. Generally, there is a trend that housekeeping genes – genes that are constitutively expressed despite any fluctuating condition – also essential genes for replication, translation and central metabolism [372,373]. Between two essential genes, *rpoB* (RNA polymerase, subunit β) and 16*S* rDNA, *rpoB* was the most stably expressed under the performed incubations. Although highly context-specific, expression of 16*S* rDNA is mostly linked to general activity of a cell [374,375]. The variation in efficiencies is due to PCR inhibitors that have accumulated during RNA extraction and cDNA synthesis and different primers [376].

Incubation for 72 h (but not after 48 h) elicits a statistically highly significant reduction in *aprA* gene expression. The two genes for sulfide oxidation, *aprA* (APS reductase, alpha subunit) and *dsrA* (dissimilatory sulfite reductase, alpha subunit), showed a decrease upon 72 h likely because the symbionts' stored sulfur granules were consumed, as no additional sulfur source was added. Upregulation of the APS reductase pathway in hydrothermal vent snail *Ifremeria nautilei* symbionts and of reverse-type dissimilatory sulfite reductase and APS reductase pathway in *Allochromatium vinosum* was shown as a direct response if reduced sulfur compounds are supplemented [374,375]. The upregulation in *Cand.* T. quadrati of these two S oxidation genes is likely connected to the upregulation of *norB* (nitric oxide reductase cytochrome, beta subunit), a key enzyme involved in denitrification. Since both oxygen and nitrate can be used as electron acceptors [118], they both may serve as such. Moreover, denitrification is not strictly an anaerobic process [377,378] and its gene transcription can be uncoupled from oxygen concentrations [379]. In contrast, symbioses in vent ecosystems seem not to rely on nitrate as an electron acceptor because oxygen concentrations can be high [380]. This boost of chemosynthesis by simultaneous respiration of oxygen and nitrate might as well

explain the upregulation *cbbL* (ribulose bisphosphate carboxylase large chain), and therefore carbon fixation, in the hypoxic incubations irrespective of the time point. The same response was also shown in *I. nautilei* symbionts [381] and is supported by incubations with stable carbon isotopes (Gabriela Paredes, pers. comm.). Since nitrogen fixation is highly sensitive to oxygen and therefore tightly downregulated in its presence due to irreversible inhibition of the catalytic center [382,383], *nifH* (nitrogenase iron protein) is not expressed in *Cand.* T. quadrati within the first 48 h. Presence of ammonium in the incubation medium, as well as host-secreted ammonium might explain this. Nonetheless, after 72 h there is an upregulation that might be connected to depletion of ammonia in the incubation medium.

Conclusions

The genome of *Cand.* T. oneisti was assembled by combining short, highly accurate Illumina reads (100 bp) and long, error-prone ONT reads (< 121 kbp). The synergy between the two sequencing techniques drastically improved the available, Illumina-based only assembly.

Although all pathways for a host-independent lifestyle are present in the *Cand.* T. oneisti genome (no evidence of size reduction), putative bacterial adaptations for a symbiotic lifestyle were identified. These include a high number of transposons and TA-systems, and points to an importance in fine-tuning the metabolic responses in its dynamic, host-attached environment. Moreover, the high number of repeats within its genome is indicative of a high level of genome plasticity and promiscuous ecological lifestyle. However, closure of the genome is crucial to confirm the presence of repeats. Since repeats and possible within population heterogeneity pose a problem in the assembly, long-read sequencing approaches have to be pursued, such as higher ONT-based coverage or even single-cell sequencing. Closure of the genome and comparative approaches could shed light on symbiosis-specific functions across different nematode-associated bacteria.

Concerning the vertical distribution of two stilbonematid nematodes (*Laxus oneistus* and *Stilbonema* sp.) in the interstitial pore water in the Caribbean Sea, their highest abundance was recorded at micro-oxic (< 20 µM) and low sulfidic (< 20 µM) conditions, with low nitrate (< 1.5 µM) and moderate ammonium concentrations (< 126 µM). The use of needle-type microsensors for *in situ* measurements, including the redox potential, might confirm and refine the observed trend.

Finally, the metabolic response of the nematode symbionts to different oxygen regimes was tested for the first time. By simultaneous respiration of oxygen and nitrate, sulfide oxidation and carbon fixation are both fuelled and upregulated. Comparative analysis of the holobiont's transcriptomes in the whole range of environmental conditions it may encounter is necessary to understand how these affect not only its metabolism and immunity but, more generally, its physiology. In turn, grasping symbiosis physiology is mandatory to establish laboratory cultures and genetic tools for testing the functions of genetic repertoires.

Based on the vertical distribution and the metabolic response, this suggests that the nematode host transports its symbiont to conditions that optimize the metabolic activity of the latter. Nevertheless, the putative bacterial factors (e.g. ncRNA, metabolites) that might control

host behaviour await to be discovered. Moreover, to which degree the host profits from its symbiont's well-being is still under investigation.

German Abstract

Freilebende marine Fadenwürmer, die zur Unterfamilie Stilbonematinae gehören, tragen symbiotische, autotrophe Schwefel-oxidierende Gammaproteobakterien der Gattung *Candidatus* Thiosymbion auf ihrer Kutikula (Ektosymbionten). Als prominentes Mitglied des Thiobios können sie in extrem hoher Anzahl (> 10^5 pro m^2) in Flachwassersedimenten vorkommen, die durch oxygenierte obere und anoxische, tiefer liegende sulfidreiche Schichten gekennzeichnet sind. Daher könnte diese chemoautotrophe Symbiose wesentlich zu S, C und N-Zyklen in marinen Sedimenten im Flachwasser beitragen und ihre Biogeochemie beeinflussen. Es wurde lange angenommen, dass die Symbionten mit den Nematoden eine Symbiose eingehen, um ihre vertikale Migration durch diese Redoxzone auszunutzen. Dies würde ihnen den Zugang zu Sulfid (Elektronendonor) als auch Sauerstoff (Elektronenakzeptor) für den Prozess der Schwefeloxidation ermöglichen. In dieser Arbeit untersuchten wir die metabolischen Anpassungen von stilbonematid Symbionten durch: (1) Rekonstruktion von Stoffwechselwegen der Symbionten und Adaptionen, die für eine symbiotische Existenz von Nutzen sein könnten. Hierfür wurde eine Kombination von kurzen (Illumina) und ultra-langen (Oxford Nanopore Technologies) Sequenziertechnologien für den Genomzusammenbau verwendet; (2) Messung ihrer vertikalen Verteilung und der physikalisch-chemischen Parameter, denen Nematoden im Sediment von Carrie Bow Cay, Belize, und Piran, Slowenien, begegnen; (3) Auswirkung von hohem und niedrigem Sauerstoffgehalt auf den S, C, N-Metabolismus von Symbionten mittels Quantifizierung der Transkription von metabolischen Schlüsselgenen (*aprA*, *dsrA*, *norB*, *cbbL*, *nifH*) über 72 h.

Die Ergänzung von Illumina-Sequenzen mit langen Sequenzen (max. 121 kbp) verbesserte die Gesamtstatistik der Genomanordnung erheblich. Wie durch COG und Pfam Annotation bestimmt, besitzt *Cand.* Thiosymbion oneisti eine hohe Anzahl von Transposasen und Toxin-Antitoxin-Systemen zusätzlich zu einer großen Zahl an sich wiederholenden Genomabschnitten, und kodiert für einen vollständigen Typ-II-Sekretionsweg von Proteinen (mit Sec- und Tat-Pfaden), Typ IV-Pili und einem Sekretionssystem vom Typ VI. All dies deutet auf ein mobiles Genom und einen extrazellulären, vielseitigen ökologischen Lebensstil hin. Darüber hinaus wird die Vielfalt der Toxin-Antitoxin-Systeme als zelluläre Anpassung an Nährstofflimitierung und Umweltstress gesehen. Im Gegensatz dazu zeigte die metabolische Rekonstruktion, dass alle Stoffwechselwege, die für einen Wirt-unabhängigen Lebensstil notwendig sind, vollständig vorhanden sind und das Symbionten-Genom (4,3 Mbp) nicht

reduziert ist. Dazu gehören Auto- und Heterotrophie (Calvin-Zyklus, Citratzyklus), Schwefeloxidation (Sox/Reverser-Dsr-Weg), Denitrifikation, Stickstofffixierung, Biosynthese aller Aminosäuren, Gene für Cofaktor- und Vitaminbiosynthese (Biotin, Folat, Polyhydroxybutyrat, Riboflavin, Cobalamin, Häm) und ABC-Transporter (z.B. für Acetat, Ammonium, Molybdat, Harnstoff, Phosphat, Zink, Lipoproteine, Häm).

Die vertikale Verteilung von Stilbonematinae, insbesondere *Laxus oneistus*, zeigte ein ausgeprägtes Maximum bei niedrigen Sulfid- (< 20 µM) und Sauerstoffkonzentrationen (< 20 µM). Die Konzentrationen von Ammonium, Nitrat, Nitrit und gelöstem organischen Kohlenstoff variierten zwischen den Standorten, wobei Ammonium die Haupt-Stickstoffquelle für die Ektosymbionten sein könnte.

Die auf dem Genom basierenden Hypothesen, die in oxischen und hypoxischen Inkubationen getestet wurden, zeigten eine simultane Atmung von Sauerstoff und Nitrat zur Kohlenstofffixierung, die beide in der hypoxischen Inkubation überexprimiert waren. Beide Gene für Schwefeloxidation (*aprA*, *dsrA*) nahmen im Laufe der Zeit ab, vermutlich da der interne Schwefelspeicher aufgebraucht wurde. Darüber hinaus könnte die Stickstofffixierung (Transkription von *nifH*) bei einer 72 h langen Hypoxie zunehmen.

Zusammenfasend deuten die Daten auf einen vielseitigen Stoffwechselweg der stilbonematid Symbionten hin, der darauf optimiert ist, in einer Umwelt mit geringem Redoxpotential zu leben.

Acknowledgements

I am profoundly indebted to Silvia Bulgheresi as my supervisor for introducing me to the nematode-bacteria symbiosis, and for her invaluable advice, encouragement and insightful questions. Silvia's patient guidance and keenness assisted me in each step of this work. Her careful editing enormously improved this thesis.

To be able to stand on my own feet would have been impossible was it not for the continuous support, useful comments and friendship provided by Gabriela Paredes. Besides the fun we had in Carrie Bow Cay, the data on the sediment cores and qPCR would have been impossible to acquire without that joint effort.

Special thanks go to Jean Marie Volland for constantly providing specimen and helping me at various stages of the project. I would also like to thank Lena König for the RNA extraction protocol, the bioinformatics support and positive feedback. To Nika Pende, Philipp Weber and Friedrich Mössel for help in the lab and for keeping a sharp eye on the figures I produced.

The sequencing part would have been impossible to develop without the help and assistance of Patrick Hyden with whom the library preparation and the sequencing was done, Thomas Rattei (Department of Microbiology and Ecosystem Science) and Filipa Sousa. I want to express my appreciation to Michaela Mauß and Yin Chen (University of Warwick), Andreas Maier (Department of Geography and Regional Research, University of Vienna) and Harald Gruber-Vodicka (Max-Planck-Institute for Marine Microbiology).

I am thankful to Monika Bright, not only for broadening my understanding on chemosynthetic symbioses, but also for the delightful dialog over the whole time. I am thankful to Jörg Ott for the valuables on the work. Moreover, I thank Christa Schleper, everyone at the Archaea Biology and Ecogenomics Division and Wolfgang Miller and his group at the Medical University of Vienna for creating a marvelous working environment and many fruitful discussions.

References

1. Fenchel TM, Riedl RJ. The sulfide system: a new biotic community underneath the oxidized layer of marine sand bottoms. Mar Biol 7(3) 255-268. 1970;7: 255–268. doi:10.1007/BF00367496
2. Powell ES, Bright TJ. A Thiobios Does Exist - Gnathostomulid Domination of the Canyon Community at the East Flower Garden Brine Seep. Int Rev der gesamten Hydrobiol und Hydrogr. 1981;66: 675–683. doi:10.1002/iroh.19810660504
3. Jorgensen BB, Bak F. Pathways and microbiology of thiosulfate transformations and sulfate reduction in a marine sediment (Kattegat, Denmark). Appl Environ Microbiol. American Society for Microbiology; 1991;57: 847–856. Available: http://www.ncbi.nlm.nih.gov/pubmed/16348450
4. Jørgensen BB. Bacterial sulfate reduction within reduced microniches of oxidized marine sediments. Mar Biol. Springer-Verlag; 1977;41: 7–17. doi:10.1007/BF00390576
5. Schwinghamer P. Characteristic size distributions of integral benthic communities. Can J Fish Aquat Sci. NRC Research Press Ottawa, Canada; 1981;38: 1255–1263. doi:10.1139/f81-167
6. Warwick RM, Clarke KR. Species size distributions in marine benthic communities. Oecologia. Springer-Verlag; 1984;61: 32–41. doi:10.1007/BF00379085
7. Duplisea DE, Hargrave BT. Response of meiobenthic size-structure, biomass and respiration to sediment organic enrichment. Hydrobiologia. Kluwer Academic Publishers; 1996;339: 161–170. doi:10.1007/BF00008924
8. Giere O. Meiobenthology: The microscopic motile fauna of aquatic sediments. Meiobenthology: The Microscopic Motile Fauna of Aquatic Sediments. 2009. doi:10.1007/978-3-540-68661-3
9. Bright M, Arndt C, Keckeis H, Felbeck H. A temperature-tolerant interstitial worm with associated epibiotic bacteria from the shallow water fumaroles of Deception Island, Antarctica. Deep Res Part II Top Stud Oceanogr. 2003;50: 1859–1871. doi:10.1016/S0967-0645(03)00095-X
10. Ott JA, Novak R. Living at an interface: Meiofauna at the oxygen/sulfide boundary of marine sediments. Reprod Genet Distrib Mar Org 23rd Eur Mar Biol Symp. 1989; 415–422.
11. Ott JA, Novak R, Schiemer F, Hentschel U, Nebelsick M, Polz M. Tackling the Sulfide

Gradient: A Novel Strategy Involving Marine Nematodes and Chemoautotrophic Ectosymbionts. Mar Ecol. Wiley Online Library; 1991;12: 261–279. doi:10.1111/j.1439-0485.1991.tb00258.x

12. Ott JA, Bright M, Bulgheresi S. Symbioses between marine nematodes and sulfur-oxidizing chemoautotrophic bacteria. Symbiosis. 2004;36: 103–126.
13. Levin LA. Ecology of cold seep sediments: Interactions of fauna with flow, chemistry and microbes. An Annu Rev. CRC Press; 2005;43: 1–46. doi:doi:10.1201/9781420037449.ch1
14. Van Gaever S, Moodley L, de Beer D, Vanreusel A. Meiobenthos at the Arctic Hakon Mosby Mud Volcano, with a parental-caring nematode thriving in sulphide-rich sediments SO MARINE ECOLOGY-PROGRESS SERIES LA English DT Article DE deep-sea cold methane seep; sulphidic environment; meiobenthos; nematodes; Ge. Mar Ecol Prog Ser. Inter-Research Science Center; 321: 143–155. doi:10.2307/24870840
15. Kamenev GM, Fadeev VI, Selin NI, Tarasov VG, Malakhov V V. Composition and distribution of macro- and meiobenthos around sublittoral hydrothermal vents in the Bay of Plenty, New Zealand. New Zeal J Mar Freshw Res. 1993;27: 407–418. doi:10.1080/00288330.1993.9516582
16. Offer RW. Selected meiofauna around shallow water hydrot hermal vents off milos (greece) : eco log ical and ultrastructural aspects. Vie Milieu. 1994;44: 215–226.
17. Zekely J, Van Dover CL, Nemeschkal HL, Bright M. Hydrothermal vent meiobenthos associated with mytilid mussel aggregations from the Mid-Atlantic Ridge and the East Pacific Rise. Deep Res Part I Oceanogr Res Pap. 2006;53: 1363–1378. doi:10.1016/j.dsr.2006.05.010
18. Zeppilli D, Leduc D, Fontanier C, Fontaneto D, Fuchs S, Gooday AJ, et al. Characteristics of meiofauna in extreme marine ecosystems : a review. Mar Biodivers. Marine Biodiversity; 2017; doi:10.1007/s12526-017-0815-z
19. Ott JA, Schiemer F. Respiration and anaerobiosis of free living nematodes from marine and limnic sediments. Netherlands J Sea Res. 1973;7: 233–243. doi:10.1016/0077-7579(73)90047-1
20. Ott JA. Determination of Fauna Boundaries of Nematodes in an Intertidal Sand Flat. Int Rev der gesamten Hydrobiol und Hydrogr. 1972;57: 645–663. doi:10.1002/iroh.19720570413

21. Giere O. Beziehungen zwischen abiotischem Faktorensystem, Zonierung und Abundanz mariner Oligochäten in einem Küstengebiet der Nordsee. Thalass Jugosl. 1971;7: 67-.
22. Moore HB. The muds of the Clyde Sea area. III. Chemical and physical conditions; rate and nature of sedimentation; and fauna. J Mar Biol Assoc United Kingdom. Cambridge University Press; 1931;24: 325–365. doi:10.1017/S0025315400050876
23. Fenchel TM. The Ecology of Micro-and Meiobenthos. Annu Rev Ecol Syst. Annual Reviews 4139 El Camino Way, P.O. Box 10139, Palo Alto, CA 94303-0139, USA; 1978;9: 99–121. doi:10.1146/annurev.es.09.110178.000531
24. Reise K, Ax P. A meiofaunal "thiobios" limited to the anaerobic sulfide system of marine sand does not exist. Mar Biol. Springer-Verlag; 1979;54: 225–237. doi:10.1007/BF00395785
25. Reise K, Ax P. Statement on the Thiobios-Hypothesis. Mar Biol. Springer-Verlag; 1981;32: 80215. doi:10.1007/BF00386876
26. Powell EN, Bright TJ, Woods A, Gittings S. Meiofauna and the thiobios in the East Flower Garden brine seep. Mar Biol. Springer; 1983;73: 269–283.
27. Giere O, Langheld C. Structural organisation, transfer and biological fate of endosymbiotic bacteria in gutless oligochaetes. Mar Biol. Springer-Verlag; 1987;93: 641–650. doi:10.1007/BF00392801
28. Powell E. Oxygen , sulfide and diffusion : Why thiobiotic meiofauna must be sulfide-insensitive first-order respirers. J Mar Res. 1989;47: 887–932. doi:10.1357/002224089785076082
29. Schiemer F, Novak R, Ott JA. Metabolic studies on thiobiotic marine free-living nematodes (Desmodoridae: Stilbonematinae) and their symbiotic microorganisms. Mar Biol. Springer; 1990;106: 129–137.
30. Vopel K, Dehmlow J, Arlt G. Vertical distribution of Cletocamptus confluens (Copepoda, Harpacticoida) in relation to oxygen and sulphide microprofiles of a brackish water sulphuretum [Internet]. Marine Ecology Progress Series. Inter-Research Science Center; 1996. pp. 129–137. doi:10.2307/24857198
31. Grieshaber MK, Völkel S. Animal Adaptations for Tolerance and Exploitation of Poisonous Sulfide. Annu Rev Physiol. Annual Reviews 4139 El Camino Way, P.O. Box 10139, Palo Alto, CA 94303-0139, USA ; 1998;60: 33–53.

doi:10.1146/annurev.physiol.60.1.33

32. Bernhard JM, Buck KR, Farmer MA, Bowser SS. The Santa Barbara Basin is a symbiosis oasis. Nature. 2000;403: 77–80. doi:10.1038/47476
33. Powell EN, Crenshaw MA, Rieger RM. Adaptation to sulfide in sulfide-system meiofauna. End products of sulfide detoxification in three tubellarians and a gastrotrich. Mar Ecol Prog Ser. 1980;2: 169–177.
34. Somero GN, Childress JJ, Anderson AE. Transport, metabolism, and detoxification of hydrogen sulfide in animals from sulfide-rich marine environments. Rev Aquat Sci RAQSEL. 1989;1.
35. Bonn EW, Follis BJ. Effects of hydrogen sulfide on channel catfish, Ictalurus punctatus. Trans Am Fish Soc. Taylor & Francis Group; 1967;96: 31–36. doi:10.1577/1548-8659(1967)96[31:EOHSOC]2.0.CO;2
36. Evans CL. The toxicity of hydrogen sulphide and other sulphides. Q J Exp Physiol Cogn Med Sci. 1967;52: 231–248. doi:10.1113/expphysiol.1967.sp001909
37. Oseid DM, Smith Jr. LL. Chronic toxicity of hydrogen sulfide to Gammarus pseudolimneatus. Trans Am Fish Soc. Taylor & Francis Group; 1974;103: 819–822. doi:10.1577/1548-8659(1974)103<819:CTOHST>2.0.CO;2
38. Oseid DM, Smith LL. Factors influencing acute toxicity estimates of hydrogen sulfide to freshwater invertebrates. Water Res. Pergamon; 1974;8: 739–746. doi:10.1016/0043-1354(74)90018-9
39. Hendelberg M, Jensen P. Vertical distribution of the nematode fauna in a coastal sediment influenced by seasonal hypoxia in the bottom water. Ophelia. 1993;37: 83–94. doi:10.1080/00785326.1993.10429909
40. Colby PJ, Smith LL. Survival of walleye eggs and fry on paper fiber sludge deposits in Rainy River, Minnesota. Trans Am Fish Soc. Taylor & Francis Group; 1967;96: 278–296. doi:10.1577/1548-8659(1967)96[278:SOWEAF]2.0.CO;2
41. Thiermann F, Vismann B, Giere O. Sulphide tolerance of the marine nematode Oncholaimus campylocercoides - A result of internal sulphur formation? Mar Ecol Prog Ser. 2000;193: 251–259. doi:10.3354/meps193251
42. Vetter RD, Powell MA, Somero GN. Metazoan adaptations to hydrogen sulphide. Metazoan life without Oxyg. Chapman and Hall London; 1991; 109–128.
43. Veldkamp H, Jannasch HW. Mixed culture studies with the chemostat. J Appl Chem

Biotechnol. John Wiley & Sons, Ltd; 1972;22: 105–123. doi:10.1002/jctb.2720220113

44. Powell EN, Crenshaw MA, Rieger RM. Adaptations to sulfide in the meiofauna of the sulfide system. I. 35S-sulfide accumulation and the presence of a sulfide detoxification system. J Exp Mar Bio Ecol. 1979;37: 57–76. doi:10.1016/0022-0981(79)90026-1
45. Powell A, Arp AJ. Hydrogen Sulfide Oxidation by Abundant Norhemoglobin Heme Compounds i n Marine Invertebrates From Sulfide-Rich Habitats. J Exp Biol. 1989;2.
46. Childress JJ, Arp AJ, Fisher CR. Metabolic and blood characteristics of the hydrothermal vent tube worm Riftia pachypitila. Mar Biol. The University of Chicago PressDivision of Comparative Physiology and Biochemistry, Society for Integrative and Comparative Biology; 1984;83: 109–124. doi:10.1007/BF00394718
47. Morrill AC, Powell EN, Bidigare RR, Shick JM. Adaptations to life in the sulfide system: a comparison of oxygen detoxifying enzymes in thiobiotic and oxybiotic meiofauna (and freshwater planarians). J Comp Physiol B. Springer-Verlag; 1988;158: 335–344. doi:10.1007/BF00695332
48. Giere O, Rhode B, Dubilier N. Structural peculiarities of the body wall of Tubificoides benedii (Oligochaeta) and possible relations to its life in sulphidic sediments. Zoomorphology. 1988;108: 29–39.
49. Thiermann F, Windoffer R, Giere O. Selected meiofauna around shallow water hydrothermal vents off Milos (Greece): ecological and ultrastructural aspects. Vie milieu. Laboratoire Arago, Université Pierre et Marie Curie; 1994;44: 215–226.
50. Dubilier N, Giere OO, Distel DL, Cavanaugh CM. Characterization of chemoautotrophic bacterial symhbionts in a gutless marine worm (Oligotropchaeta, Annelida) by phylogentetic 16S rRNA sequence analysis and in situ hybridization. Appl Environ Microbiol. 1995;61: 2346–2350.
51. Jahn A, Janas U, Theede H, Szaniawska A. Significance of body size in sulphide detoxification in the Baltic clam Macoma balthica (Bivalvia, Tellinidae) in the Gulf of Gdansk. Mar Ecol Prog Ser. Inter-Research Science Center; 1997;154: 175–183. doi:10.3354/meps154175
52. Jahn A, Gamenick I, Theede H. Physiological adaptations of Cyprideis torosa (Crustacea, Ostracoda) to hydrogen sulphide. Mar Ecol Prog Ser. Inter-Research Science Center; 1996;142: 215–223. doi:10.3354/meps142215
53. Powell MA, Somero GN. Adaptations to sulfide by hydrothermal vent animals: sites and

mechanisms of detoxification and metabolism. Biol Bull. Marine Biological Laboratory; 1986;171: 274–290. doi:10.2307/1541923

54. Völkel S, Grieshaber MK. Mitochondrial sulfide oxidation in Arenicola marina. Evidence for alternative electron pathways. Eur J Biochem. Blackwell Science Ltd; 1996;235: 231–7. doi:10.1111/j.1432-1033.1996.00231.x
55. Theede H, Oeschger R, Jahn A. Adaptive responses of marine benthic invertebrates to hydrogen sulphide. Olsen & Olsen, Fredensborg. 1995. pp. 149–152.
56. Fox CA, Powell EN. Meiofauna and the sulfide system: the effects of oxygen and sulfide on the adenylate pool of three turbellarians and a gastrotrich. Comp Biochem Physiol -- Part A Physiol. Pergamon; 1986;85: 37–44. doi:10.1016/0300-9629(86)90458-5
57. Fisher CR. Chemoautotrophic and methanotrophic symbioses in marine invertebrates. Rev Aquat Sci. 1990;2: 399–436.
58. Vismann B. Sulfide tolerance: Physiological mechanisms and ecological implications. Ophelia. Taylor & Francis; 1991;34: 1–27. doi:10.1080/00785326.1991.10429703
59. Bagarinao T. Sulfide as an environmental factor and toxicant: tolerance and adaptations in aquatic organisms. Aquat Toxicol. 1992;24: 21–62. doi:10.1016/0166-445X(92)90015-F
60. Fenchel T, Finlay BJ. Ecology and evolution in anoxic worlds. 1995. doi:10.1016/0169-5347(96)81069-X
61. Moodley L, Van Der Zwaan GJ, Herman PMJ, Kempers L, Van Breugel P. Differential response of benthic meiofauna to anoxia with special reference to Foraminifera (Protista: Sarcodina). Mar Ecol Prog Ser. Inter-Research Science Center; 1997;158: 151–163. doi:10.3354/meps158151
62. Danovaro R, Dell'Anno A, Pusceddu A, Gambi C, Heiner I, Kristensen RM. The first metazoa living in permanently anoxic conditions. BMC Biol. BioMed Central; 2010;8: 30. doi:10.1186/1741-7007-8-30
63. Danovaro R, Gambi C, Dell'Anno A, Corinaldesi C, Pusceddu A, Neves RC, et al. The challenge of proving the existence of metazoan life in permanently anoxic deep-sea sediments. BMC Biol. BioMed Central; 2016;14: 43. doi:10.1186/s12915-016-0263-4
64. Mentel M, Martin W. Anaerobic animals from an ancient, anoxic ecological niche. BMC Biol. BioMed Central; 2010;8: 32. doi:10.1186/1741-7007-8-32
65. Bernhard JM, Morrison CR, Pape E, Beaudoin DJ, Todaro MA, Pachiadaki MG, et al.

Metazoans of redoxcline sediments in Mediterranean deep-sea hypersaline anoxic basins. BMC Biol. 2015;13: 105. doi:10.1186/s12915-015-0213-6

66. Jensen P. Feeding ecology of free-living aquatic nematodes. Mar Ecol Prog Ser. 1987;35: 187–196. doi:10.3354/meps035187

67. Jensen P. Differences in microhabitat, abundance, biomass and body size between oxybiotic and thiobiotic free-living marine nematodes. Oecologia. 1987;71: 564–567. doi:10.1007/BF00379298

68. Jensen R. nematode fauna in the sulphide-richbrine seep and jacent bottoms of the East Flower Garden, NW Gulf of exico. Ill. Enoplida. Mar Biol. 1986;92: 93–99.

69. Vanreusel A, De Groote A, Gollner S, Bright M. Ecology and Biogeography of Free-Living Nematodes associated with Chemosynthetic Environments in the Deep Sea: A Review. PLoS One. 2010;5: e12449.

70. Southward AJ, Southward EC, Dando PR, Rau GH, Felbeck H, Flügel H. Bacterial symbionts and low 13C/12C ratios in tissues of Pogonophora indicate unusual nutrition and metabolism. Nature. 1981;293: 616–619. doi:10.1038/293616a0

71. Stewart FJ, Newton ILG, Cavanaugh CM. Chemosynthetic endosymbioses: Adaptations to oxic-anoxic interfaces. Trends Microbiol. 2005;13: 439–448. doi:10.1016/j.tim.2005.07.007

72. Brissac T, Mer??ot H, Gros O. Lucinidae/sulfur-oxidizing bacteria: Ancestral heritage or opportunistic association? Further insights from the Bohol Sea (the Philippines). FEMS Microbiol Ecol. 2011;75: 63–76. doi:10.1111/j.1574-6941.2010.00989.x

73. Boaden PJS. Thiobiotic facts and fancies (aspects of the distribution and evolution of anaerobic meiofauna). Mikrofauna Meeresboden. 1977;61: 45–63.

74. Boaden PJS. Anaerobiosis, Meiofauna and Early Metazoan Evolution. Zool Scr. Blackwell Publishing Ltd; 1975;4: 21–24. doi:10.1111/j.1463-6409.1975.tb00714.x

75. Tsurumi M, Tunnicliffe V. Tubeworm-associated communities at hydrothermal vents on the Juan de Fuca Ridge, northeast Pacific. Deep Res Part I Oceanogr Res Pap. Pergamon; 2003;50: 611–629. doi:10.1016/S0967-0637(03)00039-6

76. Colacino JM, Kraus DW. Hemoglobin-containing cells of Neodasys (gastrotricha, chaetonotida)-II. Respiratory significance. Comp Biochem Physiol -- Part A Physiol. Pergamon; 1984;79: 363–369. doi:10.1016/0300-9629(84)90528-0

77. Zajcev J, Ancupova L, Vorobyoya L, Garkayaya G, Kulakova I, Rusnak E. Nematodes

from the deep-water zone of the Black Sea. Dokl Acad Sci Ukr SSR, Ser B, Geol Chim Biol Nauk. 1987;11: 77–79.

78. Wieser W, Kanwisher J. Ecological and Physiological Studies on Marine Nematodes From a Small Salt Marsh Near Woods Hole, Massachusetts1. Limnol Oceanogr. 1961;6: 262–270. doi:10.4319/lo.1961.6.3.0262
79. Fonseca G, Hutchings P, Vieira DC, Gallucci F. Meiobenthic community underneath the carcass of a stingray a snapshot after natural death. Aquat Biol. 2011;13: 27–33. doi:10.3354/ab00347
80. Steyaert M, Moodley L, Nadong T, Moens T, Soetaert K, Vincx M. Responses of intertidal nematodes to short-term anoxic events. J Exp Mar Bio Ecol. 2007;345: 175–184. doi:10.1016/j.jembe.2007.03.001
81. Cook AA, John P, Hawkins LE, Mitchell N, Levin LA. Nematode abundance at the oxygen minimum zone in the Arabian Sea. Deep Res Part II Top Stud Oceanogr. Pergamon; 2000;47: 75–85. doi:10.1016/S0967-0645(99)00097-1
82. Aramayo Navarro VH, Aramayo Navarro VH. Análisis comunitario de la meiofauna metazoaria en sedimentos de la plataforma y talud continentales frente a Perú [Internet]. Repositorio de Tesis - UNMSM. Universidad Nacional Mayor de San Marcos. 2015. Available: http://cybertesis.unmsm.edu.pe/handle/cybertesis/4782
83. Luth C, Luth U, Gebruk A V., Thiel H. Methane gas Seeps Along the Oxic/Anoxic Gradient in the Black Sea: Manifestations, Biogenic Sediment Compounds and Preliminary Results on Benthic Ecology. Mar Ecol. 1999;20: 221–249. doi:10.1046/j.1439-0485.1999.t01-1-00073.x
84. Sergeeva NG, Gulin MB. Meiobenthos from an active methane seepage area in the NW Black Sea. Mar Ecol. Blackwell Publishing Ltd; 2007;28: 152–159. doi:10.1111/j.1439-0485.2006.00143.x
85. Sergeeva NG. Meiobenthos of deep-water anoxic hydrogen sulphide zone of the Black Sea. T$\ddot{\nu}$bitak Publ.; 2003;
86. Wieser W, Ott JA, Schiemer F, Gnaiger E. An ecophysiological study of some meiofauna species inhabiting a sandy beach at Bermuda. Mar Biol. 1974;26: 235–248. doi:10.1007/BF00389254
87. Por FD, Masry D. Survival of a nematode and an oligochaete species in anaerobic benthal of Lake Tiberias. Hydrobiol Bull. WileyNordic Society Oikos; 1968;17: 109.

doi:10.2307/3565023

88. Jensen P. Species distribution and a microhabitat theory for marine mud dwelling Comesomatidae (Nematoda) in european waters. Cah Biol Mar. Editions de la Station biologique de Roscoff; 1981;22: 231–241. Available: http://www.vliz.be/en/imis?refid=62875

89. Jensen P. Meiofaunal abundance and vertical zonation in a sublittoral soft bottom, with a test of the Haps corer. Mar Biol. Springer-Verlag; 1983;74: 319–326. doi:10.1007/BF00403458

90. Jensen P. Ecology of benthic and epiphytic nematodes in brackish waters. Hydrobiologia. Kluwer Academic Publishers; 1984;108: 201–217. doi:10.1007/BF00006329

91. Bouwman LA, Romeijn K, Admiraal W. On the ecology of meiofauna in an organically polluted estuarine mudflat. Estuar Coast Shelf Sci. Academic Press; 1984;19: 633–653. doi:10.1016/0272-7714(84)90020-9

92. Jensen KM, Cox RP. Effects of sulfide and low redox potential on the inhibition of nitrous oxide reduction by acetylene in Pseudomonas nautica. FEMS Microbiol Lett. No longer published by Elsevier; 1992;96: 13–18. doi:10.1016/0378-1097(92)90449-X

93. Theede H, Ponat A, Hiroki K, Schlieper C. Studies on the resistance of marine bottom invertebrates to oxygen-deficiency and hydrogen sulphide. Mar Biol. Springer-Verlag; 1969;2: 325–337. doi:10.1007/BF00355712

94. Oertsen JA, Schlungbaum G. Experimentell-ökologische Untersuchungen über O2-Mangel und H2S-Resistenz an marinen Evertebraten der westlichen Ostsee. Beitr Meereskd. 1972;29: 79–91.

95. Theede H. Comparative studies on the influence of oxygen deficiency and hydrogen sulphide on marine bottom invertebrates. Netherlands J Sea Res. Elsevier; 1973;7: 244–252. doi:10.1016/0077-7579(73)90048-3

96. Oeschger R. Long-term anaerobiosis in sublittoral marine invertebrates from the Western Baltic Sea: Halicryptus spinulosus (Priapulida), Astarte borealis and Arctica islandica (Bivalvia). Mar Ecol Prog Ser. Inter-Research Science Center; 1990;59: 133–143. doi:10.3354/meps059133

97. Oeschger R, Vetter RD. Sulfide detoxification and tolerance in Halicryptus spinulosus (Priapulida): a multiple strategy. Mar Ecol Prog Ser. Inter-Research Science Center; 86:

167–179. doi:10.2307/24830498

98. Rosenberg R, Hellman B, Johansson B. Hypoxic tolerance of marine benthic fauna. Mar Ecol Prog Ser. 1991;79: 127–131. doi:10.3354/meps079127

99. Gnaiger E. Animal energetics at very low oxygen: information from calorimetry and respirometry. Physiological strategies for gas exchange and metabolism (Society for experimental biology: Seminar series 41) Cambridge Univ Press, London. 1991. pp. 149–171.

100. Hodkinson ID, Bird JM. Anoxia tolerance in high Arctic terrestrial microarthropods. Ecol Entomol. Blackwell Science Ltd; 2004;29: 506–509. doi:10.1111/j.0307-6946.2004.00619.x

101. Fortey RA, Briggs DEG, Wills MA. The Cambrian evolutionary "explosion": Decoupling cladogenesis from morphological disparity. Biol J Linn Soc. Blackwell Publishing Ltd; 1996;57: 13–33. doi:10.1111/j.1095-8312.1996.tb01693.x

102. Schiemer F. Respiration rates of two species of Gnathostomulids. Oecologia. Springer-Verlag; 1973;13: 403–406. doi:10.1007/BF01825529

103. Heip C, Vincx M, Vrank. The ecology of marine nematodes. Oceanogr. Mar. Biol. Ann. Rev. 1985. pp. 399–489.

104. Duffy JE, Tyler S. Quantitative differences in mitochondrial ultrastructure of a thiobiotic and an oxybiotic turbellarian. Mar Biol. Springer-Verlag; 1984;83: 95–102. doi:10.1007/BF00393089

105. Giere O, Wirsen CO, Schmidt C, Jannasch HW. Contrasting effects of sulfide and thiosulfate on symbiotic CO2-assimilation of Phallodrilus leukodermatus (Annelida). Mar Biol. Springer-Verlag; 1988;97: 413–419. doi:10.1007/BF00397771

106. Jennings JB, Hick AJ. Differences in the distribution, mitochondrial content and probable roles of haemoglobin-containing parenchymal cells in four species of entosymbiotic turbellarians (Rhabdocoela: Umagillidae and pterastericolidae). Ophelia. Taylor & Francis Group; 1990;31: 163–175. doi:10.1080/00785326.1990.10430859

107. Famme P, Knudsen J. Anoxic survival, growth and reproduction by the freshwater annelid, Tubifex sp., demonstrated using a new simple anoxic chemostat. Comp Biochem Physiol -- Part A Physiol. 1985;81: 251–253. doi:10.1016/0300-9629(85)90130-6

108. de Zwaan A, Putzer V. Metabolic adaptations of intertidal invertebrates to

environmental hypoxia (a comparison of environmental anoxia to exercise anoxia). Symp Soc Exp Biol. 1985;39: 33–62. Available: http://www.ncbi.nlm.nih.gov/pubmed/3914721

109. Schöttler U, Bennet EM. Annelids. Metazoan life without Oxyg Chapman Hall, London. 1991; 165–185.
110. Steyaert M, Moodley L, Vanaverbeke J, Vandewiele S, Vincx M. Laboratory experiments on the infaunal activity of intertidal nematodes. Hydrobiologia. 2005;540: 217–223. doi:10.1007/s10750-004-7145-4
111. Ritt B, Sarrazin J, Caprais JC, Noël P, Gauthier O, Pierre C, et al. First insights into the structure and environmental setting of cold-seep communities in the Marmara Sea. Deep Res Part I Oceanogr Res Pap. Pergamon; 2010;57: 1120–1136. doi:10.1016/j.dsr.2010.05.011
112. Moens T, dos Santos GAPG, Thompson F, Swings J, Fonsêca-Genevois V, Vincx M, et al. Do nematode mucus secretions affect bacterial growth? Aquat Microb Ecol. 2005;40: 77–83. doi:10.3354/ame040077
113. Moens T, Braeckman U, Derycke S, Fonseca G, Gallucci F, Gingold R, et al. 3. Ecology of free-living marine nematodes. Nematoda. 2013; doi:10.1515/9783110274257.109
114. Ott JA, Rieger G, Rieger R, and Enderes F. New mouthless interstitial worms from the sulfide system: symbiosis with prokaryotes. Mar Ecol. 1982;3: 313–333.
115. Lee RW. Physiological adaptations of the invasive cordgrass Spartina anglica to reducing sediments: Rhizome metabolic gas fluxes and enhanced O2 and H2S transport. Mar Biol. Springer-Verlag; 2003;143: 9–15. doi:10.1007/s00227-003-1054-3
116. Wetzel MA, Jensen P, Giere O. Oxygen/sulfide regime and nematode fauna associated with Arenicola marina burrows: new insights in the thiobios case. Mar Biol. Springer-Verlag; 1995;124: 301–312. doi:10.1007/BF00347134
117. Fenchel T. Worm burrows and oxic microniches in marine sediments. 1. Spatial and temporal scales. Mar Biol. Springer-Verlag; 1996;127: 289–295. doi:10.1007/BF00942114
118. Hentschel U, Berger E, Bright M, Felbeck H, Ott JA. Metabolism of nitrogen and sulfur in ectosymbiotic bacteria of marine nematodes(Nematoda, Stilbonematinae). Mar Ecol Prog Ser. 1999;183: 149–158.
119. Cavanaugh CM, Gardiner SL, Jones ML, Jannasch HW, Waterbury JB. Prokaryotic Cells

in the Hydrothermal Vent Tube Worm Riftia pachyptila Jones: Possible Chemoautotrophic Symbionts. Science (80-). American Association for the Advancement of Science; 1981;213: 340–342. doi:10.1126/science.213.4505.340

120. Felbeck H. Chemoautotrophic Potential of the Hydrothermal Vent Tube Worm, Riftia pachyptila Jones (Vestimentifera). Science (80-). American Association for the Advancement of Science; 1981;213: 336–338. doi:10.1126/science.213.4505.336
121. Childress JJ, Fisher CR. The biology of hidrothermal vent animals: physiolgy, biochemistry, and autotrophic symbioses. Ocean Mar Biol Annu Rev. 1992;30: 337–441.
122. Southward E. Gill symbionts in thyasirids and other bivalve molluscs. J Mar Biol Assoc United Kingdom. Cambridge University Press; 1986;66: 889–914. doi:10.1017/S0025315400048517
123. Nelson DC, Fisher CR, Karl DM. The Microbiology of Deep-Sea Hydrothermal Vents. Microbiol Deep Hydrothermal Vent. CRCBoca Raton; 1995;
124. Fisher CR. Toward an Appreciation of Hydrothennal-Vent Animals: Their Environment, Physiological Ecology, and Tissue Stable Isotope Values. Seafloor Hydrothermal Systems: Physical, Chemical, Biological, and Geological Interactions. American Geophysical Union; 1995. pp. 297–316. doi:10.1029/GM091p0297
125. Giere O. Bacterial endosymbioses in marine littoral worms. Deep-sea and extreme shallow-water habitats: affinities and adaptations. na; 1996.
126. Bright M, Giere O. Microbial Symbiosis in Annelida. Environments. 2005;38: 1–45.
127. Dubilier N, Blazejak A, Ruehland C. Symbioses between Bacteria and Gutless Marine Oligochaetes. In: Overmann J, editor. Molecular Basis of Symbiosis. Springer; 2006. doi:10.1007/3-540-28221-1_9
128. Musat N, Giere O, Gieseke A, Thiermann F, Amann R, Dubilier N. Molecular and morphological characterization of the association between bacterial endosymbionts and the marine nematode Astomonema sp. from the Bahamas: Brief report. Environ Microbiol. England; 2007;9: 1345–1353. doi:10.1111/j.1462-2920.2006.01232.x
129. Miljutin D, Tchesunov A V, Hope D. Rhaptothyreus typicus Hope Murphy, 1969 (Nematoda: Rhaptothyreidae): an anatomical study of an unusual deep-sea nematode. Nematology. Brill; 2006;8: 1–20. doi:10.1163/156854106776179971
130. Felbeck H, Liebezeit G, Dawson R, Giere O. CO2 fixation in tissues of marine oligochaetes (Phallodrilus leukodermatus and P. planus) containing symbiotic,

chemoautotrophic bacteria. Mar Biol. Springer-Verlag; 1983;75: 187–191. doi:10.1007/BF00406001

131. Dubilier N, Bergin C, Lott C. Symbiotic diversity in marine animals: the art of harnessing chemosynthesis. Nat Rev Microbiol. 2008/09/17. Nature Publishing Group; 2008;6: 725–40. doi:10.1038/nrmicro1992

132. Muller F, Brissac T, Le Bris N, Felbeck H, Gros O. First description of giant Archaea (Thaumarchaeota) associated with putative bacterial ectosymbionts in a sulfidic marine habitat. Environ Microbiol. Blackwell Publishing Ltd; 2010;12: 2371–2383. doi:10.1111/j.1462-2920.2010.02309.x

133. Roeselers G, Newton ILGG. On the evolutionary ecology of symbioses between chemosynthetic bacteria and bivalves. Appl Microbiol Biotechnol. Springer; 2012;94: 1–10. doi:10.1007/s00253-011-3819-9

134. Distel DL, Morrill W, MacLaren-Toussaint N, Franks D, Waterbury J. Teredinibacter turnerae gen. nov., sp. nov., a dinitrogen-fixing, cellulolytic, endosymbiotic γ-proteobacterium isolated from the gills of wood-boring molluscs (Bivalvia: Teredinidae). Int J Syst Evol Microbiol. 2002;52: 2261–2269. doi:10.1099/ijs.0.02184-0

135. Herry A, Diouris M, Le Pennec M. Chemoautotrophic symbionts and translocation of fixed carbon from bacteria to host tissues in the littoral bivalve Loripes lucinalis (Lucinidae). Mar Biol. Springer-Verlag; 1989;101: 305–312. doi:10.1007/BF00428126

136. Glover EA, Taylor JD, Rowden AA. Bathyaustriella Thionipta, a New Lucinid Bivalve From a Hydrothermal Vent on the Kermadec Ridge, New Zealand and Its Relationship To Shallow-Water Taxa (Bivalvia: Lucinidae). J Molluscan Stud. Oxford University Press; 2004;70: 283–295. doi:10.1093/mollus/70.3.283

137. Hentschel U, Felbeck H. Nitrate respiration in chemoautotrophic symbionts of the bivalve Lucinoma aequizonata is not regulated by oxygen. Appl Environ Microbiol. 1995;61: 1630–1633. Available: http://www.ncbi.nlm.nih.gov/pubmed/16535006

138. Wilmot DB, Vetter RD. Oxygen-and nitrogen-dependent sulfur metabolism in the thiotrophic clam Solemya reidi. Biol Bull. Marine Biological Laboratory; 1992;182: 444. doi:10.2307/1542264

139. Duplessis MR, Ziebis W, Gros O, Caro A, Robidart J, Felbeck H. Respiration strategies utilized by the gill endosymbiont from the host lucinid Codakia orbicularis (Bivalvia: Lucinidae). Appl Environ Microbiol. 2004;70: 4144–4150. doi:10.1128/AEM.70.7.4144-

4150.2004

140. Stewart FJ, Dmytrenko O, Delong EF, Cavanaugh CM. Metatranscriptomic analysis of sulfur oxidation genes in the endosymbiont of Solemya velum. Front Microbiol. Frontiers; 2011;2: 134. doi:10.3389/fmicb.2011.00134

141. Duperron S, Bergin C, Zielinski F, Blazejak A, Pernthaler A, McKiness ZP, et al. A dual symbiosis shared by two mussel species, Bathymodiolus azoricus and Bathymodiolus puteoserpentis (Bivalvia: Mytilidae), from hydrothermal vents along the northern Mid-Atlantic Ridge. Environ Microbiol. 2006;8: 1441–1447. doi:10.1111/j.1462-2920.2006.01038.x

142. DeChaine EG, Cavanaugh CM. Symbioses of methanotrophs and deep-sea mussels (Mytilidae: Bathymodiolinae). Prog Mol Subcell Biol. 2006;41: 227–249. Available: http://www.ncbi.nlm.nih.gov/pubmed/16623396

143. Stein JL, Haygood M, Felbeck H. Nucleotide-Sequence and Expression of a Deep-Sea Ribulose-1,5-Bisphosphate Carboxylase Gene Cloned from a Chemoautotrophic Bacterial Endosymbiont. Proc Natl Acad Sci U S A. 1990;87: 8850–8854. doi:Doi 10.1073/Pnas.87.22.8850

144. Ponnudurai R, Kleiner M, Sayavedra L, Petersen JM, Moche M, Otto A, et al. Metabolic and physiological interdependencies in the Bathymodiolus azoricus symbiosis. ISME J. Nature Publishing Group; 2017;11: 463–477. doi:10.1038/ismej.2016.124

145. Scott KM, Cavanaugh CM. CO2 uptake and fixation by endosymbiotic chemoautotrophs from the bivalve Solemya velum. Appl Environ Microbiol. 2007;73: 1174–1179. doi:10.1128/AEM.01817-06

146. Schwedock J, Harmer TL, Scott KM, Hektor HJ, Seitz AP, Fontana MC, et al. Characterization and expression of genes from the RubisCO gene cluster of the chemoautotrophic symbiont of Solemya velum: cbbLSQO. Arch Microbiol. 2004;182: 18–29. doi:10.1007/s00203-004-0689-x

147. Petersen JM, Kemper A, Gruber-Vodicka H, Cardini U, van der Geest M, Kleiner M, et al. Chemosynthetic symbionts of marine invertebrate animals are capable of nitrogen fixation. Nat Microbiol. Nature Publishing Group; 2016;2: 16195. doi:10.1038/nmicrobiol.2016.195

148. König S, Gros O, Heiden SE, Hinzke T, Thürmer A, Poehlein A, et al. Nitrogen fixation in a chemoautotrophic lucinid symbiosis. Nat Microbiol. Nature Publishing Group;

2016;2: 16193. doi:10.1038/nmicrobiol.2016.193

149. Caro A, Got P, Bouvy M, Troussellier M, Gros O. Effects of long-term starvation on a host bivalve (Codakia orbicularis, lucinidae) and its symbiont population. Appl Environ Microbiol. American Society for Microbiology; 2009;75: 3304–3313. doi:10.1128/AEM.02659-08

150. Brissac T, Gros O, Merçot H, Mer??ot H. Lack of endosymbiont release by two Lucinidae (Bivalvia) of the genus Codakia: Consequences for symbiotic relationships. FEMS Microbiol Ecol. The Oxford University Press; 2009;67: 261–267. doi:10.1111/j.1574-6941.2008.00626.x

151. König S, Le Guyader H, Gros O. Thioautotrophic bacterial endosymbionts are degraded by enzymatic digestion during starvation: Case study of two lucinids Codakia orbicularis and C. orbiculata. Microsc Res Tech. 2015;78: 173–179. doi:10.1002/jemt.22458

152. Higgs ND, Newton J, Attrill MJ. Caribbean Spiny Lobster Fishery Is Underpinned by Trophic Subsidies from Chemosynthetic Primary Production. Curr Biol. Elsevier Ltd.; 2016;26: 3393–3398. doi:10.1016/j.cub.2016.10.034

153. van der Heide T, Govers LL, de Fouw J, Olff H, van der Geest M, van Katwijk MM, et al. A Three-Stage Symbiosis Forms the Foundation of Seagrass Ecosystems. Science (80-). 2012;336: 1432–1434. doi:10.1126/science.1219973

154. Johnson KS, Childress JJ, Beehler CL, Sakamoto CM. Biogeochemistry of hydrothermal vent mussel communities: the deep-sea analogue to the intertidal zone. Deep Res Part I. Pergamon; 1994;41: 993–1011. doi:10.1016/0967-0637(94)90015-9

155. Zal F, Leize E, Oros DR, Hourdez S, Dorsselaer A Van, Childress JJ. Haemoglobin structure and biochemical characteristics of the sulphide-binding component from the deep-sea clam Calyptogena magnifica. Cah Biol Mar. 2000;41: 413–423. Available: https://www.researchgate.net/profile/James_Childress2/publication/250003140_Haemoglobin_structure_and_biochemical_characteristics_of_the_sulphide-binding_component_from_the_deep-sea_clam_Calyptogena_magnifica/links/00b4953a1687799c97000000.pdf

156. Doeller JE, Kraus DW, Colacino JM, Wittenberg JB. Gill Hemoglobin May Deliver Sulfide to Bacterial Symbionts of Solemya velum (Bivalvia, Mollusca). Biol Bull. Marine Biological Laboratory; 1988;175: 388–396. doi:10.2307/1541730

157. Distel DL, Beaudoin DJ, Morrill W. Coexistence of multiple proteobacterial

endosymbionts in the gills of the wood-boring bivalve Lyrodus pedicellatus (Bivalvia: Teredinidae). Appl Environ Microbiol. American Society for Microbiology; 2002;68: 6292–6299. doi:10.1128/AEM.68.12.6292-6299.2002

158. O'Connor RM, Fung JM, Sharp KH, Benner JS, McClung C, Cushing S, et al. Gill bacteria enable a novel digestive strategy in a wood-feeding mollusk. Proc Natl Acad Sci. National Academy of Sciences; 2014;111: E5096–E5104. doi:10.1073/pnas.1413110111
159. Carpenter EJ, Culliney JL. Nitrogen fixation in marine shipworms. Science (80-). American Association for the Advancement of Science; 1975;187: 551–552. doi:10.1126/science.187.4176.551
160. Giere O, Liebezeit G, Dawson R. Habitat conditions and distribution pattern of the gutless oligochaete Phallodrilus leukodermatus. Mar Ecol Prog Ser. Inter-Research Science Center; 1982;8: 291–299. doi:10.3354/meps008291
161. Erséus C. Inanidrilus bulbosus gen. et sp.n., a Marine Tubificid (Oligochaeta) from Florida, USA. Zool Scr. Blackwell Publishing Ltd; 1979;8: 209–210. doi:10.1111/j.1463-6409.1979.tb00632.x
162. Erséus C. Taxonomic Revision of the Marine Genus Phallodrilus Pierantoni (Oligochaeta, Tubificidae), with Descriptions of Thirteen New Species. Zool Scr. Blackwell Publishing Ltd; 1979;8: 187–208. doi:10.1111/j.1463-6409.1979.tb00631.x
163. Giere O. Studies on Marine Oligochaeta From Bermuda , With Emphasis on New Phallodrilus-Spicies (Tubificidae). Cah Biol Mar. 1979; 301–314.
164. Erséus C. A generic revision of the Phallodrilinae (Oligochaeta, Tubificidae). Zool Scr. Blackwell Publishing Ltd; 1992;21: 5–48. doi:10.1111/j.1463-6409.1992.tb00308.x
165. Giere O. The gutless marine oligochaete Phallodrilus leukodermatus. Structural studies on an aberrant tubificid associated with bacteria. Mar Ecol Prog Ser. Inter-Research Science Center; 1981;5: 353–357. doi:10.3354/meps005353
166. Richards KS, Fleming TP, Jamieson BGM. An ultrastructural study of the distal epidermis and the occurrence of subcuticular bacteria in the gutless tubificid phallodrilus albidus (Oligochaeta: Annelida). Aust J Zool. CSIRO PUBLISHING; 1982;30: 159–168. doi:10.1071/ZO9820327
167. Woyke T, Teeling H, Ivanova NN, Huntemann M, Richter M, Gloeckner FO, et al. Symbiosis insights through metagenomic analysis of a microbial consortium. Nature. 2006;443: 950–955. doi:10.1038/nature05192

168. Heindl NR, Gruber-Vodicka HR, Bayer C, Lucker S, Ott JA, Bulgheresi S. First detection of thiotrophic symbiont phylotypes in the pelagic marine environment. FEMS Microbiol Ecol. 2011/03/26. England; 2011;77: 223–227. doi:10.1111/j.1574-6941.2011.01096.x

169. Zimmermann J, Wentrup C, Sadowski M, Blazejak A, Gruber-Vodicka HR, Kleiner M, et al. Closely coupled evolutionary history of ecto- and endosymbionts from two distantly related animal phyla. Mol Ecol. England; 2016;25: 3203–3223. doi:10.1111/mec.13554

170. Ferry JG. CO Dehydrogenase. Annu Rev Microbiol. 1995;49: 305–333. doi:10.1146/annurev.micro.49.1.305

171. Kleiner M, Wentrup C, Lott C, Teeling H, Wetzel S, Young J, et al. Metaproteomics of a gutless marine worm and its symbiotic microbial community reveal unusual pathways for carbon and energy use. Proc Natl Acad Sci U S A. 2012;109: E1173-82. doi:10.1073/pnas.1121198109

172. Kleiner M, Petersen JM, Dubilier N. Convergent and divergent evolution of metabolism in sulfur-oxidizing symbionts and the role of horizontal gene transfer. Curr Opin Microbiol. Elsevier Ltd; 2012;15: 621–631. doi:10.1016/j.mib.2012.09.003

173. Dubilier N, Mülders C, Ferdelman T, de Beer D, Pernthaler A, Klein M, et al. Endosymbiotic sulphate-reducing and sulphide-oxidizing bacteria in an oligochaete worm. Nature. Nature Publishing Group; 2001;411: 298–302. doi:10.1038/35077067

174. Blazejak A, Erseus C, Amann R, Dubilier N. Coexistence of bacterial sulfide oxidizers, sulfate reducers, and spirochetes in a gutless worm (Oligochaeta) from the Peru margin. Appl Env Microbiol. 2005/03/05. 2005;71: 1553–1561. doi:10.1128/aem.71.3.1553-1561.2005

175. Dubilier N, Amann R, Erséus C, Muyzer G, Park S, Giere O, et al. Phylogenetic diversity of bacterial endosymbionts in the gutless marine oligochete Olavius loisae (Annelida). Mar Ecol Prog Ser. 1999;178: 271–280. doi:10.3354/meps178271

176. Blazejak A, Kuever J, Erséus C, Amann R, Dubilier N. Phylogeny of 16S rRNA, ribulose 1,5-bisphosphate carboxylase/oxygenase, and adenosine 5′-phosphosulfate reductase genes from gamma- and alphaproteobacterial symbionts in gutless marine worms (oligochaeta) from Bermuda and the Bahamas. Appl Environ Microbiol. American Society for Microbiology (ASM); 2006;72: 5527–5536. doi:10.1128/AEM.02441-05

177. Cobb NA. Nematodes and their relationships. Yearb Dep Agric 1914. 1915; 1–36.

178. Needham T. A letter concerning certain chalky tubulous concretions called malm; with some microscopical observations on the farina of the red lily, and of worms discovered in smutty corn. Philos Trans R Soc London. 1774;42: 634–641.

179. Van Gaever S, Vanreusel A, Hughes JA, Bett BJ, Kiriakoulakis K. The macro- and micro-scale patchiness of meiobenthos associated with the Darwin Mounds (north-east Atlantic). J Mar Biol Assoc UK. 2004;84: 547–556. doi:10.1017/S0025315404009555h

180. Zeppilli D, Sarrazin J, Leduc D, Arbizu PM, Fontaneto D, Fontanier C, et al. Is the meiofauna a good indicator for climate change and anthropogenic impacts? Mar Biodivers. 2015;45: 505–535. doi:10.1007/s12526-015-0359-z

181. Bary A de. Die Erscheinung der Symbiose [Internet]. Oxford University. K. J. Trübner; 1879. Available: http://books.google.fr/books?id=7oQ_AAAAYAAJ

182. Chitwood BG. Some marine nematodes from North Carolina. Proc Helminthol Soc Wash. 1936;3: 1–15.

183. Wieser W. Eine ungewöhnliche Assoziation zwischen Blaualgen und freilebenden marinen Nematoden. Österreichische Bot Zeitschrift. 1959;106: 81–87. doi:10.1007/BF01278998

184. Hopper BE, Cefalu RC. Free-living marine nematodes from Biscayne Bay, Florida V. Stilbonematinae: Contributions to the taxonomy and morphology of the genus Eubostrichus Greeff and related genera. Trans Am Microsc Soc. [American Microscopical Society, Wiley]; 1973;92: 578–591. doi:10.2307/3225268

185. Tchesunov A V. Marine free-living nematodes of the subfamily Stilbonematinae taxonomic review with descriptions of a few species from the Nha Trang Bay , Central Vietnam. Meiofauna Mar. 2013;20: 71–94.

186. Wieser W. Benthic Studies in Buzzards Bay Ii. the Meiofauna1. Limnol Oceanogr. 1960;5: 121–137. doi:10.4319/lo.1960.5.2.0121

187. Morgan AR, Gerlach AR. Striped bass studies on Coos Bay, Oregon in 1949 and 1950. Oregon Fish Commission. 1950.

188. Gerlach SA. Free-living nemtodes from the Red Sea. Kieler Meeresforschungen. 1964;20: 18–34. Available: https://www.cabdirect.org/cabdirect/abstract/19660800840

189. Cobb N. One hundred new nemas. Contrib to a Sci Nematol. 1920; Available: http://www.vliz.be/imisdocs/publications/237787.pdf

190. Bayer C, Heindl NR, Rinke C, Lücker S, Ott JA, Bulgheresi S. Molecular characterization

of the symbionts associated with marine nematodes of the genus Robbea. Environ Microbiol Rep. 2009/10/20. Wiley-Blackwell; 2009;1: 136–144. doi:10.1111/j.1758-2229.2009.00019.x

191. Bright M, Bulgheresi S. A complex journey: transmission of microbial symbionts. Nat Rev Microbiol. 2010/02/17. England: Nature Publishing Group; 2010;8: 218–230. doi:10.1038/nrmicro2262
192. Bulgheresi S, Schabussova I, Chen T, Mullin NP, Maizels RM, Ott JA. A new C-type lectin similar to the human immunoreceptor DC-SIGN mediates symbiont acquisition by a marine nematode. Appl Environ Microbiol. 2006/04/07. United States; 2006;72: 2950–2956. doi:10.1128/AEM.72.4.2950-2956.2006
193. Urbancik W, Bauer-nebelsick M, Ott JA. The ultrastructure of the cuticle of Nematoda - I. The body cuticle within the Stilbonematinae (Adenophorea, Desmodoridae). Zoomorphology. 1996;116: 51–64. doi:10.1007/BF02526870
194. Nebelsick M, Blumer M, Urbancik W, Ott JA. The glandular sensory organ of Desmodoridae (Nematoda)-ultrastructure and phylogenetic implications. Invertebr Biol. JSTOR; 1995;114: 211–219. doi:10.2307/3226876
195. Ott JA, Nebelsick M, Novak R, Polz MF, Felbeck H. Chemoautotrophic, sulfur-oxidizing symbiotic bacteria on marine nematodes: Morphological and biochemical characterization. Microb Ecol. Springer-Verlag; 1992;24: 313–329. doi:10.1007/BF00167789
196. Gooday AJ, Jorissen F, Levin LA, Middelburg JJ, Naqvi SWA, Rabalais NN, et al. Historical records of coastal eutrophication-induced hypoxia. Biogeosciences. 2009;6: 1707–1745. doi:10.5194/bg-6-1707-2009
197. Riemann F, Thiermann F, Bock L. Leptonemella species (Desmodoridae, Stilbonematinae), benthic marine nematodes with ectosymbiotic bacteria, from littoral sand of the North Sea island of Sylt: taxonomy and ecological aspects. Helgol Mar Res. 2003;57: 118–131.
198. Boaden PJS, Platt HM. Daily migration patterns in an interstidal meiobenthonic community. Thalass jugosl. 1971;7: 1–12.
199. Giere O, Conway NM, Gastrock G, Schmidt C. "Regulation' of gutless annelid ecology by endosymbiotic bacteria. Mar Ecol Prog Ser. 1991;68: 287–299. doi:10.3354/meps068287

200. Connell JH, Slatyer RO. Mechanisms of Succession in Natural Communities and Their Role in Community Stability and Organization. Am Nat. University of Chicago Press; 1977;111: 1119–1144. doi:10.1086/283241

201. Jensen P. Theristus anoxybioticus. Mar Biol. 1995; 131–136.

202. Gerlach SA. Food-chain relationships in subtidal silty sand marine sediments and the role of meiofauna in stimulating bacterial productivity. Oecologia. 1978;33: 55–69. doi:10.1007/BF00376996

203. Giordano F, Aigrain L, Quail MA, Coupland P, Bonfield JK, Davies RM, et al. De novo yeast genome assemblies from MinION, PacBio and MiSeq platforms. Sci Rep. Springer US; 2017;7: 1–10. doi:10.1038/s41598-017-03996-z

204. Deamer D, Akeson M, Branton D. Three decades of nanopore sequencing. Nat Biotechnol. Nature Publishing Group; 2016;34: 518–524. doi:10.1038/nbt.3423

205. Bettencourt R, Pinheiro M, Egas C, Gomes P, Afonso M, Shank T, et al. High-throughput sequencing and analysis of the gill tissue transcriptome from the deep-sea hydrothermal vent mussel Bathymodiolus azoricus. BMC Genomics. BioMed Central; 2010;11: 559. doi:10.1186/1471-2164-11-559

206. Newton ILG, Woyke T, Auchtung TA, Dilly GF, Dutton RJ, Fisher MC, et al. The Calyptogena magnifica Chemoautotrophic Symbiont Genome. Science (80-). American Association for the Advancement of Science; 2007;315: 998–1000. doi:10.1126/science.1138438

207. Ponnudurai R, Sayavedra L, Kleiner M, Heiden SE, Thürmer A, Felbeck H, et al. Genome sequence of the sulfur-oxidizing Bathymodiolus thermophilus gill endosymbiont. Stand Genomic Sci. BioMed Central; 2017;12: 50. doi:10.1186/s40793-017-0266-y

208. Schmieder R, Edwards R. Quality control and preprocessing of metagenomic datasets. Bioinformatics. 2011;27: 863–864. doi:10.1093/bioinformatics/btr026

209. Loman NJ, Quinlan AR. Poretools: A toolkit for analyzing nanopore sequence data. Bioinformatics. 2014;30: 3399–3401. doi:10.1093/bioinformatics/btu555

210. Leggett RM, Heavens D, Caccamo M, Clark MD, Davey RP. NanoOK: Multi-reference alignment analysis of nanopore sequencing data, quality and error profiles. Bioinformatics. 2015;32: 142–144. doi:10.1093/bioinformatics/btv540

211. Bushnell B. BBMap: A Fast, Accurate, Splice-Aware Aligner [Internet]. Ernest Orlando Lawrence Berkeley National Laboratory, Berkeley, CA (US). 2014. doi:10.1186/1471-

2105-13-238

212. Li H, Durbin R. Fast and accurate long-read alignment with Burrows-Wheeler transform. Bioinformatics. 2010;26: 589–595. doi:10.1093/bioinformatics/btp698

213. Bankevich A, Nurk S, Antipov D, Gurevich AA, Dvorkin M, Kulikov AS, et al. SPAdes: A New Genome Assembly Algorithm and Its Applications to Single-Cell Sequencing. J Comput Biol. 2012;19: 455–477. doi:10.1089/cmb.2012.0021

214. Zimin A V., Marçais G, Puiu D, Roberts M, Salzberg SL, Yorke JA. The MaSuRCA genome assembler. Bioinformatics. 2013;29: 2669–2677. doi:10.1093/bioinformatics/btt476

215. Koren S, Walenz BP, Berlin K, Miller JR, Bergman NH, Phillippy AM. Canu: Scalable and accurate long-read assembly via adaptive κ-mer weighting and repeat separation. Genome Res. 2017;27: 722–736. doi:10.1101/gr.215087.116

216. Gremme G, Steinbiss S, Kurtz S. GenomeTools: A Comprehensive Software Library for Efficient Processing of Structured Genome Annotations. IEEE/ACM Trans Comput Biol Bioinforma. 2013;10: 645–656. doi:10.1109/TCBB.2013.68

217. Gurevich A, Saveliev V, Vyahhi N, Tesler G. QUAST: Quality assessment tool for genome assemblies. Bioinformatics. Oxford University Press; 2013;29: 1072–1075. doi:10.1093/bioinformatics/btt086

218. Lagesen K, Hallin P, Rødland EA, Stærfeldt HH, Rognes T, Ussery DW. RNAmmer: Consistent and rapid annotation of ribosomal RNA genes. Nucleic Acids Res. 2007;35: 3100–3108. doi:10.1093/nar/gkm160

219. Laslett D, Canback B. ARAGORN, a program to detect tRNA genes and tmRNA genes in nucleotide sequences. Nucleic Acids Res. 2004;32: 11–16. doi:10.1093/nar/gkh152

220. Parks DH, Imelfort M, Skennerton CT, Hugenholtz P, Tyson GW. CheckM: assessing the quality of microbial genomes recovered from isolates, single cells, and metagenomes. Genome Res. Cold Spring Harbor Laboratory Press; 2015;25: 1043–55. doi:10.1101/gr.186072.114

221. Nawrocki EP, Eddy SR. Infernal 1.1: 100-fold faster RNA homology searches. Bioinformatics. Oxford University Press; 2013;29: 2933–2935. doi:10.1093/bioinformatics/btt509

222. Nawrocki EP, Burge SW, Bateman A, Daub J, Eberhardt RY, Eddy SR, et al. Rfam 12.0: Updates to the RNA families database. Nucleic Acids Res. 2015;43: D130–D137.

doi:10.1093/nar/gku1063

223. Bland C, Ramsey TL, Sabree F, Lowe M, Brown K, Kyrpides NC, et al. CRISPR Recognition Tool (CRT): a tool for automatic detection of clustered regularly interspaced palindromic repeats. BMC Bioinformatics. BioMed Central; 2007;8: 209. doi:10.1186/1471-2105-8-209
224. Nielsen H. Predicting Secretory Proteins with SignalP. Methods in molecular biology (Clifton, NJ). 2017. pp. 59–73. doi:10.1007/978-1-4939-7015-5_6
225. Kurtz S, Phillippy A, Delcher AL, Smoot M, Shumway M, Antonescu C, et al. Versatile and open software for comparing large genomes. Genome Biol. BioMed Central; 2004;5: R12. doi:10.1186/gb-2004-5-2-r12
226. Krzywinski M, Schein J, Birol I, Connors J, Gascoyne R, Horsman D, et al. Circos: An information aesthetic for comparative genomics. Genome Res. 2009;19: 1639–1645. doi:10.1101/gr.092759.109
227. Varghese NJ, Mukherjee S, Ivanova N, Konstantinidis KT, Mavrommatis K, Kyrpides NC, et al. Microbial species delineation using whole genome sequences. Nucleic Acids Res. Oxford University Press; 2015;43: 6761–6771. doi:10.1093/nar/gkv657
228. R Core Team. R: A Language and Environment for Statistical Computing [Internet]. Vienna, Austria; Available: https://www.r-project.org
229. Warnes GR, Bolker B, Bonebakker L, Gentleman R, Liaw WHA, Lumley T, et al. gplots: Various R Programming Tools for Plotting Data [Internet]. 2016. Available: http://cran.r-project.org/package=gplots
230. Seemann T. Prokka: Rapid prokaryotic genome annotation. Bioinformatics. 2014;30: 2068–2069. doi:10.1093/bioinformatics/btu153
231. Bourtzis K, Nirgianaki A, Markakis G, Savakis C. Wolbachia infection and cytoplasmic incompatibility in Drosophila species. Genetics. 1996;144: 1063–1073. doi:10.1186/1471-2105-15-293
232. Altschul SF, Gish W, Miller WT, Myers EW, Lipman DJ. Basic local alignment search tool. J Mol Biol. 1990/10/05. Academic Press; 1990;215: 403–410. doi:10.1006/jmbi.1990.9999
233. Camacho C, Coulouris G, Avagyan V, Ma N, Papadopoulos J, Bealer K, et al. BLAST+: architecture and applications. BMC Bioinformatics. 2009;10: 421. doi:10.1186/1471-2105-10-421

234. Huntemann M, Ivanova NN, Mavromatis K, Tripp HJ, Paez-Espino D, Tennessen K, et al. The standard operating procedure of the DOE-JGI Metagenome Annotation Pipeline (MAP v.4). Stand Genomic Sci. 2016;11: 17. doi:10.1186/s40793-016-0138-x

235. Eddy SR. Accelerated profile HMM searches. Pearson WR, editor. PLoS Comput Biol. Public Library of Science; 2011;7: e1002195. doi:10.1371/journal.pcbi.1002195

236. Finn RD, Coggill P, Eberhardt RY, Eddy SR, Mistry J, Mitchell AL, et al. The Pfam protein families database: Towards a more sustainable future. Nucleic Acids Res. Oxford University Press; 2016;44: D279–D285. doi:10.1093/nar/gkv1344

237. Grissa I, Vergnaud G, Pourcel C. CRISPRcompar: a website to compare clustered regularly interspaced short palindromic repeats. Nucleic Acids Res. 2008;36: W52–W57. doi:10.1093/nar/gkn228

238. Käll L, Krogh A, Sonnhammer ELL. Advantages of combined transmembrane topology and signal peptide prediction-the Phobius web server. Nucleic Acids Res. 2007;35: W429–W432. doi:10.1093/nar/gkm256

239. Krogh A, Larsson B, von Heijne G, Sonnhammer EL. Predicting transmembrane protein topology with a hidden markov model: application to complete genomes11Edited by F. Cohen. J Mol Biol. 2001;305: 567–580. doi:10.1006/jmbi.2000.4315

240. Huang L, Zhang H, Wu P, Entwistle S, Li X, Yohe T, et al. dbCAN-seq: a database of carbohydrate-active enzyme (CAZyme) sequence and annotation. Nucleic Acids Res. 2017; doi:10.1093/nar/gkx894

241. Snipen L, Liland KH. micropan: an R-package for microbial pan-genomics. BMC Bioinformatics. BioMed Central; 2015;16: 79. doi:10.1186/s12859-015-0517-0

242. Yu NY, Wagner JR, Laird MR, Melli G, Rey S, Lo R, et al. PSORTb 3.0: Improved protein subcellular localization prediction with refined localization subcategories and predictive capabilities for all prokaryotes. Bioinformatics. 2010;26: 1608–1615. doi:10.1093/bioinformatics/btq249

243. Achaz G, Boyer F, Rocha EPC, Viari A, Coissac E. Repseek, a tool to retrieve approximate repeats from large DNA sequences. Bioinformatics. 2007;23: 119–121. doi:10.1093/bioinformatics/btl519

244. Ogata H, Goto S, Sato K, Fujibuchi W, Bono H, Kanehisa M. KEGG: Kyoto encyclopedia of genes and genomes. Nucleic Acids Res. 1999;27: 29–34. doi:10.1093/nar/27.1.29

245. Kanehisa M, Sato Y, Morishima K. BlastKOALA and GhostKOALA: KEGG Tools for

Functional Characterization of Genome and Metagenome Sequences. J Mol Biol. 2016;428: 726–731. doi:10.1016/j.jmb.2015.11.006

246. Norris JN, Bucher KE. Marine algae and seagrasses from Carrie Bow Cay, Belize. Atl Barrier Reef Ecosyst Carrie Bow Cay, Belize I Struct Communities. 1982;12: 167–223. Available: c:%5CArchivos de programa%5CEndNote%5CBASES DE DATOS%5CArticulos en PDF%5C115-Norris and Bucher_1982.pdf
247. Cline JD. Spectrophotometric Determination of Hydrogen Sulfide in Natural Waters. Limnol Oceanogr. 1969;14: 454–458. doi:10.4319/lo.1969.14.3.0454
248. Green LC, Wagner DA, Glogowski J, Skipper PL, Wishnok JS, Tannenbaum SR. Analysis of nitrate, nitrite, and [15N]nitrate in biological fluids. Anal Biochem. 1982;126: 131–138. doi:10.1016/0003-2697(82)90118-X
249. Schnetger B, Lehners C. Determination of nitrate plus nitrite in small volume marine water samples using vanadium(III)chloride as a reduction agent. Mar Chem. Elsevier B.V.; 2014;160: 91–98. doi:10.1016/j.marchem.2014.01.010
250. Solórzano L. Determination of ammonia in natural waters by the phenolhypochlorite method. Limnol Oceanogr. 1969;14: 799–801. doi:10.4319/lo.1969.14.5.0799
251. KESTER DR, DUEDALL IW, CONNORS DN, PYTKOWICZ RM. Preparation of Artificial Seawater1 [Internet]. Limnology and Oceanography. 1967. pp. 176–179. doi:10.4319/lo.1967.12.1.0176
252. Ligges U, Martin M. Scatterplot3d – an R package for Visualizing Multivariate Data. Cran. Dortmund: SFB 475, Universität Dortmund; 2003; 1–36. doi:10.18637/jss.v008.i11
253. Aziz RK, Bartels D, Best AA, DeJongh M, Disz T, Edwards RA, et al. The RAST Server: Rapid Annotations using Subsystems Technology. BMC Genomics. 2008;9: 75. doi:10.1186/1471-2164-9-75
254. Untergasser A, Nijveen H, Rao X, Bisseling T, Geurts R, Leunissen JAM. Primer3Plus, an enhanced web interface to Primer3. Nucleic Acids Res. Oxford University Press; 2007;35: W71–W74. doi:10.1093/nar/gkm306
255. Schefe JH, Lehmann KE, Buschmann IR, Unger T, Funke-Kaiser H. Quantitative real-time RT-PCR data analysis: Current concepts and the novel "gene expression's C T difference" formula. J Mol Med. 2006;84: 901–910. doi:10.1007/s00109-006-0097-6
256. Bohlin J, Snipen L, Hardy SP, Kristoffersen AB, Lagesen K, Dønsvik T, et al. Analysis of intra-genomic GC content homogeneity within prokaryotes. BMC Genomics. 2010;11:

464. doi:10.1186/1471-2164-11-464

257. Bowers RM, Kyrpides NC, Stepanauskas R, Harmon-Smith M, Doud D, Reddy TBK, et al. Minimum information about a single amplified genome (MISAG) and a metagenome-assembled genome (MIMAG) of bacteria and archaea [Internet]. Nature Biotechnology. 2017. pp. 725–731. doi:10.1038/nbt.3893

258. Konstantinidis KT, Rosselló-Móra R, Amann R. Uncultivated microbes in need of their own taxonomy. ISME J. Nature Publishing Group; 2017; doi:10.1038/ismej.2017.113

259. Gzyl KE, Wieden HJ. Tetracycline does not directly inhibit the function of bacterial elongation factor Tu. Jan E, editor. PLoS One. 2017;12: e0178523. doi:10.1371/journal.pone.0178523

260. Gerdes K, Christensen SK, Løbner-Olesen A. Prokaryotic toxin-antitoxin stress response loci. Nat Rev Microbiol. Nature Publishing Group; 2005;3: 371–382. doi:10.1038/nrmicro1147

261. Cantarel BI, Coutinho PM, Rancurel C, Bernard T, Lombard V, Henrissat B. The Carbohydrate-Active EnZymes database (CAZy): An expert resource for glycogenomics. Nucleic Acids Res. Oxford University Press; 2009;37: D233-8. doi:10.1093/nar/gkn663

262. Blattner FR. The Complete Genome Sequence of Escherichia coli K-12. Science (80-). 1997;277: 1453–1462. doi:10.1126/science.277.5331.1453

263. Garcia HE, Gordon LI. Oxygen Solubility Sin Seawater: Better Fitting Equations. Limnol Oceanogr. 1992;37: 1307–1312. doi:10.2307/2837876

264. Polz MF, Harbison C, Cavanaugh CM. Diversity and heterogeneity of epibiotic bacterial communities on the marine nematode Eubostrichus dianae. Appl Environ Microbiol. 1999/09/03. 1999;65: 4271–4275. Available: http://www.ncbi.nlm.nih.gov/pubmed/10473452

265. Ott JA, Leisch N, Gruber-Vodicka H. Eubostrichus fertilis sp. n., a new marine nematode (Desmodoridae: Stilbonematinae) with an extraordinary reproductive potential from Belize, Central America. Nematology. 2014;16: 1–11. doi:10.1163/15685411-00002807

266. Pende N, Leisch N, Gruber-Vodicka HR, Heindl NR, Ott JA, den Blaauwen T, et al. Size-independent symmetric division in extraordinarily long cells. Nat Commun. England; 2014;5: 4803. doi:10.1038/ncomms5803

267. Greeff R. Untersuchungen liber einige Formen des Arthropoden- und Wurm-Typus.

Arch Gesch Naturwiss. 1869;35: 117–118.

268. Koren S, Schatz MC, Walenz BP, Martin J, Howard JT, Ganapathy G, et al. Hybrid error correction and de novo assembly of single-molecule sequencing reads. Nat Biotechnol. Nature Publishing Group; 2012;30: 693–700. doi:10.1038/nbt.2280

269. Ono Y, Asai K, Hamada M. PBSIM: PacBio reads simulator - Toward accurate genome assembly. Bioinformatics. Oxford University Press; 2013;29: 119–121. doi:10.1093/bioinformatics/bts649

270. Loman NJ, Quick J, Simpson JT. A complete bacterial genome assembled de novo using only nanopore sequencing data. Nat Methods. Nature Publishing Group; 2015;12: 733–735. doi:10.1038/nmeth.3444

271. Lemon JK, Khil PP, Frank KM, Dekker JP. Rapid Nanopore Sequencing of Plasmids and Resistance Gene Detection in Clinical Isolates. J Clin Microbiol. American Society for Microbiology; 2017;55: JCM.01069-17. doi:10.1128/JCM.01069-17

272. Byrne A, Beaudin AE, Olsen HE, Jain M, Cole C, Palmer T, et al. Nanopore long-read RNAseq reveals widespread transcriptional variation among the surface receptors of individual B cells. Nat Commun. Nature Publishing Group; 2017;8: 16027. doi:10.1038/ncomms16027

273. Quick J, Loman NJ, Duraffour S, Simpson JT, Severi E, Cowley L, et al. Real-time, portable genome sequencing for Ebola surveillance. Nature. Europe PMC Funders; 2016;530: 228–232. doi:10.1038/nature16996

274. Pomerantz A, Penafiel N, Arteaga A, Bustamante L, Pichardo F, Coloma LA, et al. Real-time DNA barcoding in a remote rainforest using nanopore sequencing. bioRxiv. Cold Spring Harbor Laboratory; 2017; 189159. doi:10.1101/189159

275. Castro-Wallace SL, Chiu CY, John KK, Stahl SE, Rubins KH, Mcintyre ABR, et al. Nanopore DNA Sequencing and Genome Assembly on the International Space Station. bioRxiv Prepr. 2016; doi:10.1038/s41598-017-18364-0

276. Simpson JT, Workman RE, Zuzarte PC, David M, Dursi LJ, Timp W. Detecting DNA cytosine methylation using nanopore sequencing. Nat Methods. Nature Publishing Group; 2017;14: 407–410. doi:10.1038/nmeth.4184

277. Cretu Stancu M, van Roosmalen MJ, Renkens I, Nieboer M, Middelkamp S, de Ligt J, et al. Mapping And Phasing Of Structural Variation In Patient Genomes Using Nanopore Sequencing. bioRxiv. Cold Spring Harbor Laboratory; 2017;22: 1–33.

doi:10.1101/129379

278. Bolisetty MT, Rajadinakaran G, Graveley BR. Determining exon connectivity in complex mRNAs by nanopore sequencing. Genome Biol. 2015;16: 204. doi:10.1186/s13059-015-0777-z

279. Smith AM. Reading canonical and modified nucleotides in 16S ribosomal RNA using nanopore direct RNA sequencing. bioRxiv. Cold Spring Harbor Laboratory; 2017; 132274. doi:10.1101/132274

280. Pevzner PA, Tang H, Waterman MS. An Eulerian path approach to DNA fragment assembly. Proc Natl Acad Sci. National Academy of Sciences; 2001;98: 9748–9753. doi:10.1073/pnas.171285098

281. Magoc T, Pabinger S, Canzar S, Liu X, Su Q, Puiu D, et al. GAGE-B: An evaluation of genome assemblers for bacterial organisms. Bioinformatics. Oxford University Press; 2013;29: 1718–1725. doi:10.1093/bioinformatics/btt273

282. Utturkar SM, Klingeman DM, Land ML, Schadt CW, Doktycz MJ, Pelletier DA, et al. Evaluation and validation of de novo and hybrid assembly techniques to derive high-quality genome sequences. Bioinformatics. Oxford University Press; 2014;30: 2709–2716. doi:10.1093/bioinformatics/btu391

283. Goodwin S, McPherson JD, McCombie WR. Coming of age: ten years of next-generation sequencing technologies. Nat Rev Genet. Nature Publishing Group; 2016;17: 333–351. doi:10.1038/nrg.2016.49

284. Lu H, Giordano F, Ning Z. Oxford Nanopore MinION Sequencing and Genome Assembly. Genomics, Proteomics Bioinforma. Elsevier; 2016;14: 265–279. doi:10.1016/j.gpb.2016.05.004

285. Vaser R, Sović I, Nagarajan N, Šikić M. Fast and accurate de novo genome assembly from long uncorrected reads. Genome Res. Cold Spring Harbor Laboratory Press; 2017;27: 737–746. doi:10.1101/gr.214270.116

286. Walker BJ, Abeel T, Shea T, Priest M, Abouelliel A, Sakthikumar S, et al. Pilon: An integrated tool for comprehensive microbial variant detection and genome assembly improvement. Wang J, editor. PLoS One. Public Library of Science; 2014;9: e112963. doi:10.1371/journal.pone.0112963

287. José Gosalbes M, Latorre A, Lamelas A, Moya A. Genomics of intracellular symbionts in insects. Int J Med Microbiol. Urban & Fischer; 2010;300: 271–278.

doi:10.1016/j.ijmm.2009.12.001

288. Luo H, Gao F, Lin Y. Evolutionary conservation analysis between the essential and nonessential genes in bacterial genomes. Sci Rep. Nature Publishing Group; 2015;5: 13210. doi:10.1038/srep13210

289. Touchon M, Rocha EPC. Causes of insertion sequences abundance in prokaryotic genomes. Mol Biol Evol. Oxford University Press; 2007;24: 969–981. doi:10.1093/molbev/msm014

290. Moran NA, Plague GR. Genomic changes following host restriction in bacteria [Internet]. Current Opinion in Genetics and Development. Elsevier Current Trends; 2004. pp. 627–633. doi:10.1016/j.gde.2004.09.003

291. Werren JH. Selfish genetic elements, genetic conflict, and evolutionary innovation. Proc Natl Acad Sci. National Academy of Sciences; 2011;108: 10863–10870. doi:10.1073/pnas.1102343108

292. Edwards RJ, Brookfield JFY. Transiently beneficial insertions could maintain mobile DNA sequences in variable environments. Mol Biol Evol. Oxford University Press; 2003;20: 30–37. doi:10.1093/molbev/msg001

293. Leavis HL, Willems RJL, Van Wamel WJB, Schuren FH, Caspers MPM, Bonten MJM. Insertion sequence-driven diversification creates a globally dispersed emerging multiresistant subspecies of E. faecium. PLoS Pathog. Public Library of Science; 2007;3: 0075–0096. doi:10.1371/journal.ppat.0030007

294. Chao L, McBroom SM. Evolution of transposable elements: an IS10 insertion increases fitness in Escherichia coli. Mol Biol Evol. Oxford University Press; 1985;2: 359–69. doi:10.1093/oxfordjournals.molbev.a040356

295. Newton ILG, Bordenstein SR. Correlations between bacterial ecology and mobile DNA. Curr Microbiol. Springer-Verlag; 2011;62: 198–208. doi:10.1007/s00284-010-9693-3

296. Kleiner M, Young JC, Shah M, Verberkmoes NC, Dubilier N. Metaproteomics reveals abundant transposase expression in mutualistic endosymbionts. MBio. American Society for Microbiology; 2013;4: e00223-13. doi:10.1128/mBio.00223-13

297. Sberro H, Leavitt A, Kiro R, Koh E, Peleg Y, Qimron U, et al. Discovery of Functional Toxin/Antitoxin Systems in Bacteria by Shotgun Cloning. Mol Cell. 2013;50: 136–148. doi:10.1016/j.molcel.2013.02.002

298. Moll I, Engelberg-Kulka H. Selective translation during stress in Escherichia coli. Trends

Biochem Sci. Elsevier Current Trends; 2012;37: 493–498. doi:10.1016/j.tibs.2012.07.007

299. Di Fossalunga AS, Lipuma J, Venice F, Dupont L, Bonfante P. The endobacterium of an arbuscular mycorrhizal fungus modulates the expression of its toxin-antitoxin systems during the life cycle of its host. ISME J. Nature Publishing Group; 2017;11: 2394–2398. doi:10.1038/ismej.2017.84
300. Slaby BM, Hackl T, Horn H, Bayer K, Hentschel U. Metagenomic binning of a marine sponge microbiome reveals unity in defense but metabolic specialization. ISME J. Nature Publishing Group; 2017;11: 2465–2478. doi:10.1038/ismej.2017.101
301. Sayavedra L, Kleiner M, Ponnudurai R, Wetzel S, Pelletier E, Barbe V, et al. Abundant toxin-related genes in the genomes of beneficial symbionts from deep-sea hydrothermal vent mussels. Elife. eLife Sciences Publications, Ltd; 2015;4: e07966. doi:10.7554/eLife.07966.001
302. Arcus VL, Mckenzie JL, Robson J, Cook GM. The PIN-domain ribonucleases and the prokaryotic VapBC toxin-antitoxin array. Protein Eng Des Sel. 2011;24: 33–40. doi:10.1093/protein/gzq081
303. Masuda H, Inouye M. Toxins of prokaryotic toxin-antitoxin systems with sequence-specific endoribonuclease activity. Toxins (Basel). Multidisciplinary Digital Publishing Institute (MDPI); 2017;9. doi:10.3390/toxins9040140
304. Cruz JW, Sharp JD, Hoffer ED, Maehigashi T, Vvedenskaya IO, Konkimalla A, et al. Growth-regulating Mycobacterium tuberculosis VapC-mt4 toxin is an isoacceptor-specific tRNase. Nat Commun. NIH Public Access; 2015;6: 7480. doi:10.1038/ncomms8480
305. Winther KS, Brodersen DE, Brown AK, Gerdes K. VapC20 of mycobacterium tuberculosis cleaves the sarcin-ricin loop of 23S rRNA. Nat Commun. Nature Publishing Group; 2013;4: 2796. doi:10.1038/ncomms3796
306. Bodogai M, Ferenczi S, Bashtovyy D, Miclea P, Papp P, Dusha I. The *ntrPR* Operon of *Sinorhizobium meliloti* Is Organized and Functions as a Toxin-Antitoxin Module. Mol Plant-Microbe Interact. 2006;19: 811–822. doi:10.1094/MPMI-19-0811
307. Oláh B, Kiss E, Györgypál Z, Borzi J, Cinege G, Csanádi G, et al. Mutation in the *ntrR* Gene, a Member of the *vap* Gene Family, Increases the Symbiotic Efficiency of *Sinorhizobium meliloti*. Mol Plant-Microbe Interact. 2001;14: 887–894. doi:10.1094/MPMI.2001.14.7.887

308. Coussens NP, Daines DA. Wake me when it's over – Bacterial toxin–antitoxin proteins and induced dormancy. Exp Biol Med. SAGE Publications; 2016;241: 1332–1342. doi:10.1177/1535370216651938

309. Anantharaman V, Aravind L. New connections in the prokaryotic toxin-antitoxin network: relationship with the eukaryotic nonsense-mediated RNA decay system. Genome Biol. 2003;4: R81. doi:10.1186/gb-2003-4-12-r81

310. Yuan J, Yamaichi Y, Waldor MK. The three Vibrio cholerae chromosome II-encoded ParE toxins degrade chromosome I following loss of chromosome II. J Bacteriol. 2011;193: 611–619. doi:10.1128/JB.01185-10

311. Pandey DP, Gerdes K. Toxin-antitoxin loci are highly abundant in free-living but lost from host-associated prokaryotes. Nucleic Acids Res. Oxford University Press; 2005;33: 966–976. doi:10.1093/nar/gki201

312. Pedersen K, Zavialov A V., Pavlov MY, Elf J, Gerdes K, Ehrenberg M. The bacterial toxin RelE displays codon-specific cleavage of mRNAs in the ribosomal A site. Cell. Elsevier; 2003;112: 131–140. doi:10.1016/S0092-8674(02)01248-5

313. Starosta AL, Lassak J, Jung K, Wilson DN. The bacterial translation stress response. FEMS Microbiol Rev. NIH Public Access; 2014;38: 1172–1201. doi:10.1111/1574-6976.12083

314. Mets T, Lippus M, Schryer D, Liiv A, Kasari V, Paier A, et al. Toxins MazF and MqsR cleave Escherichia coli rRNA precursors at multiple sites. RNA Biol. Taylor & Francis; 2017;14: 124–135. doi:10.1080/15476286.2016.1259784

315. Thomas T, Rusch D, DeMaere MZ, Yung PY, Lewis M, Halpern A, et al. Functional genomic signatures of sponge bacteria reveal unique and shared features of symbiosis. ISME J. Nature Publishing Group; 2010;4: 1557–1567. doi:10.1038/ismej.2010.74

316. Rodriguez-Lanetty M, Phillips W, Weis V, Margulis L, Colley N, Trench R, et al. Transcriptome analysis of a cnidarian – dinoflagellate mutualism reveals complex modulation of host gene expression. BMC Genomics. 2006;7: 23. doi:10.1186/1471-2164-7-23

317. Hentschel U, Piel J, Degnan SM, Taylor MW. Genomic insights into the marine sponge microbiome. Nat Rev Microbiol. Nature Publishing Group; 2012;10: 641–654. doi:10.1038/nrmicro2839

318. Horn H, Slaby BM, Jahn MT, Bayer K, Moitinho-Silva L, Förster F, et al. An Enrichment

of CRISPR and other defense-related features in marine sponge-associated microbial metagenomes. Front Microbiol. Frontiers Media SA; 2016;7: 1751. doi:10.3389/fmicb.2016.01751

319. Murooka Y, Ishibashi K, Yasumoto M, Sasaki M, Sugino H, Azakami H, et al. A sulfur- and tyramine-regulated Klebsiella aerogenes operon containing the arylsulfatase (atsA) gene and the atsB gene. J Bacteriol. 1990;172: 2131–2140. Available: http://pubmedcentralcanada.ca/pmcc/articles/PMC208713/pdf/jbacter01046-0461.pdf
320. Bond CS, Clements PR, Ashby SJ, Collyer CA, Harrop SJ, Hopwood JJ, et al. Structure of a human lysosomal sulfatase. Structure. Cell Press; 1997;5: 277–289. doi:10.1016/S0969-2126(97)00185-8
321. Parenti G, Meroni G, Ballabio A. The sulfatase gene family. Curr Opin Genet Dev. Elsevier Current Trends; 1997;7: 386–391. doi:10.1016/S0959-437X(97)80153-0
322. Ve T, Williams SJ, Kobe B. Structure and function of Toll/interleukin-1 receptor/resistance protein (TIR) domains. Apoptosis. Springer US; 2015;20: 250–261. doi:10.1007/s10495-014-1064-2
323. Yang S, Tang F, Gao M, Krishnan HB, Zhu H. R gene-controlled host specificity in the legume-rhizobia symbiosis. Proc Natl Acad Sci. National Academy of Sciences; 2010;107: 18735–18740. doi:10.1073/pnas.1011957107
324. Kelly DJ, Thomas GH. The tripartite ATP-independent periplasmic (TRAP) transporters of bacteria and archaea [Review]. FEMS MicrobiolRev. 2001;25: 405–424. doi:S0168-6445(01)00061-4 [pii]
325. Katz RA, Skalka AM. The retroviral enzymes. Annu Rev Biochem. 1994;63: 133–73. doi:10.1146/annurev.bi.63.070194.001025
326. Weissgerber T, Sylvester M, Kröninger L, Dahl C. A comparative quantitative proteomic study identifies new proteins relevant for sulfur oxidation in the purple sulfur bacterium allochromatium vinosum. Appl Environ Microbiol. American Society for Microbiology (ASM); 2014;80: 2279–2292. doi:10.1128/AEM.04182-13
327. Ma D, Cook DN, Alberti M, Pon NG, Nikaido H, Hearst JE. Molecular cloning and characterization of acrA and acrE genes of Escherichia coli. J Bacteriol. American Society for Microbiology (ASM); 1993;175: 6299–6313. doi:10.1128/jb.175.19.6299-6313.1993
328. Jasper Kieboom. Active Efflux Systems in the Solvent-Tolerant Bacterium Pseudomonas Putida S12 [Internet]. Wageningen University. 2002. Available:

http://edepot.wur.nl/198993

329. Desai MS, Seekatz AM, Koropatkin NM, Kamada N, Hickey CA, Wolter M, et al. A Dietary Fiber-Deprived Gut Microbiota Degrades the Colonic Mucus Barrier and Enhances Pathogen Susceptibility. Cell. Cell Press; 2016;167: 1339–1353.e21. doi:10.1016/j.cell.2016.10.043

330. Sonnenburg JL, Angenent LT, Gordon JI. Getting a grip on things: How do communities of bacterial symbionts become established in our intestine? Nat Immunol. Nature Publishing Group; 2004;5: 569–573. doi:10.1038/ni1079

331. Treangen TJ, Abraham AL, Touchon M, Rocha EPC. Genesis, effects and fates of repeats in prokaryotic genomes. FEMS Microbiol Rev. Oxford University Press; 2009;33: 539–571. doi:10.1111/j.1574-6976.2009.00169.x

332. Meng A, Marchet C, Corre E, Peterlongo P, Alberti A, Wincker P, et al. A de novo approach to disentangle partner identity and function in holobiont systems. 2017;

333. Williamson CHD, Sanchez A, Vazquez A, Gutman J, Sahl JW. Bacterial genome reduction as a result of short read sequence assembly. bioRxiv. 2016; doi:10.1101/091314

334. The C. elegans Sequencing Consortium. Genome Sequence of the Nematode *Caenorhabditis elegans*: A Platform for Investigating Biology [Internet]. Science. American Association for the Advancement of Science; 1998. pp. 2012–2018. doi:10.1126/science.282.5396.2012

335. Markert S, Gardebrecht A, Felbeck H, Sievert SM, Klose J, Becher D, et al. Status quo in physiological proteomics of the uncultured Riftia pachyptila endosymbiont. Proteomics. WILEY-VCH Verlag; 2011;11: 3106–3117. doi:10.1002/pmic.201100059

336. Tsuchimoto S, Ohtsubo H, Ohtsubo E. Two genes, pemK and pemI, responsible for stable maintenance of resistance plasmid R100. J Bacteriol. 1988;170: 1461–1466. doi:10.1128/jb.170.4.1461-1466.1988

337. Wilkinson JF. The problem of energy-storage compounds in bacteria. Exp Cell Res. Academic Press; 1959;7: 111–130. doi:10.1016/0014-4827(59)90237-X

338. Rao AU, Carta LK, Lesuisse E, Hamza I. Lack of heme synthesis in a free-living eukaryote. Proc Natl Acad Sci U S A. National Academy of Sciences; 2005;102: 4270–4275. doi:10.1073/pnas.0500877102

339. Hogle SL, Barbeau KA, Gledhill M. Heme in the marine environment: from cells to the iron cycle. Metallomics. The Royal Society of Chemistry; 2014;6: 1107–1120.

doi:10.1039/C4MT00031E

340. Alcaraz LD, Olmedo G, Bonilla G, Cerritos R, Hernández G, Cruz A, et al. The genome of Bacillus coahuilensis reveals adaptations essential for survival in the relic of an ancient marine environment. Proc Natl Acad Sci U S A. National Academy of Sciences; 2008;105: 5803–8. doi:10.1073/pnas.0800981105

341. Benning C. Biosynthesis and Function of the Sulfolipid Sulfoquinovosyl Diacylglycerol. Annu Rev Plant Physiol Plant Mol Biol. 1998;49: 53–75. doi:10.1146/annurev.arplant.49.1.53

342. Dulla GFJ, Go RA, Stahl DA, Davidson SK. Verminephrobacter eiseniae type IV pili and flagella are required to colonize earthworm nephridia. ISME J. 2012;6: 1166–1175. doi:10.1038/ismej.2011.183

343. Chavez-Dozal A, Hogan D, Gorman C, Quintanal-Villalonga A, Nishiguchi MK. Multiple Vibrio fischeri genes are involved in biofilm formation and host colonization. FEMS Microbiol Ecol. 2012;81: 562–573. doi:10.1111/j.1574-6941.2012.01386.x

344. Ryu CM. Against friend and foe: Type 6 effectors in plant-associated bacteria. J Microbiol. The Microbiological Society of Korea; 2015;53: 201–208. doi:10.1007/s12275-015-5055-y

345. Green ER, Mecsas J. Bacterial Secretion Systems: An Overview. Virulence Mech Bact Pathog Fifth Ed. : 215–239. doi:10.1128/microbiolspec.VMBF-0012-2015

346. Böck D, Medeiros JM, Tsao HF, Penz T, Weiss GL, Aistleitner K, et al. In situ architecture, function, and evolution of a contractile injection system. Science (80-). American Association for the Advancement of Science; 2017;357: 713–717. doi:10.1126/science.aan7904

347. Leiman PG, Basler M, Ramagopal UA, Bonanno JB, Sauder JM, Pukatzki S, et al. Type VI secretion apparatus and phage tail-associated protein complexes share a common evolutionary origin. Proc Natl Acad Sci. National Academy of Sciences; 2009;106: 4154–4159. doi:10.1073/pnas.0813360106

348. Schwarz S, Hood RD, Mougous JD. What is type VI secretion doing in all those bugs? Trends Microbiol. NIH Public Access; 2010;18: 531–537. doi:10.1016/j.tim.2010.09.001

349. Hachani A, Wood TE, Filloux A. Type VI secretion and anti-host effectors. Curr Opin Microbiol. Elsevier Current Trends; 2016;29: 81–93. doi:10.1016/j.mib.2015.11.006

350. Gerwing TG, Allen Gerwing AM, Hamilton DJ, Barbeau MA. Apparent redox potential

discontinuity (aRPD) depth as a relative measure of sediment oxygen content and habitat quality. Int J Sediment Res. Elsevier; 2015;30: 74–80. doi:10.1016/S1001-6279(15)60008-7

351. Bush T, Diao M, Allen RJ, Sinnige R, Muyzer G, Huisman J. Oxic-Anoxic regime shifts mediated by feedbacks between biogeochemical processes and microbial community dynamics. Nat Commun. 2017;8. doi:10.1038/s41467-017-00912-x
352. Falter JL, Sansone FJ. Shallow pore water sampling in reef sediments. Coral Reefs. 2000;19: 93–97. doi:10.1007/s003380050233
353. Kanwisher J. Gas exchange of shallow marine sediments. Symposium on the environmental chemistry of marine sediments. 1962. pp. 13–19.
354. Pamatmat MM. Ecology and Metabolism of a Benthic Community on an Intertidal Sandflat. Int Rev der gesamten Hydrobiol und Hydrogr. 1968;53: 211–298. doi:10.1002/iroh.19680530203
355. Fernex F, Baratie R, Span D, Vandelei Fernandes L. Variations of nitrogen nutrient concentrations in the sediment pore waters of the northwestern Mediterranean continental shelf. Cont Shelf Res. Pergamon; 1989;9: 767–794. doi:10.1016/0278-4343(89)90013-7
356. Riemann F, Schrage M. The mucus-trap hypothesis on feeding of aquatic nematodes and implications for biodegradation and sediment texture. Oecologia. 1978;34: 75–88. doi:10.1007/BF00346242
357. Riemann F, Ernst W, Ernst R. Acetate uptake from ambient water by the free-living marine nematode Adoncholaimus thalassophygas. Mar Biol. Springer-Verlag; 1990;104: 453–457. doi:10.1007/BF01314349
358. Jørgensen BB. The sulfur cycle of a coastal marine sediment (Limfjorden, Denmark)1. Limnol Oceanogr. 1977;22: 814–832. doi:10.4319/lo.1977.22.5.0814
359. Furla P, Allemand D, Shick JM, Ferrier-Pagès C, Richier S, Plantivaux A, et al. The symbiotic anthozoan: A physiological chimera between alga and animal. Integrative and Comparative Biology. 2005. pp. 595–604. doi:10.1093/icb/45.4.595
360. Touchette BW, Burkholder JAM. Review of nitrogen and phosphorus metabolism in seagrasses. J Exp Mar Bio Ecol. 2000;250: 133–167. doi:10.1016/S0022-0981(00)00195-7
361. Lee K-S, Dunton KH. Inorganic nitrogen acquisition in the seagrass Thalassia testudinum: Development of a whole-plant nitrogen budget. Limnol Oceanogr. 1999;44:

1204–1215. doi:10.4319/lo.1999.44.5.1204

362. Jorgensen NOG, Kroer N, Coffin RB, Xiao-Hua Yang, Lee C. Dissolved free amino acids, combined amino acids, and DNA as sources of carbon and nitrogen to marine bacteria. Mar Ecol Prog Ser. 1993;98: 135–148. doi:10.3354/meps098135
363. Trench RK. Microalgal-Invertebrate Symbioses - A Review. Endocytobiosis Cell Res. 1993;9: 135–175. Available: http://www.citeulike.org/group/894/article/511409
364. Venn AA, Loram JE, Douglas AE. Photosynthetic symbioses in animals. Journal of Experimental Botany. 2008. pp. 1069–1080. doi:10.1093/jxb/erm328
365. Yellowlees D, Rees TA V., Leggat W. Metabolic interactions between algal symbionts and invertebrate hosts. Plant, Cell and Environment. 2008. pp. 679–694. doi:10.1111/j.1365-3040.2008.01802.x
366. Falkowski PG, Dubinsky Z, Muscatine L, McCloskey L. Population Control in Symbiotic Corals. Bioscience. 1993;43: 606–611. doi:10.2307/1312147
367. Berner RA. Electrode studies of hydrogen sulfide in marine sediments. Geochim Cosmochim Acta. Pergamon; 1963;27: 563–575. doi:10.1016/0016-7037(63)90013-9
368. Wharfe JR. An ecological survey of the benthic invertebrate macrofauna of the lower Medway estuary, Kent. J Anim Ecol. JSTOR; 1977; 93–113.
369. Reid R, Brand D. Sulfide-Oxidizing Symbiosis in Lucinaceans: Implications for Bivalve Evolution. Veliger. 1986;29: 3–24. doi:10.1016/0300-9629(94)00211-B
370. Meyers M, Fossing H, Powell E. Microdistribution of interstitial meiofauna, oxygen and sulfide gradients, and the tubes of macro-infauna [Internet]. Marine Ecology Progress Series. Inter-Research Science Center; 1987. pp. 223–241. doi:10.3354/meps035223
371. Bright M. Life Stategies of Thiotrophic Ectosymbioses. 2002.
372. Wen S, Chen X, Xu F, Sun H. Validation of reference genes for real-time quantitative PCR (qPCR) Analysis of avibacterium paragallinarum. Reddy H, editor. PLoS One. 2016;11: e0167736. doi:10.1371/journal.pone.0167736
373. Florindo C, Ferreira R, Borges V, Spellerberg B, Gomes JP, Borrego MJ. Selection of reference genes for real-time expression studies in Streptococcus agalactiae. J Microbiol Methods. 2012;90: 220–227. doi:10.1016/j.mimet.2012.05.011
374. Stenico V, Baffoni L, Gaggìa F, Biavati B. Validation of candidate reference genes in Bifidobacterium adolescentis for gene expression normalization. Anaerobe. 2014;27: 34–39. doi:10.1016/j.anaerobe.2014.03.004

375. Bujold AR, MacInnes JI. Validation of reference genes for quantitative real-time PCR (qPCR) analysis of Actinobacillus suis. BMC Res Notes. 2015;8: 86. doi:10.1186/s13104-015-1045-8

376. Rao X, Huang X, Zhou Z, Lin X. An improvement of the 2ˆ(-delta delta CT) method for quantitative real-time polymerase chain reaction data analysis. Biostat Bioinforma Biomath. NIH Public Access; 2013;3: 71–85. doi:10.1016/j.biotechadv.2011.08.021.Secreted

377. Robertson LA, Kuenen JG. Aerobic denitrification: a controversy revived. Arch Microbiol. Springer-Verlag; 1984;139: 351–354. doi:10.1007/BF00408378

378. Lloyd D. Aerobic denitrification in soils and sediments: From fallacies to factx. Trends Ecol Evol. Elsevier Current Trends; 1993;8: 352–356. doi:10.1016/0169-5347(93)90218-E

379. Marchant HK, Ahmerkamp S, Lavik G, Tegetmeyer HE, Graf J, Klatt JM, et al. Denitrifying community in coastal sediments performs aerobic and anaerobic respiration simultaneously. ISME J. 2017;11: 1799–1812. doi:10.1038/ismej.2017.51

380. Childress JJ, Girguis PR. The metabolic demands of endosymbiotic chemoautotrophic metabolism on host physiological capacities. J Exp Biol. 2011;214: 312–325. doi:10.1242/jeb.049023

381. Seston SL, Beinart RA, Sarode N, Shockey AC, Ranjan P, Ganesh S, et al. Metatranscriptional response of chemoautotrophic Ifremeria nautilei endosymbionts to differing sulfur regimes. Front Microbiol. Frontiers Media SA; 2016;7: 1–18. doi:10.3389/fmicb.2016.01074

382. Tsoy O V., Ravcheev DA, Čuklina J, Gelfand MS. Nitrogen fixation and molecular oxygen: Comparative genomic reconstruction of transcription regulation in Alphaproteobacteria. Front Microbiol. Frontiers Media SA; 2016;7: 1343. doi:10.3389/fmicb.2016.01343

383. De Philippis R, Vincenzini M. Exocellular polysaccharides from cyanobacteria and their possible applications. FEMS Microbiol Rev. American Society for Microbiology (ASM); 1998;22: 151–175. doi:10.1016/S0168-6445(98)00012-6

384. Riedl R. Energy exchange at the bottom/water interface. Thalass Jugosl. 1971;7.

385. Ott JA, Bauer-Nebelsick M, Novotny V. The genus Laxus Cobb , 1894 (Stilbonematinae : Nematoda): Description of two new species with ectosymbiotic chemoautotrophic

bacteria. Proc Biol Soc Wash. 1995;108: 508–527.

List of Tables

List of Figures

Supplementary Figures

Sediment cores

Carrie Bow Cay, water holding capacity

Layer	Thickness of Layer (cm)	Pore water content (ml/28.27 cm^3 sediment)
1 (subsurface)	5	8
2	5	12
3	5	14
4	5	16
5	5	10
6	5	10
mean		11

Piran, water holding capacity

Layer	Thickness of Layer (cm)	Pore water content (ml/28.27 cm^3 sediment)
1 (subsurface)	5	7
2	5	14
3	6	12
mean		11

Carrie Bow Cay, cores away from seagrass beds

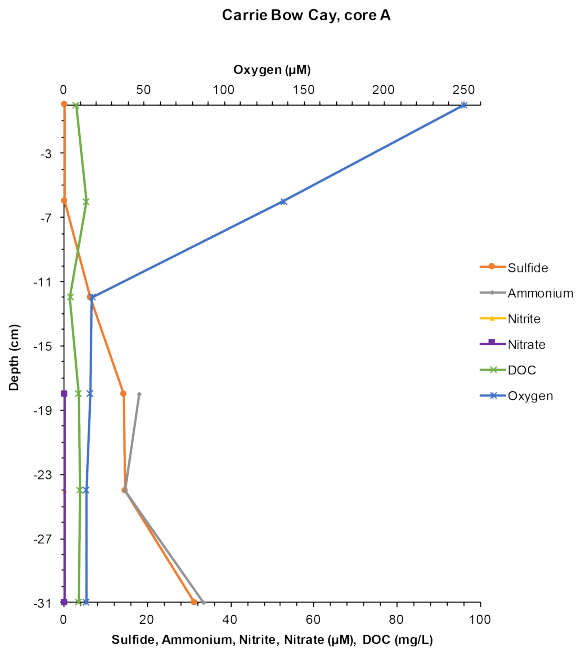

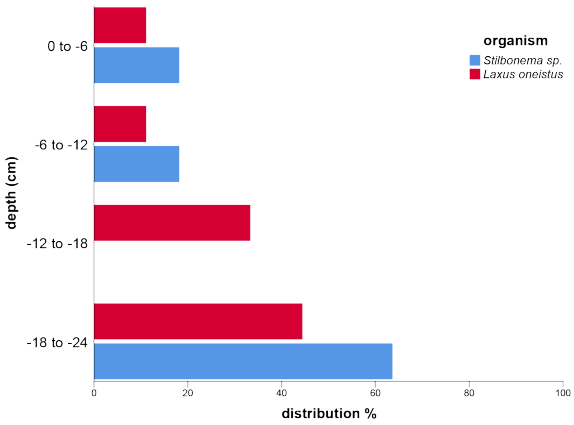

Total number of *L. oneistus*: 9
Total number of *Stilbonema* sp.: 11

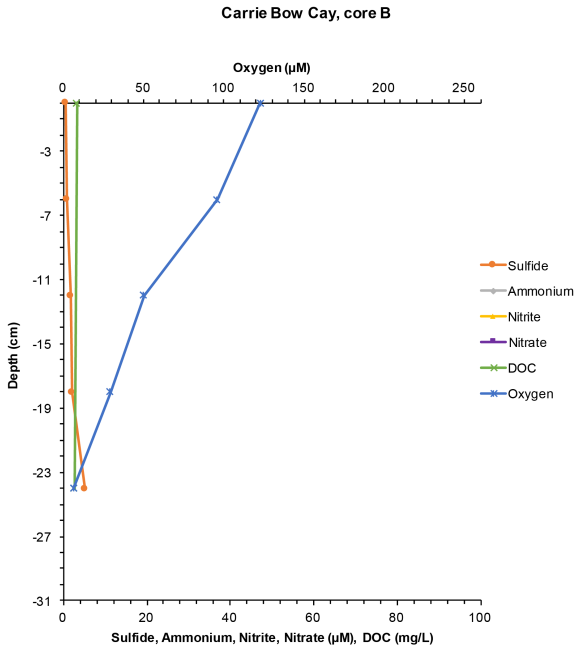

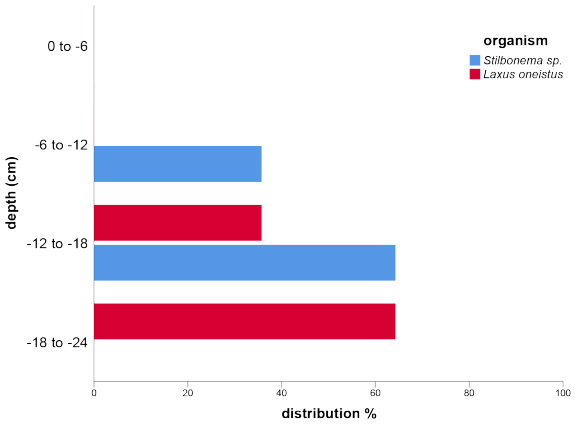

Total number of *L. oneistus*: 42
Total number of *Stilbonema* sp.: 42

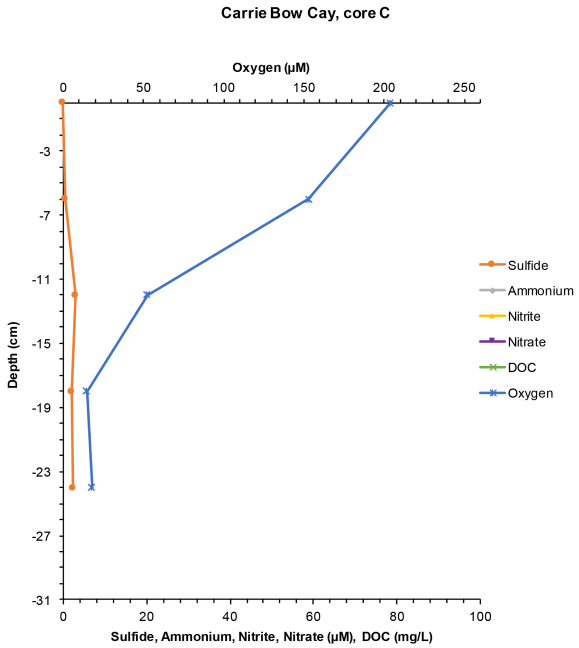

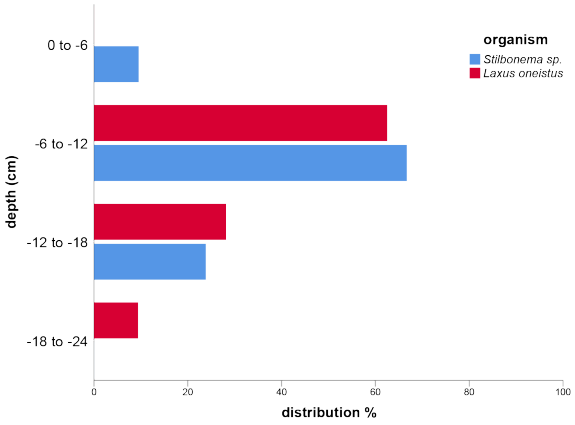

Total number of *L. oneistus*: 32
Total number of *Stilbonema* sp.: 21

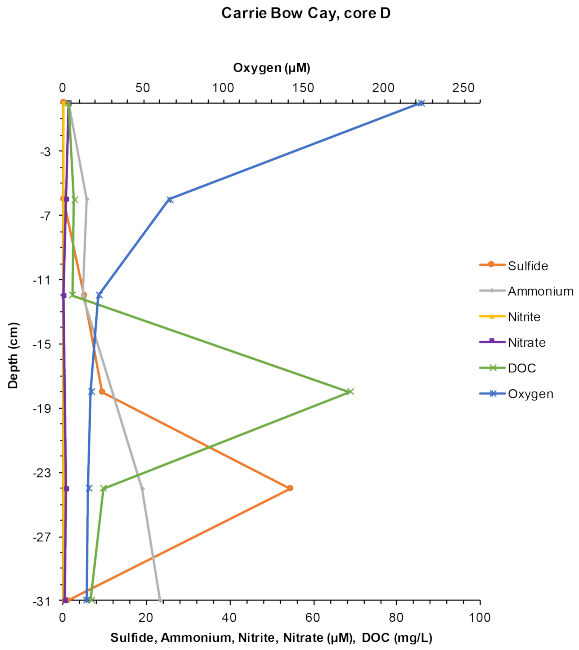

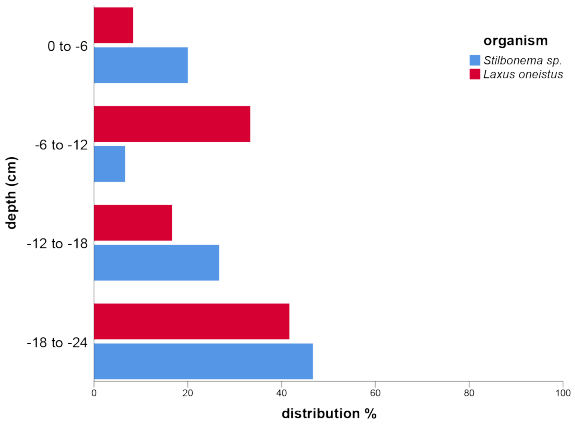

Total number of *L. oneistus*: 12
Total number of *Stilbonema* sp.: 15

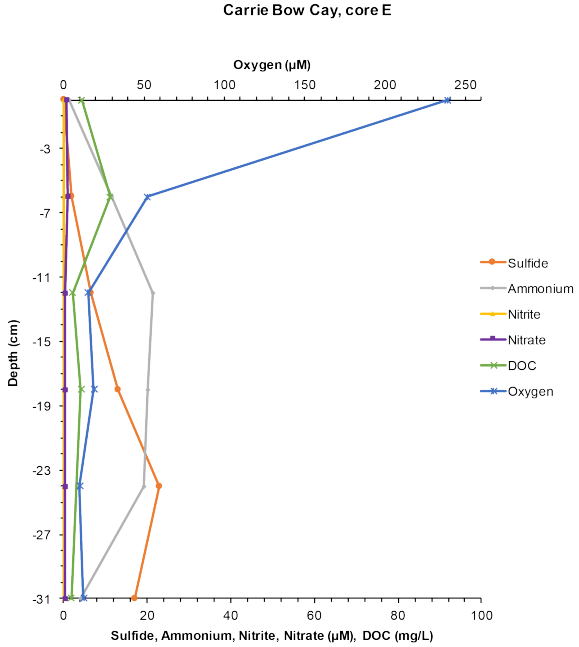

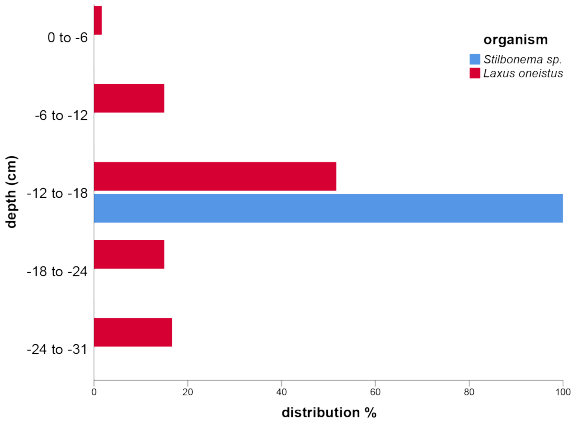

Total number of *L. oneistus*: 60
Total number of *Stilbonema* sp.: 1

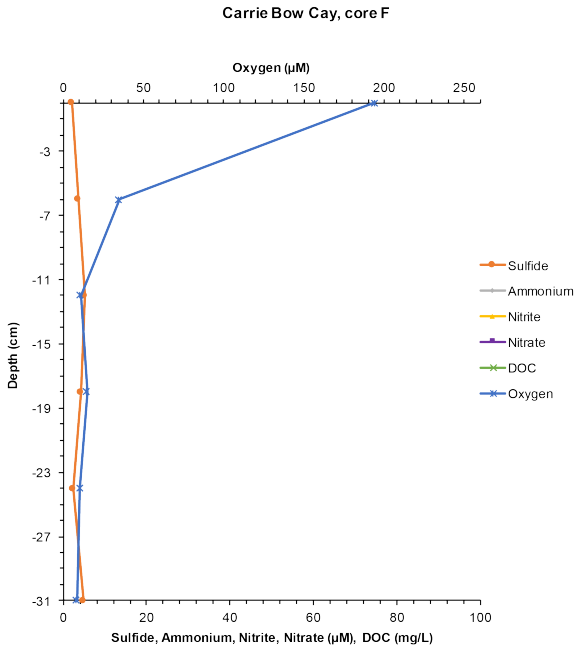

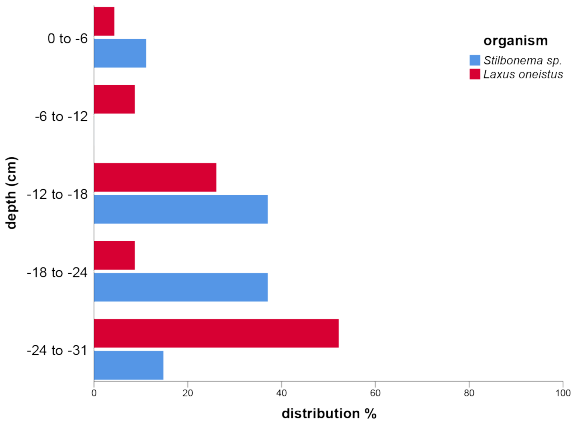

Total number of *L. oneistus*: 23
Total number of *Stilbonema* sp.: 27

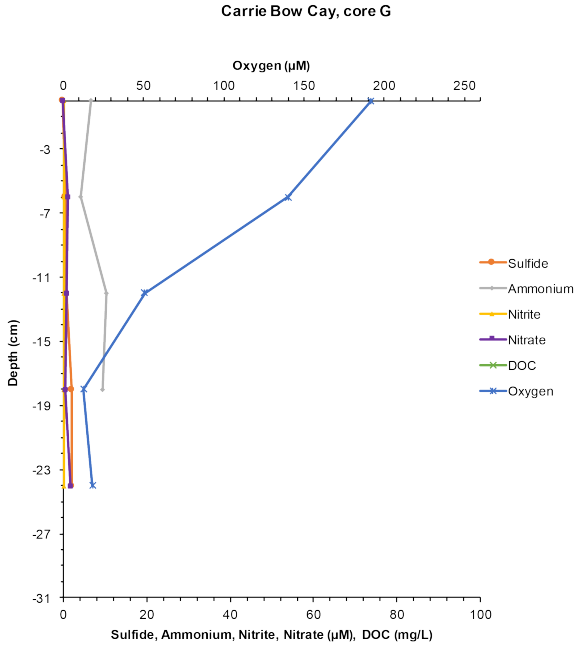

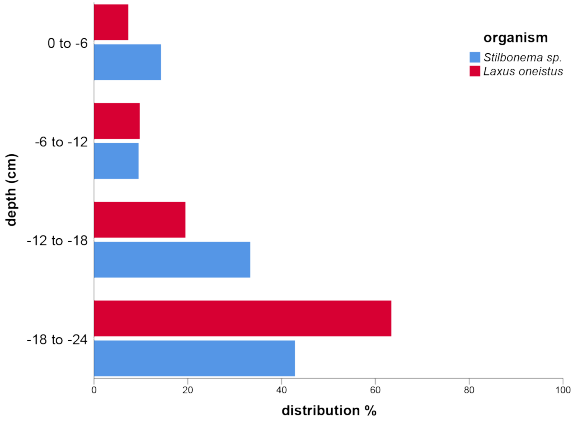

Total number of *L. oneistus*: 41
Total number of *Stilbonema* sp.: 21

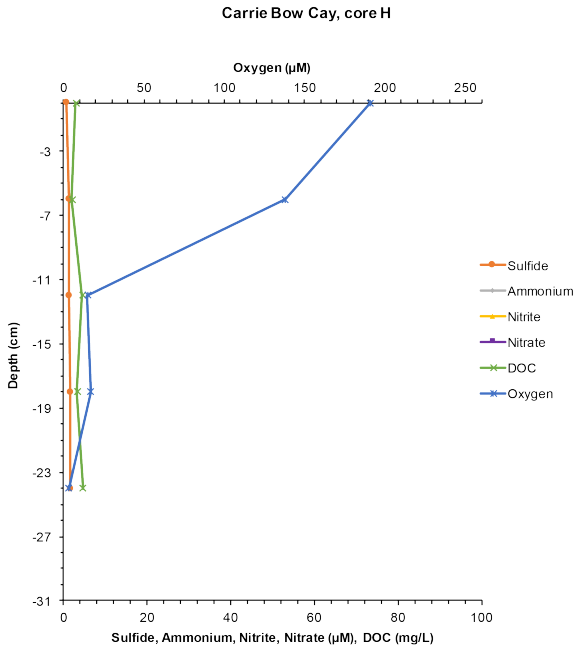

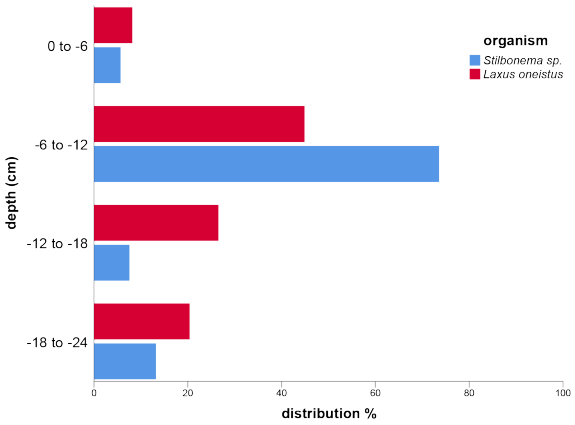

Total number of *L. oneistus*: 49
Total number of *Stilbonema* sp.: 53

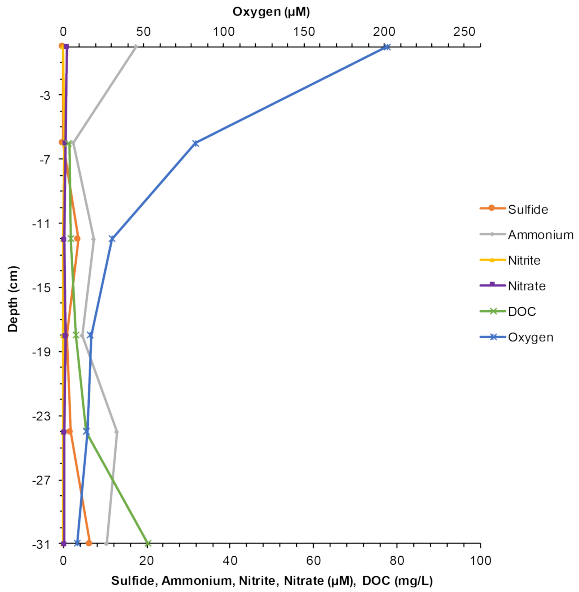

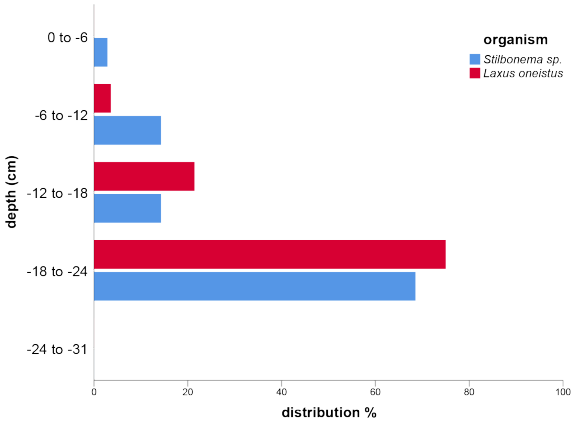

Total number of *L. oneistus*: 28
Total number of *Stilbonema* sp.: 35

Carrie Bow Cay, core O

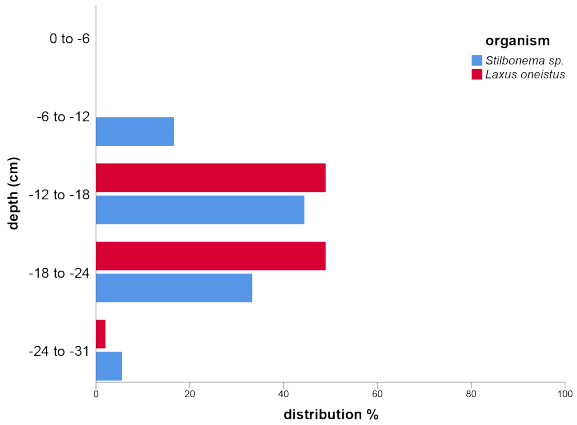

Total number of *L. oneistus*: 49
Total number of *Stilbonema* sp.: 18

Carrie Bow Cay, cores adjacent to seagrass beds

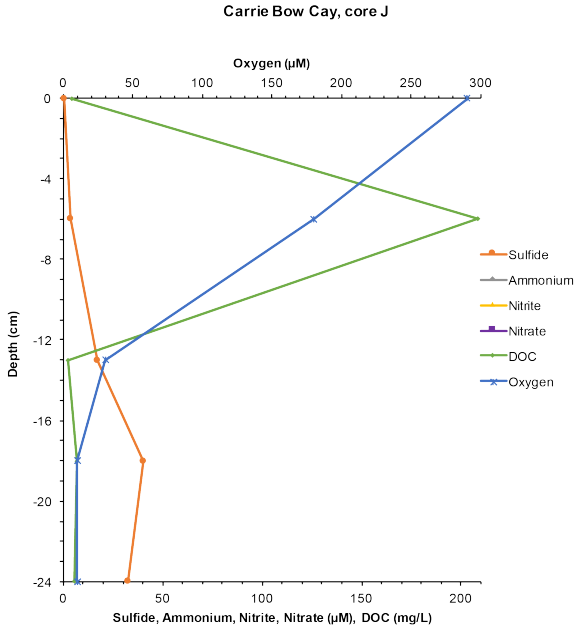

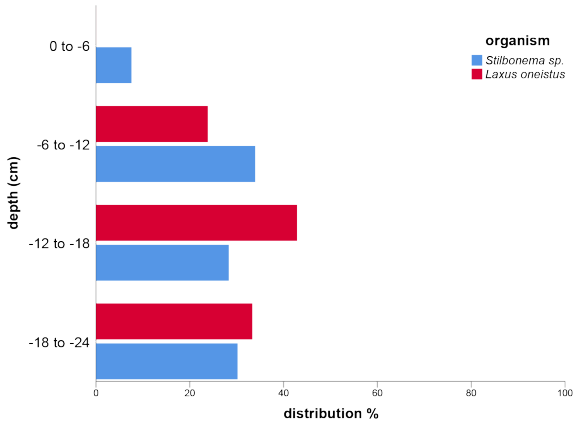

Total number of *L. oneistus*: 21
Total number of *Stilbonema* sp.: 53

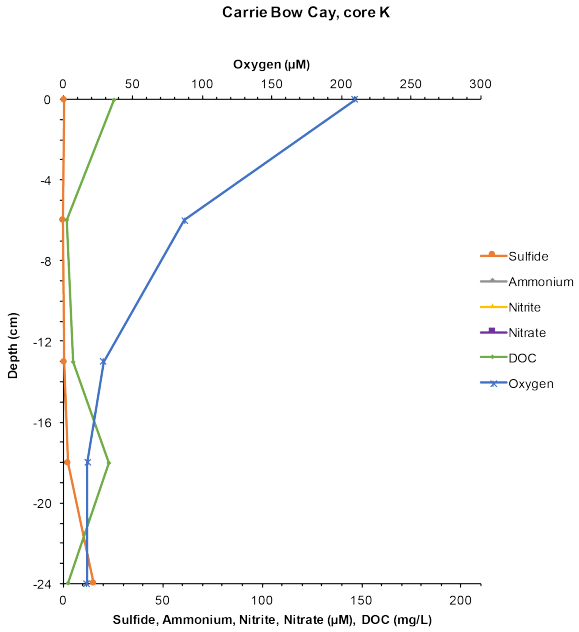

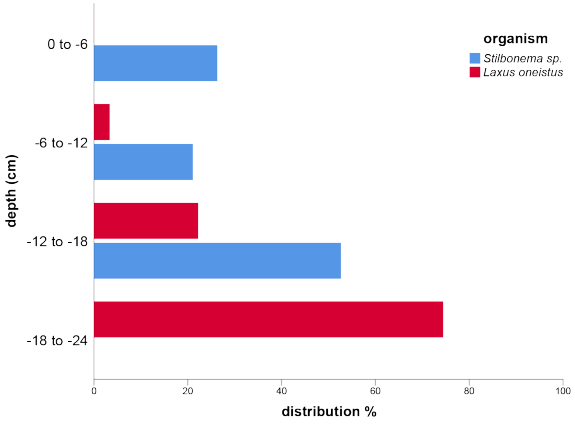

Total number of *L. oneistus*: 90
Total number of *Stilbonema* sp.: 19

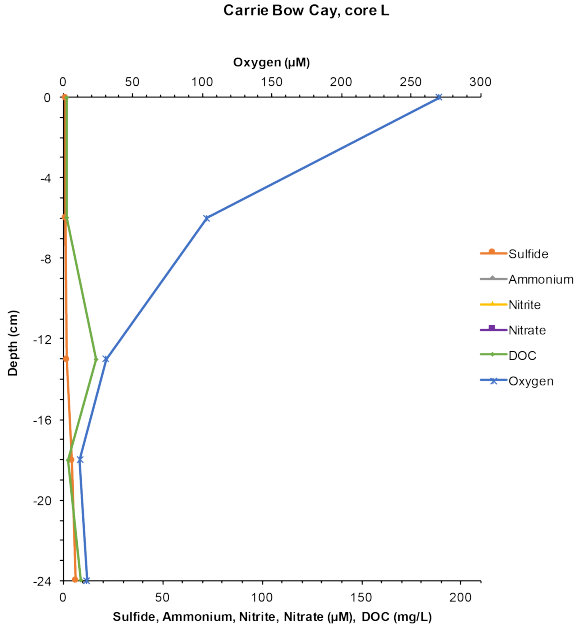

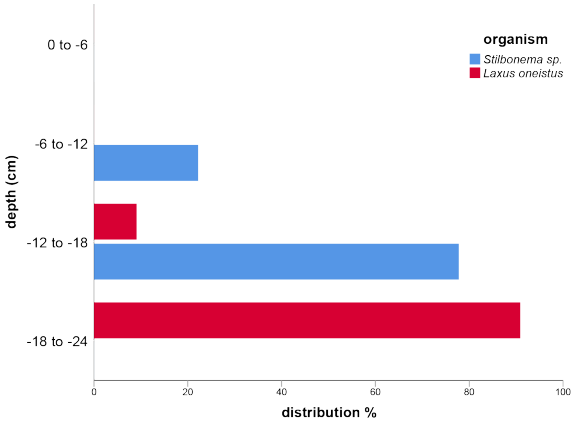

Total number of *L. oneistus*: 55
Total number of *Stilbonema* sp.: 9

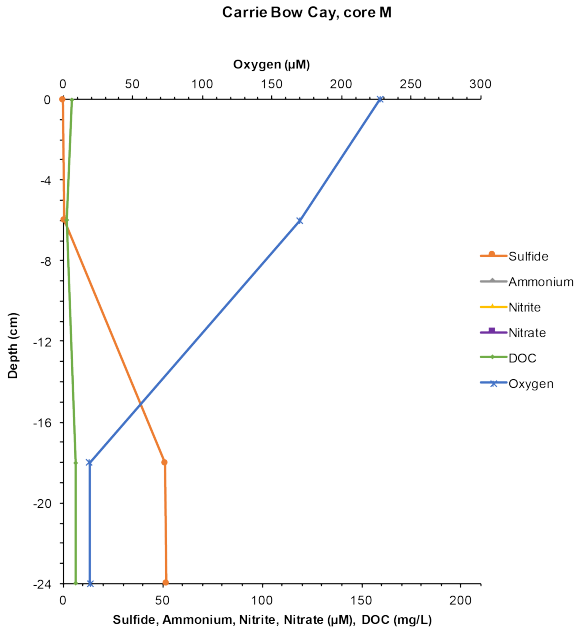

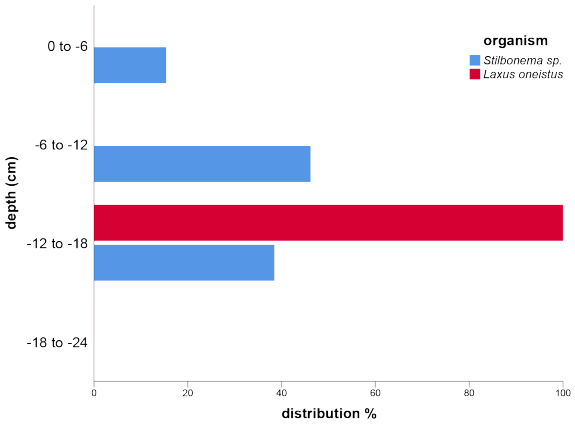

Total number of *L. oneistus*: 1
Total number of *Stilbonema* sp.: 26

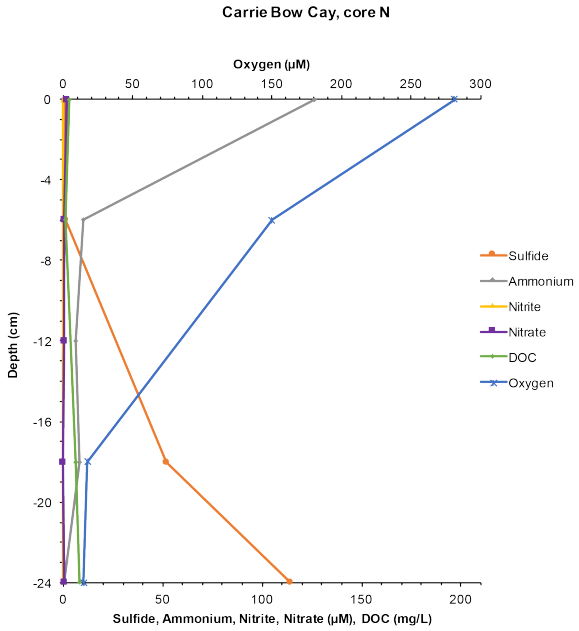

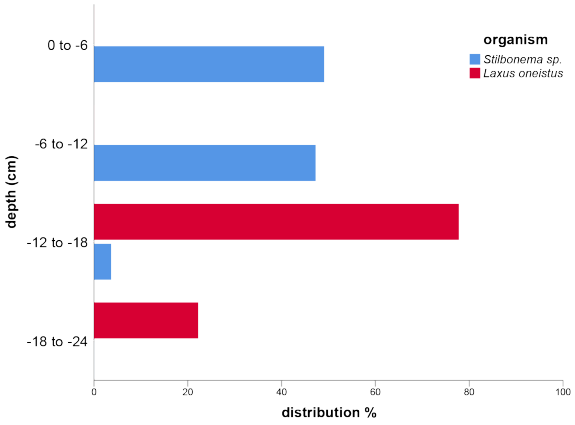

Total number of *L. oneistus*: 9
Total number of *Stilbonema* sp.: 55

3D scatter plots

Sediment cores taken in distance to seagrass beds

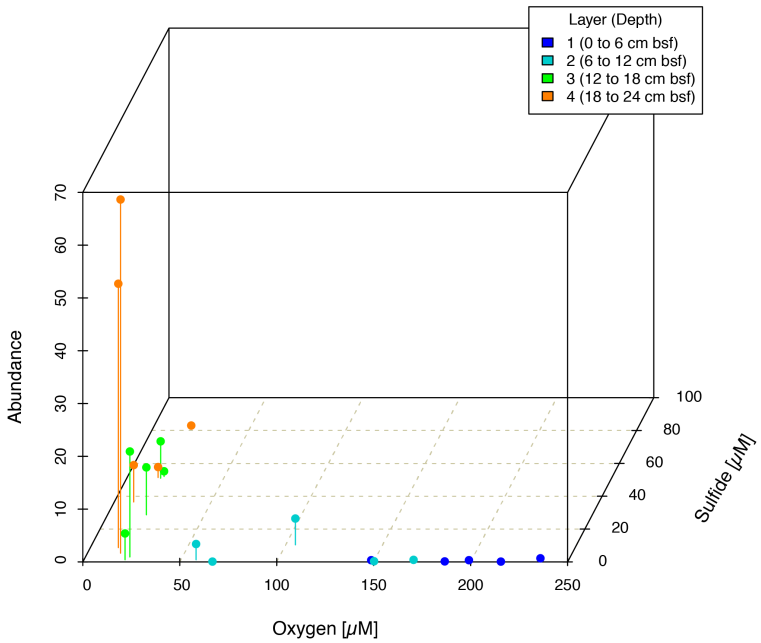

Sediment cores adjacent to seagrass beds

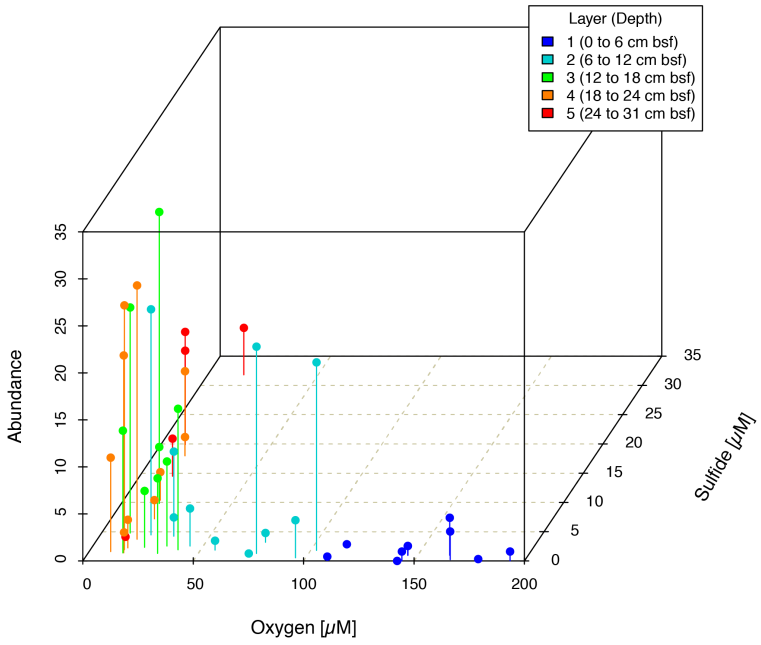

Piran

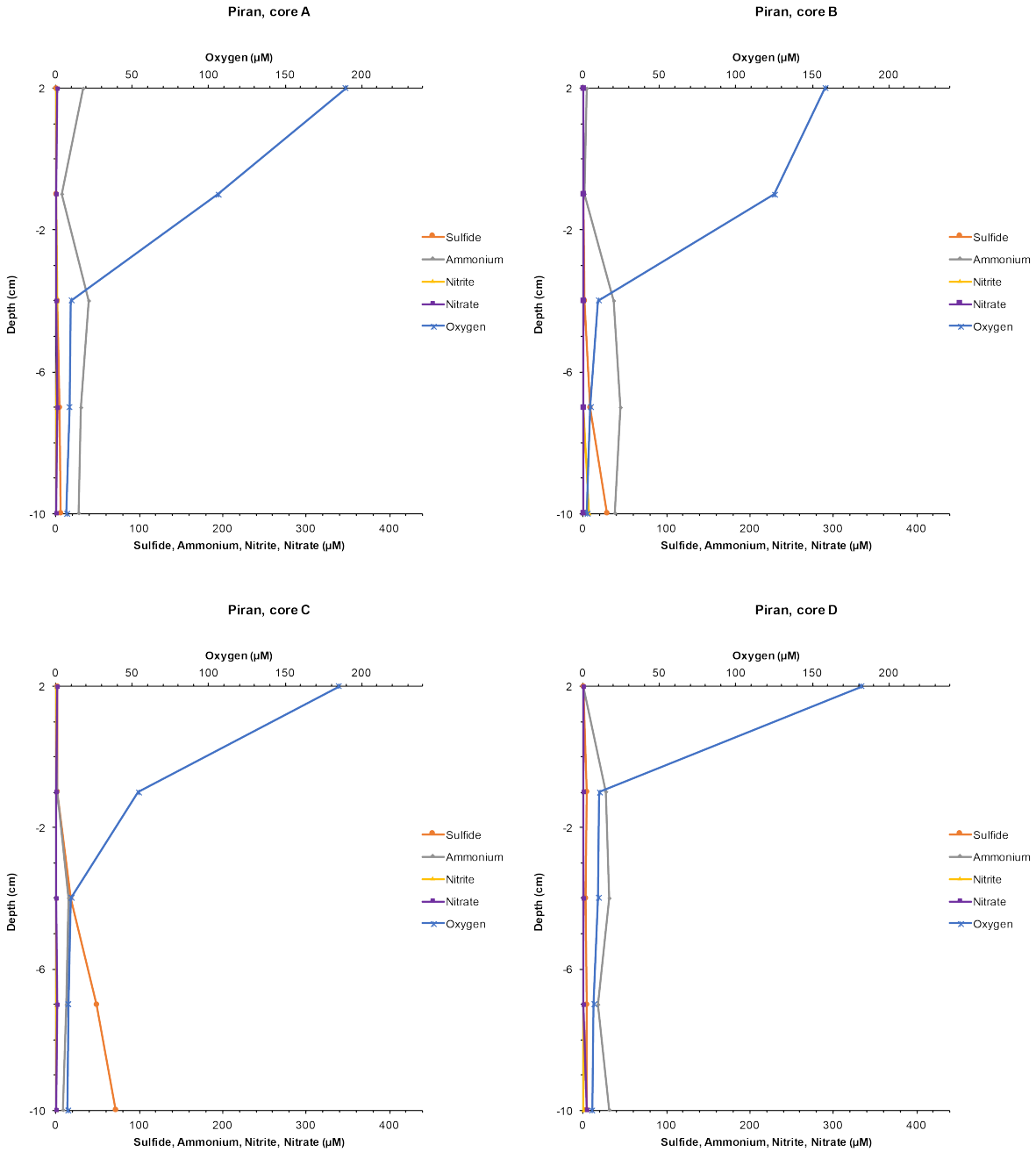
Piran, core A
Oxygen (µM)
0
50
100
150
200
2
-2
-6
-10
Depth (cm)
0
100
200
300
400
Sulfide, Ammonium, Nitrite, Nitrate (µM)
Sulfide
Ammonium
Nitrite
Nitrate
Oxygen
Piran, core B
Oxygen (µM)
Depth (cm)
Sulfide, Ammonium, Nitrite, Nitrate (µM)
Sulfide
Ammonium
Nitrite
Nitrate
Oxygen
Piran, core C
Oxygen (µM)
Depth (cm)
Sulfide, Ammonium, Nitrite, Nitrate (µM)
Sulfide
Ammonium
Nitrite
Nitrate
Oxygen
Piran, core D
Oxygen (µM)
Depth (cm)
Sulfide, Ammonium, Nitrite, Nitrate (µM)
Sulfide
Ammonium
Nitrite
Nitrate
Oxygen

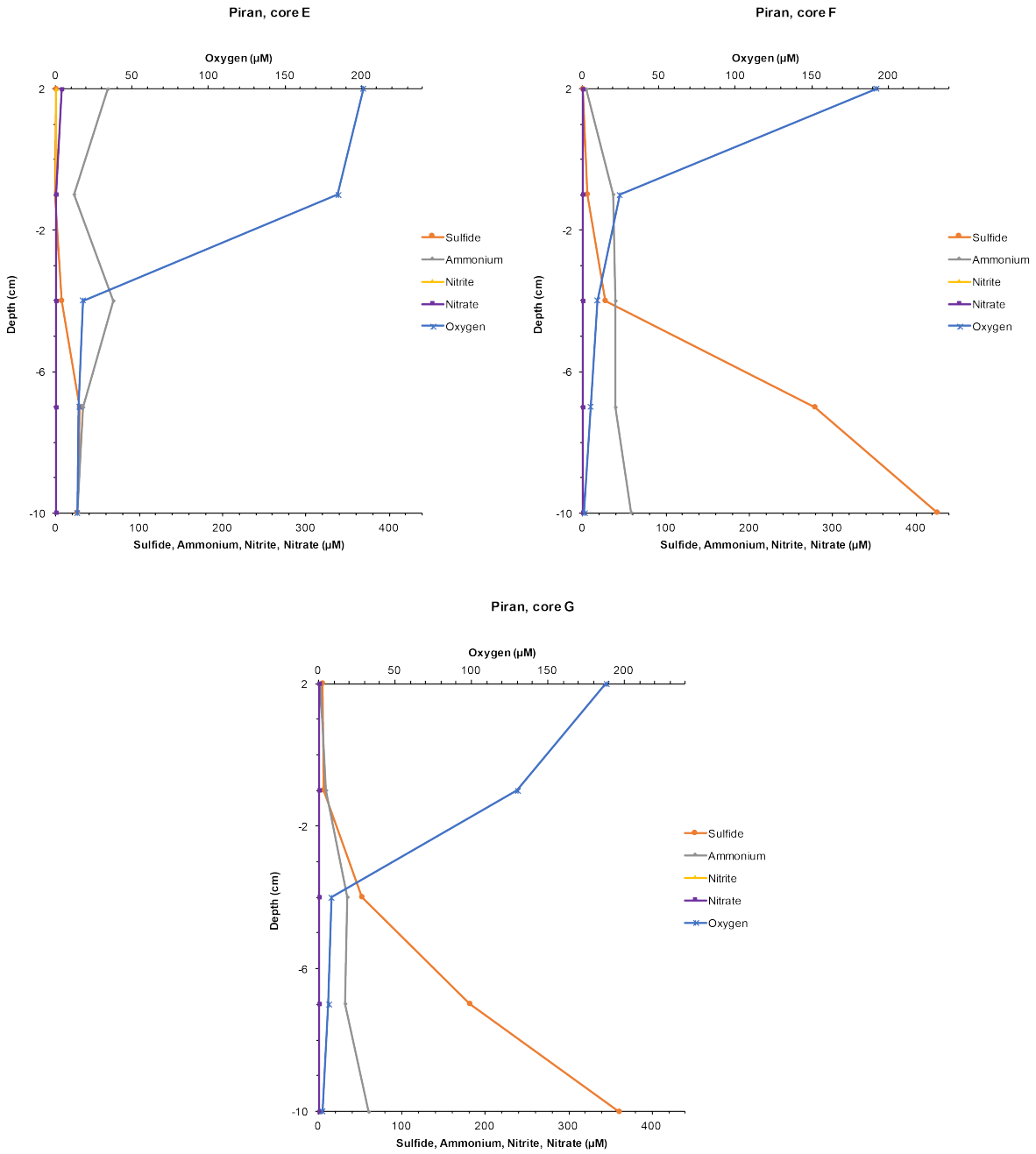
Piran, core E
Oxygen (µM)
0
50
100
150
200
2
-2
-6
-10
Depth (cm)
0
100
200
300
400
Sulfide, Ammonium, Nitrite, Nitrate (µM)
Sulfide
Ammonium
Nitrite
Nitrate
Oxygen
Piran, core F
Oxygen (µM)
0
50
100
150
200
2
-2
-6
-10
Depth (cm)
0
100
200
300
400
Sulfide, Ammonium, Nitrite, Nitrate (µM)
Sulfide
Ammonium
Nitrite
Nitrate
Oxygen
Piran, core G
Oxygen (µM)
0
50
100
150
200
2
-2
-6
-10
Depth (cm)
0
100
200
300
400
Sulfide, Ammonium, Nitrite, Nitrate (µM)
Sulfide
Ammonium
Nitrite
Nitrate
Oxygen